Stony Brook University

Synthesis and Characterization of Nitrogen Substituted Zeolites

A Dissertation Presented

by

Fulya Dogan

to

The Graduate School

in Partial Fulfillment of the Requirements

for the Degree of

Doctor of Philosophy

in

Chemistry

Stony Brook University

December 2010

Stony Brook University

Fulya Dogan

We, the dissertation committee for the above candidate for the **Doctor of Philosophy** degree, hereby recommend acceptance of this dissertation.

Clare P. Grey, D. Phil., Advisor

Professor, Department of Chemistry, Stony Brook University

Michael G. White, Ph. D., Chairperson

Professor, Department of Chemistry, Stony Brook University

Brian L. Phillips, Ph. D., Third Member

Professor, Department of Geosciences, Stony Brook University

Jonathan C. Hanson, Ph. D., Outside Member

Beamline Scientist and Research Chemist, Chemistry Department, Brookhaven National Laboratory

This dissertation is accepted by the Graduate School.

Lawrence Martin

Dean of the Graduate School

Abstract of the Dissertation

Synthesis and Characterization of Nitrogen Substituted Zeolites

by

Fulya Dogan

Doctor of Philosophy

in

Chemistry

Stony Brook University

2010

The interest in basic solid materials, particularly for basic zeolites has considerably increased in the last two decades because of their potential use in catalysis and separation. Basic zeolites have most often been obtained by ion-exchange or impregnation with alkali metal cations or grafting of organic bases onto zeolite pore walls. Such materials often suffer from instability and/or pore blockage, because none of these approaches places basic sites directly into the zeolite framework. Recently zeolitic materials have been made with some of the bridging oxygen atoms in Si–O–Si and/or Si–O–Al linkages replaced by NH groups, i.e. by substitution of framework oxygen by

nitrogen. As a result, the basic strength of the framework increases due to the lower electronegativity of nitrogen with respect to oxygen.

In this study, solid base catalysts are obtained by nitrogen substitution of the faujasite type of zeolites under ammonia flow at high temperatures. The efficiency of the reaction is tested by using zeolites with different aluminum contents and extraframework cations and varying the reaction conditions such as ammonia flow rate, reaction temperature and duration. The characterization studies show that high levels of nitrogen substitution can be achieved while maintaining porosity, particularly for NaY and low-aluminum HY zeolites, without a significant loss in the crystallinity. ^{27}Al and ^{29}Si MAS NMR experiments performed on the nitrogen substituted zeolites show dealumination of the framework and preferential substitution for Si–OH–Al sites at the early stages of the reaction (temperatures at 750–800 °C). No preference is seen for reactions performed at higher temperatures and longer reaction times (e.g., 850 °C and 48 h). X-ray PDF analysis performed on the modified zeolites show that the Si-N distance in the 1st shell is longer than Si-O bond distance and Si-Si/Al bond distance of the Si-O/N-Si/Al linkage decreases, as an indication of a decrease in bond angle. The basicity experiments performed on the zeolites show an increase basicity with increase of the nitrogen content.

Table of Contents

List of Abbreviations

1D, 2D	one dimensional, two-dimensional
BATE	boric acid trimethyl ester
BET	Brunauer Emmett Teller
CBU	composite building units
CP	cross polarization
CSA	chemical shift anisotropy
CT	central transition
CTAB	cetyl trimethylammonium bromide
DFT	density functional theory
DOR	double rotation
EDX	energy-dispersive X-ray spectroscopy
EFG	electric field gradient
ESR	electron spin resonance
FAU	faujasite
FID	free induction decay
FT-IR	fourier transform infrared
HETCOR	heteronuclear correlation
LF	laboratory frame
MAS	magic angle spinning
MQ	multiple quantum
MQMAS	multiple quantum magic angle spinning
NMR	nuclear magnetic resonance
PAS	principal axis system
PDF	pair distribution function
QCC	quadrupolar coupling constant
SEM	scanning electron microscopy
SOD	sodalite
SP	single pulse

SQ	single quantum
TEOS	Tetraethyl orthosilicate
TMS	tetramethylsilane
TPD	temperature programmed desorption
TRAPDOR	transfer of population double resonance
USY	ultra stable Y
XRD	X-ray diffraction

List of Symbols

α, β, γ	Euler angles, relative orientation between two tensors
γ	gyromagnetic ratio
$\delta_{xx}, \delta_{yy}, \delta_{zz}$	principal components of chemical shift tensor
δ_{iso}	isotropic chemical shift
δ_{CS}	isotropic chemical shift
η	quarupolar asymmetry parameter
ν_0	Larmor frequency, s^{-1}
ω_0	Larmor frequency, rad. s^{-1}
ν_r	rotor (sample) spinning frequency s^{-1}
σ	chemical shielding tensor
τp	pulse width (rf duration)
ρ (r)	microscopic pair density
ρ_0	average number density
θ	diffracted angle
B_0	external applied magnetic field
C_Q	quadrupolar coupling constant
D	dipolar coupling constant
e	electron charge
eq	larger component of electric field gradient tensor, V_{zz}
eQ	nuclear quadrupole moment
$G(r)$	pair distribution function
H	Hamiltonian operator
H_D	dipolar coupling Hamiltonian
H_Q	quadrupolar Hamiltonian
$\hbar$	Planck's constant
I	nuclear spin number
I_z	z-component angular momentum operator, spin I

p	coherence order
P_Q	size of the quadrupolar product
Q	nuclear quadrupole moment
Q	magnitude of scattering vector
r_{IS}	internuclear distance between spin I and S
S	nuclear spin number
S_z	z-component angular momentum operator, spin S
$S(Q)$	normalized scattering intensity
t_1, t_2	first, second dimension FID in a two dimensional spectrum
$\mathbf{V}$	EFG tensor
V_{XX}, V_{YY}, V_{ZZ}	principal components of the EFG tensor

List of Figures

Chapter 1

Chapter 2

Chapter 3

Chapter 4

Chapter 5

List of Tables

Chapter 3

Chapter 4

Chapter 5

Acknowledgements

First and foremost, I would like to thank my advisor, Professor Clare P. Grey, for her guidance, kindness, encouragement and endless support. I'm grateful her for giving me a research opportunity in her team. Her dedication to science and her enthusiasm will always inspire me to become a good researcher and a scientist.

I would also like to thank my committee members: Professors Michael G. White and Brian L. Phillips for their guidance, help and constructive criticism in the past five years. Dr. Jonathan C. Hanson is thanked for serving as outside member. I also wish to acknowledge Dr. Jonathan C. Hanson for all his help in running the experiments at NSLS (Brookhaven National Laboratory) and for useful discussions.

Professors Scott M. Auerbach and W. Curtis Conner Jr., Dr. Karl D. Hammond and Dr. Geoffrey A. Tompsett are acknowledged for fruitful discussions and collaborations. I am thankful for the assistance from the beamline scientists, Dr. Peter J. Chupas, Dr. Karena Chapman (Argonne National Laboratory) and Dr. Laura Barrio-Pliego (Brookhaven National Laboratory). Dr. Zhehong Gan (National High Magnetic Field Lab at Tallahassee) and Dr. Boris Itin (New York Structural Biology Center) are acknowledged for their help on running High Field NMR experiments. The US Department of Energy has provided the financial support.

I would also like to thank all the past and present group members for the friendly and fun working environment, for their kindness and help. I thank to Hua Huo, Frédéric Blanc, Rosa Roberts, Nicole Trease and especially Rangeet Bhattacharyya for their great help and support.

Finally I would like to thank to my parents and my sister back in Turkey for all their support, sacrifice, encouragement, unconditional love and all the comforting video chats. Thank you for always believing in me. And to my beloved husband, Baris Key… Thank you for starting this journey with me. I could have never done this without you. Thank you for all your patience, encouragement, support and endless love. You bring joy and happiness to my life.

List of Publications

1. Investigation of the Structural Changes and Reaction Mechanism of Nitrogen Substituted Zeolite Y by Multinuclear NMR Spectroscopy, Dogan F., Bhattacharya R. and Grey, C. P., **2010**, manuscript in preparation

basis of Chapter 4

2. Liquid Phase Aldol Condensation Reactions with MgO-ZrO_2 and Shape-Selective Amine-Substituted NaY", Shen W.; Tompsett, G. A.; Hammond, K. D.;Xing R.; Dogan, F; Grey, C. P Conner, W. C.; Auerbach, S. M.; Huber G. W., Applied Catalysis A: General, **2010**, excepted

3. Optimizing the Synthesis of Nitrogen-Substituted Zeolites, Hammond, K. D.; Gharibeh, M.; Tompsett, G. A.; Dogan, F.; Brown, A. V.; Grey, C. P.; Auerbach, S. M.; Conner, W. C. *Chemistry of Materials*, **2010**, *22*, 130-142

basis of Chapter 2

4. Searching for Microporous, Strongly Basic Catalysts: Experimental and Calculated ^{29}Si NMR Spectra of Heavily Nitrogen-Doped Y Zeolites, Dogan, F.; Hammond, K. D.; Tompsett, G. A.; Huo, H.; Conner, W. C.; Auerbach, S. M.; Grey, C. P. *J. Am. Chem. Soc.* **2009**, *131*, 11062-11079

basis of Chapter 3

5. Spectroscopic Signatures of Nitrogen-Substituted Zeolites, Hammond, K. D.; Dogan, F.; Tompsett, G. A.; Agarwal, V.; Conner, W. C.; Grey, C. P.; Auerbach, S. M. *J. Am. Chem. Soc.* **2008**, *130*, 14912-14913

Chapter 1

Introduction

The interest in basic solid materials, particularly basic zeolites, has considerably increased in the last two decades because of their potential use in catalysis and separations. Basic zeolites have most often been obtained by ion-exchange with alkali metal cations, impregnation with alkali metal ions/basic salts or grafting of organic bases onto zeolite pore walls[1,2]. The resulting materials often suffer from instability and/or pore blockages, because none of these approaches places basic sites directly into the zeolite framework. Recently, zeolitic materials have been made with some of the bridging oxygen atoms in Si–O–Si and/or Si–O–Al linkages replaced by NH groups, by substitution of framework oxygen atoms by nitrogen[3,4]. This is achieved by treating zeolites with amines such as ammonia at high temperatures. As a result, the basic strength of the framework increases due to the lower electronegativity of nitrogen with respect to oxygen, as confirmed by recent density functional theory (DFT) calculations[5]. However, there are limited studies on; i) optimum reaction conditions for nitrogen substitution of zeolites leading to higher nitrogen content but still good crystallinity and porosity, ii) optimum zeolite composition as starting material (Al content, nature of extraframework cations) to improve nitrogen substitution efficiency and iii) the mechanism of nitrogen substitution and nature of the nitrogen sites as well as their basic strength and applicability of treated zeolites in catalytic reactions. The motivation of this research is to study most of these issues.

In this introduction chapter, I will briefly introduce the zeolites, their structural properties and applications, their acidic and basic properties as pristine materials and cover the methods to increase the basicity of the framework and the effect of these modification methods on the zeolite framework. We will then briefly introduce the characterization methods used in this research to study the nitrogen substituted zeolites and finally cover some of the methods to study the basicity of the zeolites.

1.1. Zeolites

Zeolites are microporous crystalline aluminasilicates, composed of SiO_4^{-4} and AlO_4^{-5} tetrahedra with O atoms connecting neighboring tetrahedral containing interconnecting channels and cavities which can accommodate exchangeable metal cations, organic molecules with different shapes and sizes. They have a number of industrial applications such as water softeners, cation exchangers, dehydrating agents. Their molecular sieving property and high internal surface area is critical in the separation of different gas mixtures. Another common application of zeolites is catalysis, primarily catalysis of hydrocarbon transformation reactions in which both the acidity and molecular sieve feature of zeolites are being used. Zeolites are also finding increasing use in synthesis of organic intermediates and fine chemicals[6]. This range of uses of zeolites results from a variety of zeolitic structures.

A completely siliceous structure leads to a silica polymorph, which is an uncharged solid. Addition of aluminum into the silicate framework makes the framework negatively charged. Thus, the presence of extraframework cations is needed within the structure to maintain charge neutrality. The framework structure encloses cavities that can be occupied by large ions and water molecules both having considerable freedom and movement, permitting ion exchange and reversible dehydration. So, the zeolite composition can be described as $M^{m+}_{n/m}[Si_{1-n}\ Al_nO_2].xH_2O$ where $M^{m+}_{n/m}$ is extraframework cation, $[Si_{1-n}\ Al_nO_2]$ is framework and nH_2O is the adsorbed phase. The TO_4 units (T= Si,Al) in zeolites are rigid. Generally, the O-T-O angle is close to 109^o and the T-O bond length depends on the particular metal cation. For SiO_4, the Si-O bond length is 1.59-1.64 Å and for AlO_4 the Al-O bond length it is 1.73 Å [7]. T-O-T bond angle is quite flexible allowing the formation of different zeolite frameworks by a combination of different composite building units (CBUs). The simplest CBUs are *rings*. They are formed of tetrahedra of different sizes. The combination of different sizes of rings in different dimensions results in larger CBUs such as windows, cages, cavities and channels[8]. Different types of CBUs connections form about 133 known zeolite structure types such as faujasite, mordenite, etc. with various channel and cage dimensions (Figure 1.1).

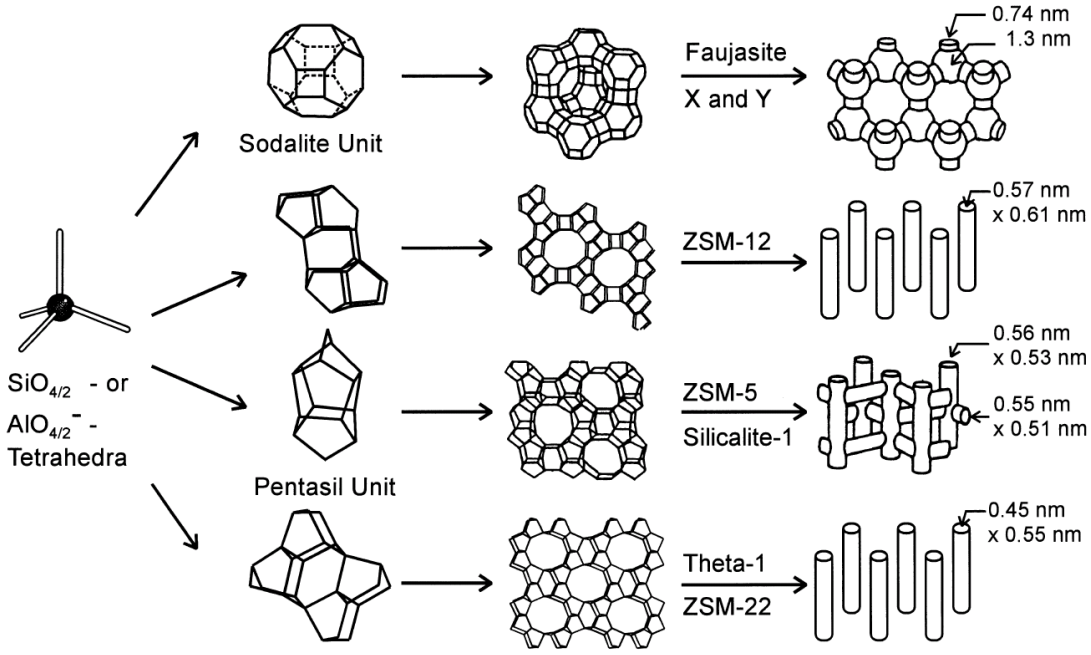

Figure 1.1. Structures of four selected zeolites and their micropore systems and dimensions, from top to bottom: faujasite or zeolites X, Y; zeolite ZSM-12; zeolite ZSM-5 or silicalite-1; zeolite Theta-1 or ZSM-22 (Figure taken from reference 8).

1.1.1. Faujasite Type of Zeolites

As described in the previous section, zeolites are classified into many different structural types depending on the types of connections. Zeolites with faujasite (FAU) topology are among the most widely used type of zeolite among about 133 known structures[9]. The characteristic framework of faujasite type zeolites (Figure 1.2) is composed of sodalite cages and hexagonal prisms. Each sodalite cage connects four hexagonal prisms with their 6-ring in a tetrahedral arrangement[10]. This connection creates supercages with a diameter of about 13 Å in the faujasite structure, allowing relatively large adsorbed molecules to be bound inside the pores. The faujasite type of zeolites can be divided into two main groups depending on their Si/Al ratio. Zeolite X has a Si/Al ratio from 1.0 to 1.5 while Zeolite Y has a Si/Al ratio of about 2.5 and zeolite USY (Ultra Stable Y) Si/Al ratio of 5.6 and higher. The Y and USY zeolites adopt the space group Fd3m (a≈ 24.7 Å) and zeolite X belongs to space group Fd3.

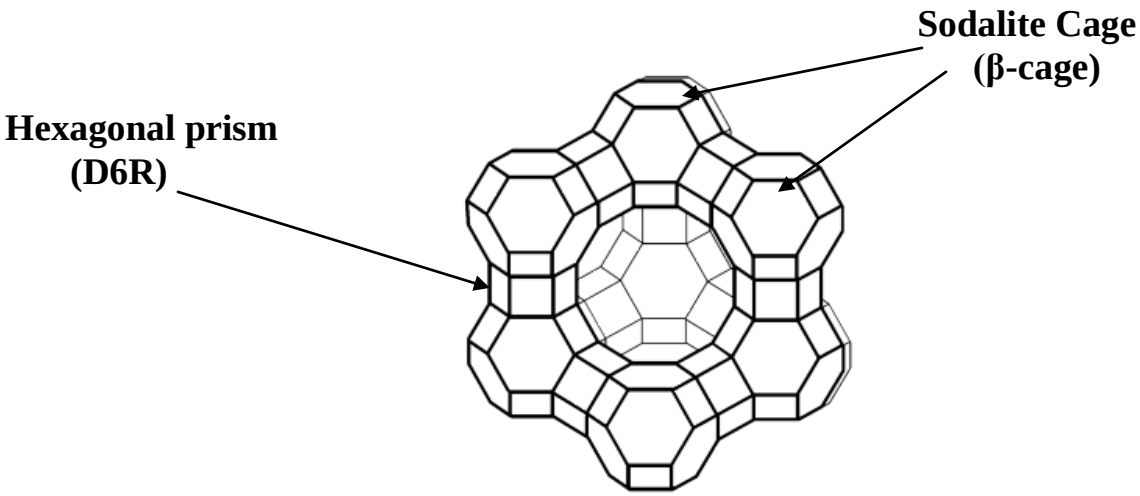

Figure 1.2. Structure of faujasite type of zeolites. Each intersection represents a silicon or an aluminum atom while each line represents an oxygen atom.

1.1.2. Zeolite Beta

Zeolite beta was the first molecular sieve to be synthesized as a high silica variety. Its most interesting property is its highly disordered framework compared to other zeolite families[6,11]. The structure consists of layers formed by five and six rings that may be stacked in different sequences forming a 12 ring pore system that has been observed as an intergrowth of two polytypes A and B.

1.1.3. Mesoporous Silicates

Since the pore sizes of zeolites are limited, materials with characteristics similar to those of zeolites but with larger pores have been studied for almost two decades. The unique characteristics of mesoporous molecular sieves, such as uniform mesoporous structure and large surface area, make the materials of potential use in catalysis, separation of large molecules and nanoelectronics. Since the first report of the mesoporous molecular sieve, MCM-41, there has been extensive study of mesoporous materials. Materials with various pore and wall sizes with a variety of morphologies, and more importantly, with better thermal and hydrothermal stabilities have been synthesized with different methods[12,13]. Out of all mesoporous materials, the most commonly studied

ones are mesoporous MCM-41 and SBA-15. MCM-41, synthesized by Mobil researchers in 1992, has pore sizes in the range of 1.5–10 nm with relatively low hydrothermal stability and weak acidity. The material is highly ordered with a hexagonal structure but the silicate walls are not crystalline and are glass like (Figure 1.3)[14]. In 1998, Zhao et al. synthesized a new type of mesoporous material SBA-15 with uniform two-dimensional hexagonal structure and larger pore sizes, up to 30 nm, allowing bulky molecules to enter into the pores[14]. Mesoporous SBA-15 has higher hydrothermal stability and a thicker pore wall (3.1–6.4 nm) compared with mesoporous MCM-41 materials. For these reasons, SBA-15 is a potentially versatile catalyst and catalyst support for conversion of large molecules.

The mesoporous molecular sieve framework consists of amorphous silica. Because of the large surface area, a large fraction of silicon is present as SiOH groups exposed on the internal surface. The high concentration of surface SiOH is generally used to introduce catalytically active sites by grafting desirable species. A large number of functionalizing groups, both organic and inorganic, have been introduced into channels of the mesoporous materials to generate catalysts, adsorbents, and to improve the hydrothermal and mechanical stabilities[15-17]. Incorporation of heteroatoms, such as aluminum, is also commonly applied to mesoporous molecular sieves, since this introduces a charge imbalance in the framework, which is balanced by protons, generating Bronsted acid sites.

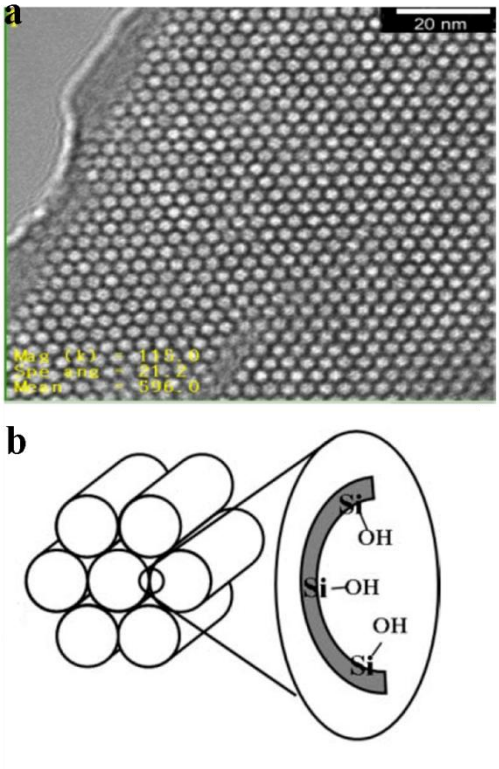

Figure 1.3. a) TEM micrograph of MCM-41. MCM-41 structure has uniform mesopores arranged into a hexagonal, honeycomb-like lattice (Figure taken from reference 13). b) Schematic representation of cylindrical mesopores of MCM-41, silanol groups on the pore surface.

1.2. Acidity and Basicity of Zeolites

The unique properties of the zeolitic materials do not only depend on the framework structure of zeolites but also the composition of the framework such as Si/ Al ratio or type of guest species such as the extraframework cations. The aluminum content within the framework can vary over a wide range with Si/Al = 1 to ∞. Lowenstein proposed that the lower limit of Si/Al = 1 of a zeolite framework arises because the location of adjacent AlO_4^{-5} tetrahedra is not favored, because of the electrostatic repulsions between the negative charges. As the Si/Al ratio of the framework increases, the hydrothermal stability and hydrophobicity increases[6]. The presence of Al also effects the formation of Bronsted acid sites in zeolites. As mentioned above the presence of Al results in a negative charge of the framework. This negative charge is primarily located at the oxygen atoms surrounding the aluminum atoms and compensated by extraframework

cations. If the extraframework cations are protons, they are always coordinated to one of these framework oxygens forming Bronsted acid sites[18]. On the other hand, the positively charged oxide clusters or ions present within the pores of zeolites can act as Lewis acid sites. These species are typically alumina generated by the extraction of aluminum from the framework (dealumination) or metal cations balancing the negative charge of the framework. Lewis and Bronsted acidity, along with the unique porous structure of zeolites plays a vital role in controlling the performances of the many zeolite-based industrial catalysts. Zeolite HY, for example, proves to be powerful in many catalytic reactions and is a cracking catalyst in the petroleum industry.

Compared to the use of acidic zeolites in industry, basic zeolites have not been widely employed since the standard zeolites do not typically exhibit strong basic sites. It would be desirable to take advantage of the properties of zeolites such as high surface area, shape selectivity and pore structure, and develop highly active, selective and stable base catalysts. To induce stronger base sites, researchers usually consider low-silica zeolites, which contain a high concentration of aluminum substitution in the zeolite framework, thereby placing a high density of negative charge on the zeolite framework oxygen atoms.

1.2.1. Framework basicity in zeolites

In a zeolite framework oxygens of the SiO_4 and AlO_4 tetrahedra are negatively charged and, in principle, are Lewis basic sites. By exchanging the protons with cations the basic character of the framework can be strengthened. The basicity of the oxygen atoms in the lattice depends on the angles between oxygen and tetrahedral atoms (T atoms), the bond length and the nature of the tetrahedral atom. Oxygen atoms in AlO_4 tetrahedra for instance are more basic than the ones in SiO_4 tetrahedra. The strength of framework basicity depends on the specific Al location in the T sites and also the Al concentration. As stated in the previous section, it requires a high number of Al atoms in the framework to generate a high number of basic oxygens. For a given number of Al sites, as the degree of connectivity's decrease, the number of basic sites increases, decreasing the basic strength[19].

1.2.2. Catalytic Applications of Basic Zeolites

Zeolites have been potential candidates for solid base catalysis due to their shape selective properties, their ability to concentrate reactants inside their pores and their high thermal stability. In comparison to the homogeneous catalysts, solid base catalysts have a number of advantages as they can be easily separated and recycled after catalytic reaction requiring no neutralization and they are non corrosive to the reactor system. Basic zeolites have been used in many reactions such as carbon-carbon bond forming reactions in fine chemistry, in petroleum refining as well as food, pharmaceutical and cosmetic industries.

One of the catalytic reactions that the basic zeolites are mostly tested and used for are Knoevenagel reactions. Knoevenagel reactions are condensation reactions of aldehydes or ketones, with reagents of the form Z-CH_2-Z' or Z-CHR-Z'. The Z groups are electron withdrawing groups, such as CHO, COR, COOH, COOR, CN, NO_2, SOR, SO_2R, SO_2OR or similar groups. Below is the knoevenagel reaction between benzaldehyde and malonitrile[2,20]. The reaction is also commonly used as a test reaction to study the basicity of the zeolites that are modified to increase their basic character (discussed in Section 1.3)

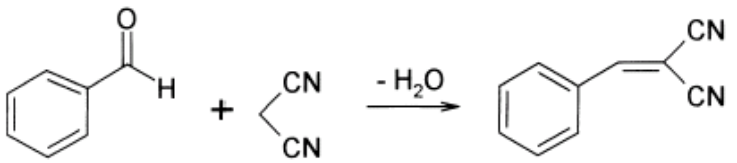

(1.1)

Base catalysts have an increasingly important role in the biorefinery. Most catalysts used in biodiesel production by transesterification of vegetable oils with methanol use base catalysts, and base catalysts are 4,000 times more active than acid catalysts for this reaction. The transesterification is the reaction of triglycerides (or other esters) with alcohols to produce alkyl esters (biodiesel) and glycerol, in the presence of acid or base catalysts as shown in Figure 1.4. Transesterification consists of a number of consecutive, reversible reactions, with diglycerides and monoglycerides as intermediates[21]. The first step in transesterification is production of diglycerides and alkyl esters, followed by monoglycerides and alkyl esters and finally alkyl esters and glycerol.

All of these reactions are reversible, and excess alcohol solvent is used to drive the reaction to completion.

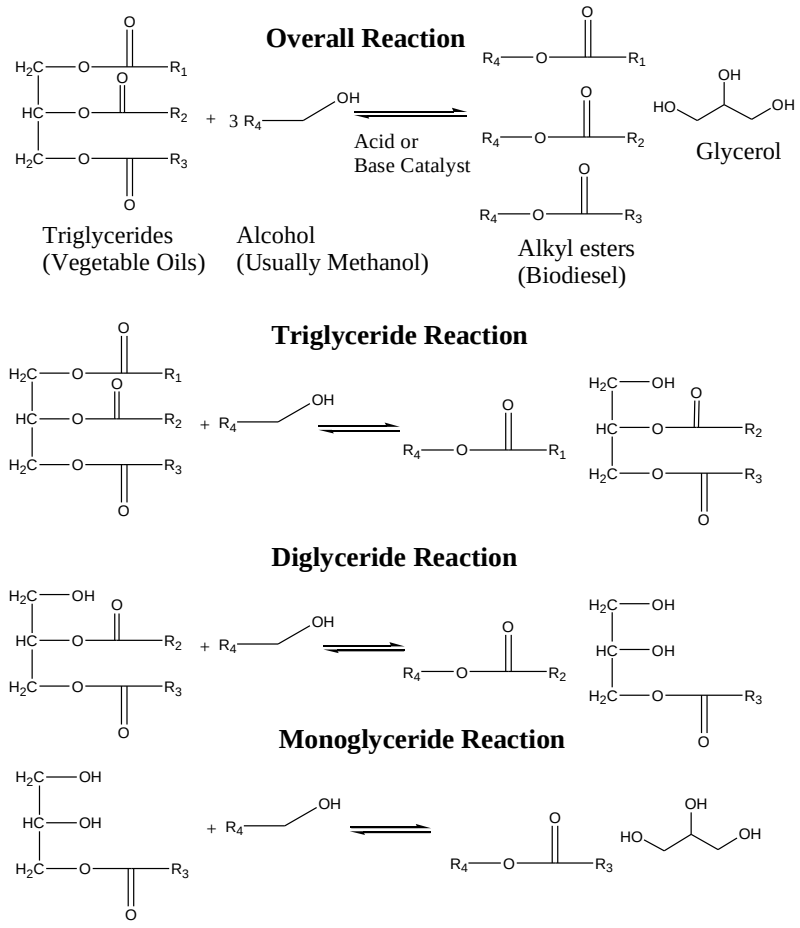

Figure 1.4. Overall and intermediate reactions for transesterification of triglyceride and alcohol to produce alkylesters (biodiesel) and glycerol.

One other important base catalyzed reaction in biorefinery include: aldol condensation reactions specifically aldol condensation of furfural with acetone as shown in Figure 1.5. The reaction is one of the key steps to convert carbohydrates into liquid alkanes ranging from n-C_7-C_{15}. The products can be either a monomer (1:1 atomic ratio furfural:acetone) or dimer (2:1 atomic ratio furfural:acetone). The dimer has a lower solubility in water than the monomer, and it is desired to control the selectivity of this reaction[22]. Therefore, shape selective materials with well defined pore structures are used in controlling product selectivity.

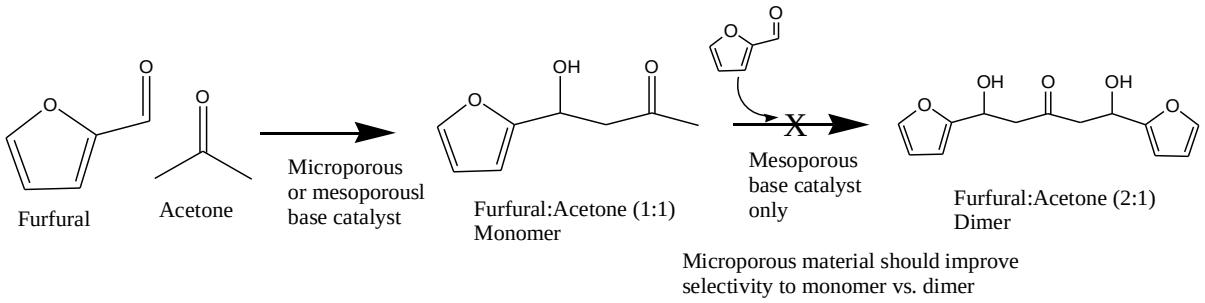

Figure 1.5. Aldol condensation of furfural with acetone.

1.3. Modifications in Zeolite Framework

1.3.1. Dehydration and Dealumination

In the as-crystallized form, zeolites are hydrated; the cavities are filled with either physisorbed water or are present in the form of a hydration shell surrounding the cations. Because of the equilibrium between the water of hydration of the cations and the physisorbed water, these two types of water are lost over a relatively wide temperature range in one continuous process. Depending on the cationic form and Si/Al ratio of the zeolitic framework the effect of thermal treatment on the zeolite framework varies. For example, the acidic forms of zeolites with low silica content are mostly unstable and easily go through dealumination which affects the crystallinity of the framework. Some thermal stability can be attained by partial exchange with ammonium ions, leaving most of the cation sites occupied by stable cations but then even a mild hydrothermal treatment can cause loss of crystallinity. In catalytic applications zeolites are always used in the activated, non-hydrated state. Various characterization studies on non-hydrated zeolites have shown that this treatment may cause changes in the zeolite framework. Van Bokhoven et al. found three-coordinate aluminum atoms at high temperatures and distorted tetrahedral aluminum atoms at room temperature[23]. In another work, they observed that the distorted tetrahedral aluminum atoms can be converted to tetrahedral aluminum upon rehydration[24]. Such changes of the coordination state of aluminum atoms in non-hydrated zeolites can affect the acidic properties of these catalysts and indicate

that investigations of the non-hydrated materials are required. Generally, changes of the local structure of AlO_4 tetrahedra in the framework of zeolites influence the Si-O bond lengths and Si-O-T bond angles[25].

Increasing the Lewis acidity of the zeolite materials requires the modification of the as synthesized material. This is often done by the dealumination of the framework, either by steaming the zeolite or acid leaching, where hydrolysis of the framework Si-O-Al linkages is induced, eventually resulting in the loss of aluminum from the framework forming extraframework aluminum cations acting as Lewis acid sites. The extraframework aluminum species in steamed zeolites can be cationic compounds, such as Al^{3+}, AlO^{+}, $Al(OH)^{2+}$, and $Al(OH)_2^{+}$, or neutral and polymerized compounds, such as AlO(OH), $Al(OH)_3$, and Al_2O_3 and the nature of extraframework aluminum species is strongly influenced by the presence of water[26]. The dealumination process is usually associated with a change in the porosity within the crystals and may sometimes cause a dramatic loss of crystallinity.

1.3.2. Increasing the basicity of the framework

As mentioned in the previous section, zeolites are generally used as solid-acid catalysts and little attention has been paid to their basic properties or to increase the basicity of zeolite framework. The origin of the basicity of zeolites is known to be the oxygen atoms in the framework. To induce stronger base sites, usually low-silica zeolites are considered, which contain a high concentration of aluminum substitution in the zeolite framework, thereby placing a high density of negative charge on the zeolite framework oxygen atoms. Even greater base strengths can be attained in zeolites through ion exchange with alkali metal ions and also impregnation of the zeolite pores with small particles that can act as bases themselves. The former produces relatively weak basic sites, while the latter results in strong basic sites. With alkali ion-exchanged zeolites, the type of alkali cations that is used affects the basic strength of the resulting zeolites. Effects of the alkali ions on basic strength are in the following order: Cs+ > Rb+ > K+ > Na+ > Li+ where the basic sites are framework oxygen. The bonding of the framework oxygen is covalent in nature. This causes the basic sites of ion-exchanged zeolites to be relatively

weak as compared to those of alkaline earth oxides[27]. Unfortunately, even the base sites in Cs-X are relatively weak and can not catalyze most of the organic additions and condensations with reasonable turnover rates. The reason for this is that although the framework oxygens in Cs-X are negatively charged, the electro-negativity of oxygen is so great that these oxygens are unwilling to share their charge, making them weak base sites. In order to create stronger base sites in the cavities of zeolites, one of the modification methods that has been tried was impregnation with various alkali salts such as NaN_3. The resulting materials were successfully employed for several bifunctional reactions by incorporating selective metal clusters. Weitkamp, however, notes that these systems are both air and water sensitive which limits their use, certainly excluding water forming reactions such as condensations & esterification reactions[28]. Another method to introduce basic sites into the zeolite framework involves grafting organic bases on the pore walls of zeolites. Zhang *et al*. grafted amino groups on to NaX and CsNaX zeolites and tested their catalytic activity for Knoevenagel condensation reactions[29]. The results showed higher conversion compared to aminopropylated MCM-41 but the catalysts suffers from pore blocking, preventing bulky molecules from reaching the inside active site.

1.3.3. Nitrogen substitution on zeolites and mesoporous materials

In the 1990`s another kind of mesoporous base catalyst with high surface area was developed which contains nitrogen rather than oxygen as basic sites. The modification of the framework was achieved replacing the oxygen by nitrogen at high temperatures under ammonia treatment. The preliminary substitution reactions were held on amorphous aluminum phosphates, zirconium phosphates, aluminum vanadate or galloaluminophosphates[28,30,31]. Substitution of framework oxygen with nitrogen has now been performed on several different oxides such as amorphous silica, silicoaluminophosphate molecular sieves (SAPO-11) and mesoporous silicon oxides such as SBA-15 and MCM-41 forming silicon oxynitrides[32-35]. The nitrogen substitution reactions were mostly performed at 900-1100^{o}C and the treated material showed nitrogen contents of up to 15% (by weight). The substitution reactions recently have also been

applied to zeolitic materials. Ernst *et al.* prepared zeolites Y by treating them with ammonia at 700–875^{o}C. They reported high catalytic activity in the Knoevenagel condensation of benzaldehyde with malononitrile, though they reported that this activity decreased with storage time if the materials were stored in a dessicator instead of an inert atmosphere. Their recent work on beta zeolite on the specific pore volume as measured from nitrogen adsorption showed a decrease consistently with nitrogen content, which may indicate that the materials' microporous structure was destroyed as nitrogen was added to the zeolite[20,36].

Zhang *et al.* performed nitrogen substitution reactions with ZSM-5, treating the material with ammonia under a temperature of about 1100^{o}C[37]. They obtained a maximum nitrogen content of 15% and nitrogen substituted ZSM-5 zeolites showed *a* high activity in the Knoevenagel condensation of benzaldehyde with malononitrile. Han *et al.* disclosed a novel route to the nitridation of MFI zeolites[3]. They treated the samples with methyl amine at room temperature and the thermogravimetric analysis results showed a replacement of up to 13% of the zeolites oxygen by nitrogen, forming Si-N-Si linkages. NH_3 and CO_2 Temperature Programmed Desorption (TPD) experiments confirmed that the zeolites had acquired strong basic properties.

1.3.4. Proposed nitrogen substitution mechanism

The substitution mechanism of nitrogen over framework oxygen in zeolites and mesoporous materials has been studied by various groups. Although the detailed mechanism is not completely known for nitrogen substitution into the zeolite framework, the structural characterization of nitridated mesoporous materials by Infrared (IR) and Raman Spectroscopy reveals that the substitution reactions starts with the surface groups and defect sites in the structure. Therefore crystalline zeolites have been claimed to be more difficult to nitride as they contain fewer silanol groups as defect sites[1,8].

Chino *et al.* studied the nitridation mechanism of mesoporous silica SBA-15[38]. The structural ordering, surface properties and local structure of the products were analyzed by X-ray Diffraction (XRD), Fourier Transform Infrared (FT-IR), Electron Spin Resonance (ESR) and ^{29}Si MAS NMR Spectroscopy. The proposed mechanism taking

the ESR and IR results into account was that the nitridation proceeds through the radical reaction of NH_3 with ≡Si–O· and ≡Si· species below 700°C. N-related defects (seen by ESR) are produced through the reaction of siloxane bridging bonds by H atoms generated from NH_3 on the pore surface above 800°C. Nitridation is then enhanced by the condensation of $\equiv SiNH_2$ species and the radical reaction of NH_3 with N-related defects. Other than this study, no other group has suggested a nitrogen substituted mechanism with radical formation but the initial steps of most them showed that the reaction starts with terminal silanol groups.

Xia *et al.* studied the nitrogen substitution reaction on mesoporous Si-MCM-48 prepared at 900°C for 20 hours and characterized the treated material by XRD and IR Spectroscopy. The suggested nitridation mechanism was as follows[32]:

$$\equiv Si - OH + NH_3 \rightarrow \equiv Si - NH_2 + H_2O \qquad (1.2)$$

and/ or

$$\equiv Si - O - Si\equiv + NH_3 \rightarrow \equiv Si - NH - Si\equiv + H_2O \text{ or } \equiv Si - NH_2 + \equiv Si - OH \qquad (1.3)$$

Han *et al.* studied nitrogen substitution of zeolite MFI by reacting the material with methyl amine at room temperature[3]. The products were studied by FT-IR and ^{29}Si MAS NMR. The group suggested a reaction mechanism as given in Figure 1.6.

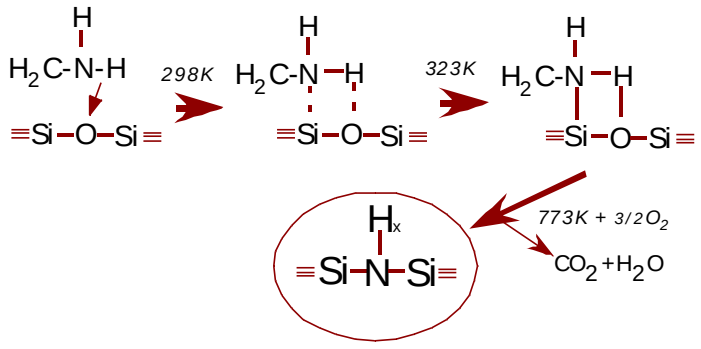

Figure 1.6. Proposed mechanism for the reactions between methylamine and MFI zeolites. First, a transition state Si-O-H-N complex is formed, which is then formed into then a tetra-ring unit. Si–NH–Si bond forms after calcination at 773K, eliminating the methyl groups of methyl amine.

According to Han *et al*., when methyl amine is adsorbed onto the zeolite surface, the H atom of amine group attacks the [Si–O] framework to form the transition state Si-O---H---N, where the Si–OH groups were observed with the ^{29}Si MAS NMR at 298K. According to the proposed mechanism then a tetra-ring unit is further formed, Si–N linkage appearing in the modified zeolite at 323K. Finally, the Si–NH–Si bond forms after calcination at 773K, eliminating the methyl groups of methyl amine. Han *et al.* specifically hypothesized a single hydrogen bound to nitrogen (x =1 in Figure 1.6) in the final basic site; however, they provided no confirmation for this. The final configurations of the basic catalytic sites for nitrogen substitution into zeolites remain poorly understood. One might envision that the ammonia treatment at high temperatures or the methylamine treatment initially near room temperature first involves interactions between these basic reactants and framework Brønsted acid sites. For silica/alumina zeolites, these interactions would result in substitution into Si-O-Al bonds, forming Si-N(H_x)-Al basic sites.

Ernst *et al.* studied the nitrogen substitution reaction on zeolite beta under a wide temperature range from 300^{o}C to 850^{o}C and proposed a mechanism for nitrogen substitution over terminal silanols, Si-O-Si framework linkages as well as Si-O-Al linkages with the flowing steps:

$$\equiv Si - OH + NH_3 \rightarrow \equiv Si - NH_2 + H_2O \quad (1.4)$$

$$\equiv Si - O - Si\equiv + NH_3 \rightarrow \equiv Si - NH_2 + \equiv Si - OH \quad (1.5)$$

$$\equiv Si\text{-}NH_2 + \equiv Si\text{-}OH \longrightarrow \equiv Si\text{-}\overset{H}{N}\text{-}Si + H_2O \quad (1.6)$$

$$\equiv Si\text{-}NH_2 + \equiv H_2N\text{-}Si \longrightarrow \equiv Si\text{-}\overset{H}{N}\text{-}Si + NH_3 \quad (1.7)$$

$$\equiv Si\text{-}\overset{H}{O}\text{-}Al\equiv + NH_3 \longrightarrow \equiv Si\text{-}NH_2\text{-}Al + H_2O \quad (1.8)$$

Apart from the summarized proposed mechanisms on nitrogen substituted to mesoporous silicon oxides and zeolite MFI, which was treated initially at room temperature with ammonia, a detailed mechanism for nitrogen substitution to aluminum containing zeolites and the nature of the local structure of the product is still speculative. Performing the substitution reaction at various reaction conditions, with starting materials

having different aluminum contents and extraframework cation, and performing a more detailed study on the products will help in our understanding of the sites, and their formation mechanism (involving acidic-basic sorption and /or Si-O-Al sites).

1.4. Characterization Methods

Various methods are being used for the characterization of zeolites. Among them the most common ones are X-ray powder diffraction (XRD) and Magic Angle Solid State (MAS) NMR spectroscopy. XRD is mainly used for determining the zeolite structure as well as the space group and unit cell parameters, whereas, MAS NMR provides information about the local environment of the framework atoms, such as Si, Al ordering, quantitative data of Si and Al sites as well as the identification of the catalytic sites. NMR is a probe of local structure and often serves as a complementary tool for the probe of long-range order, diffraction[6]. Scanning Electron Microscopy (SEM) is also a method of choice for determining the size and morphology of zeolite crystallites. IR spectroscopy and Raman spectroscopy are also commonly used for analyzing the coordination environment for nonframework and framework metal ions[20,36,37].

1.4.1. Solid State NMR Spectroscopy

1.4.1.1. Interactions in Solid State NMR Spectroscopy

The NMR spectra of solid samples are affected by various internal spin interactions between nuclear spins and magnetic or electric fields arising from the sample itself, including shielding interactions such as chemical shift, dipolar interactions and the quadrupolar interaction.

Chemical Shielding Anisotropy (CSA): The chemical shielding interaction arises because of the interaction of the nuclear spin with surrounding electrons, how the nuclear spin is affected by its electronic environment (electronegativity, hydrogen bonding). In the external magnetic field the electrons circulate around the field and produce a secondary field which opposes the applied magnetic field at the center of the circulation.

Therefore, the net magnetic field experienced by the nucleus is less than the applied static field, shielding the nucleus.

The chemical shift is an anisotropic parameter and the orientational dependence in the chemical is characterized by a tensor illustrated in Figure 1.7. The principal components of the chemical shift tensor can be defined so that $\delta_{xx} \geq \delta_{yy} \geq \delta_{zz}$ and isotropic chemical shift δ_{iso} can be written as

$$\delta_{iso} = 1/3\ (\delta_{xx} + \delta_{yy} + \delta_{zz}) \qquad [1.9]$$

In a crystalline powder sample all the orientations of the Principal Axis System (PAS) of the shielding tensor are present and for most orientations PAS does not coincide with the laboratory frame (LF) where the z axis is aligned with the direction of the applied magnetic field B_0.

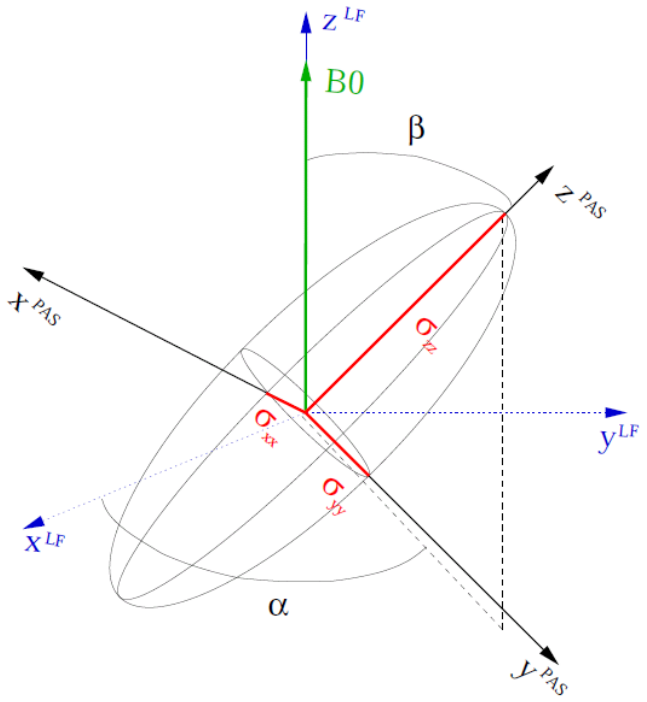

Figure 1.7. Principal tensor components for chemical shift anisotropy (defined with respect to laboratory frame) and the Euler angles (α and β) defining the orientation of the principal axis system (PAS) in the lab frame (LF). σxx, σyy, σzz, are the principal components of the chemical shielding tensor.

Dipolar Coupling: Dipole dipole interactions arise because each nucleus has a spin and this spin generates an individual magnetic field affecting the neighbor nucleus. The

interaction is strongly dependent on the distance between the nuclear spins and the angle between the vector connecting the two spins and the direction of the static magnetic field (θ). The interaction produces a shift of the NMR resonance to lower or higher frequencies depending on the value of θ and the expression for the dipolar coupling Hamiltonian between the two nuclei I and S can be written as;

$$H_D = - D (3 \cos^2 \theta - 1) I_z S_z \qquad [1.10]$$

where D is the dipolar coupling constant which is given by $\gamma_I \gamma_S h / 2\pi r^3$. γ_I and γ_S are the gyromagnetic ratios of spin I and S, respectively, and *h* is Planck`s constant. Since the term is angular dependent, the direct dipole interaction causes a distribution of resonant frequencies and broadens the NMR signal in the solid state. This often prevents the observation of the isotropic chemical shifts. Therefore, high resolution spectra require elimination of this anisotropic interaction which is usually done by Magic Angle Spinning (MAS) which will be discussed in the next section. The dipolar interaction can, however, provide useful information on nuclear connectivity. Therefore, there are MAS NMR techniques to reintroduce the dipolar interaction under MAS conditions.

Quadrupolar Interactions: Quadrupolar nuclei have a spin > 1/2, and an asymmetric distribution of nucleons giving rise to a non-spherical positive electric charge distribution; this is in contrast to spin-1/2 nuclei, which have a spherical distribution of positive electric charge. The asymmetric charge distribution in the nucleus is described by the nuclear electric quadrupole moment, *eQ*, which is an instrinsic property of the nucleus, and is the same regardless of the environment. The interaction between quadrupole moment and electric field gradient (EFG) is called the quadrupolar interaction. The EFG is caused by surrounding electrons distribution. The magnitude of the quadrupolar interaction is given by quadrupolar coupling constant C_Q, which is defined in equation (1.5).

$$C_Q = eQ \cdot eq/h \qquad [1.11]$$

The EFG at the quadrupolar nucleus can be described by asymmetric traceless tensor, which can also be diagonalized. The principal components of the EFG tensor are defined as $|V_{xx}| \leq |V_{yy}| \leq |V_{zz}|$. The asymmetry of the quadrupolar interaction is given by the asymmetry parameter:

$$\eta = (V_{xx} - V_{yy})/V_{zz} \quad (0 \leq \eta \leq 1). \qquad [1.12]$$

If $\eta = 0$, the EFG tensor is axially symmetric.

Effects of the first- and second-order interactions on the energy levels of a spin-5/2 nucleus are shown in Figure 1.8. The Zeeman splitting (H_z) gives a set of equally spaced energy levels. The transition (1/2 ↔ -1/2) is called central transition (CT), and the other transitions like (3/2↔1/2), (-1/2↔-3/2), (5/2↔3/2) and (-3/2↔-5/2) are called satellite transitions. To first order the quadrupolar splitting ($H_Q^{(1)}$), gives a set of symmetric transitions with the magnitude of the effect depending on the Q (quadrupolar interaction) and characteristic shape determined by η. For non integer quadrupolar nuclei the central transition is not effected by first order quadrupolar interaction. The second order quadrupolar interaction however effects all the transitions, including the central transition and results in broad quadrupolar lineshape. The quadrupole interaction complicates the interpretation of the NMR spectra but is valuable source for structural information as it reflects the local symmetry of the studied nucleus.

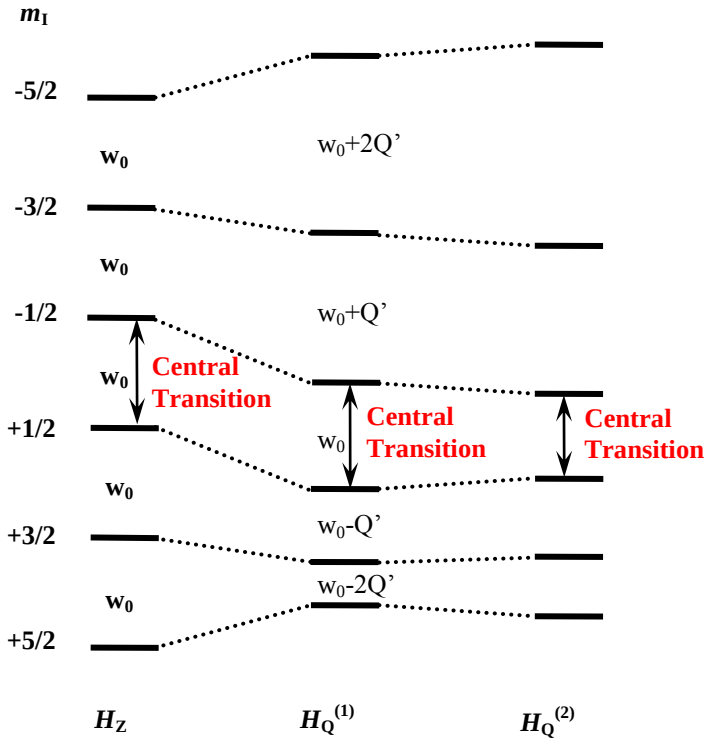

Figure 1.8. Effects of first and second-order quadrupolar interaction on a spin 5/2 nucleus.

Magic Angle Spinning (MAS): Many of these interactions depend on the orientation of the sample in the magnetic field thus they have an angular dependence. Magic Angle

Spinning (MAS) involves the physical rotation of the sample at the magic angle of 54.74^{o} with respect to external magnetic field (Figure 1.9). The angle 54.74^{o} is the solution to the term $3\cos^2(\theta)-1$, the angular dependence in the above interactions. At the magic angle this term becomes zero removing the dipole dipole interaction and chemical shift anisotropy interactions in the limit of fast spinning and first order quadrupole interactions narrowing the NMR spectra. If the spinning rate is not sufficiently large enough compared to the anisotropy, this leads to a series of peaks, spaced at integer multiples of the spinning rate from the isotropic peak, which are known as spinning sidebands. The isotropic peak is not necessarily the most intense line, but does not change position with modified spinning rate, providing an easy method to identify the isotropic resonance in the solid-NMR spectrum. The broadening effects due to higher order interactions of the quadrupolar nuclei can be eliminated by the application of different NMR pulse sequences.

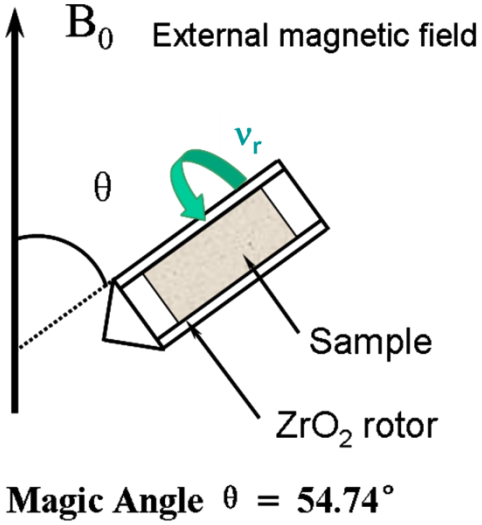

Figure 1.9. Schematic representation of the Magic Angle Spinning (MAS) technique, where θ is the angle between the rotor and the external magnetic field and νr is the spinning speed frequency.

1.4.1.2. Solid State NMR Pulse Techniques

The simplest and most generally used technique is One Pulse MAS NMR. Besides that there are many different pulse sequences which provide specific information or improve the quality of the NMR spectrum. Some of these used in this research are summarized below.

One Pulse Sequence: The one pulse sequence causes the bulk magnetization to deviate from the z axis by a certain phase angle, θ. The transverse magnetization is then recorded and transformed into a NMR spectrum via Fourier transform (Figure 1.10.a).

Heteronuclear Decoupling One Pulse Sequence: This is used to improve the signal resolution when the broadening due to the interactions between the dipole moments of two or more different nuclei is too large to be removed by MAS. A simple one pulse sequence is applied to one of the nuclei. The second nucleus is irradiated at its Larmor frequency, modulating its spin state and averaging the effect of its dipole moment, while the signal is detected for the first nucleus (Figure 1.10.b).

Spin-Echo Sequence: Spectra that contain broad resonances can suffer from artifacts and distortions caused during the first few microseconds of instrumental dead time at the beginning of the Free Induction Decay (FID). This will be particularly severe if the FID decays fast. The larger the anisotropic interactions felt by the spin system, the faster the FID decays. A spin-echo pulse sequence is used to remove artifacts and distortions. The sequence begins with a $\pi/2$ pulse bringing the magnetization from the z axis to the xy plane. After a time τ, a π pulse is applied which causes the dephasing spin system to refocus. Then after a second time interval, τ again, the transverse magnetization is measured and converted into an NMR spectrum. Figure 1.10.c shows the spin-echo pulse sequence.

Cross Polarization Pulse Sequence: In systems containing two nuclei, one of which has more abundant spins, the magnetization can be transferred from the more abundant spin (I) to the less abundant one (S) by irradiating both nuclei at their correct Larmor frequencies. Providing the Hartman-Hahn condition which is $\gamma_I B_I = \gamma_S B_S$ where B_I and B_s is the strength of the rf field applied on the I and S spin, respectively, is met, the net magnetization of the S spin is increased. Structural information can be obtained, because

the route of transfer of magnetization between I and S spins depends on their spatial proximity (Figure 1.10.d).

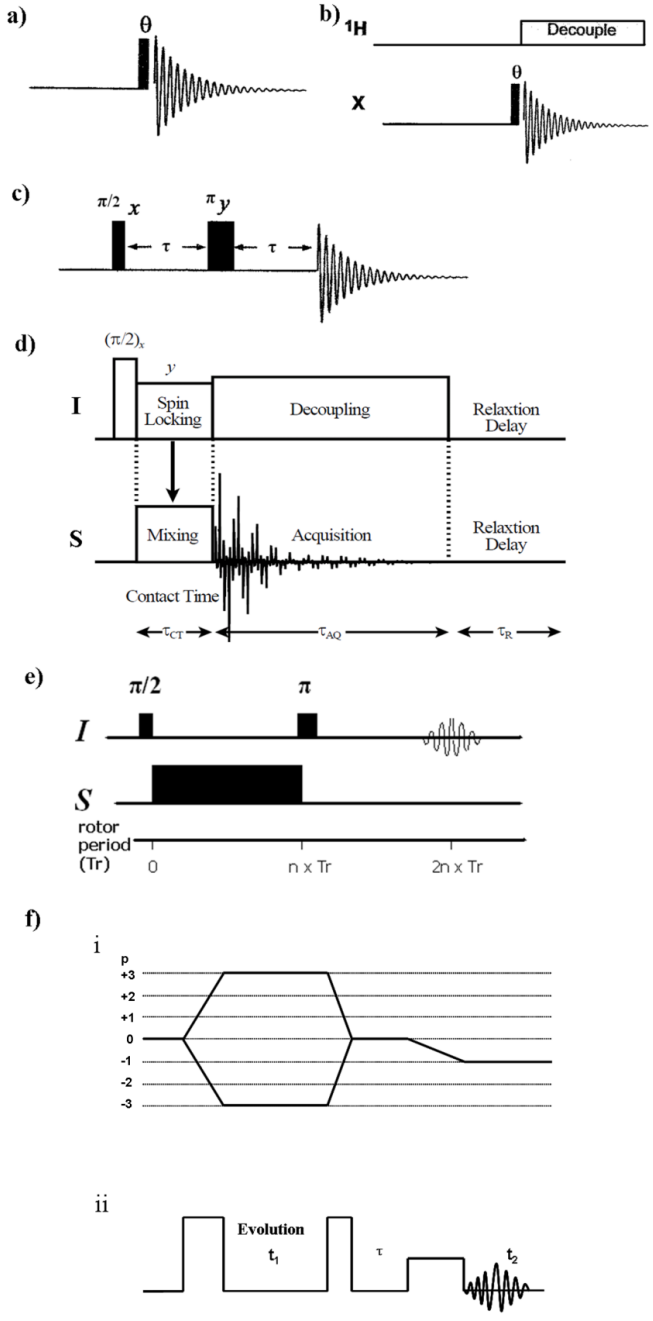

Figure 1.10. NMR Pulse Sequences a) One-Pulse b) Decoupled One-Pulse c) Spin-Echo d) Cross Polarization e) TRAPDOR and f) MQMAS Pulse Sequence (i, Coherence pathway for a 'z-filter' MQMAS NMR experiment ii, Pulse sequence for a 'z-filter' MQMAS NMR experiment).

TRAPDOR Sequence: TRAPDOR, Transfer of Populations In Double Resonance, is a pulse sequence which allows the heteronuclear dipole interactions to be measured[39]. The sequence includes a spin-echo experiment for a nucleus *I*, obtained with (double resonance) and without irradiation (control) of the nucleus *S* on a separate channel. During the rotor synchronized echo of the nucleus *I*, irradiation of *S* leads to rotationally induced level transitions. The population transfers between the S spin Zeeman levels alter the evolution of dipolar coupled I spin magnetization and prevent refocusing of its magnetization at the spin echo causing a TRAPDOR effect. The greater the dipolar coupling, the greater the dephasing of the *I* spin, and thus the greater the TRAPDOR effect[39]. The technique provides a very powerful tool in assigning linkages. If a TRAPDOR effect is observed, then the peak of the dipolar coupled species undergoes a decrease in intensity which can be checked from the difference spectra. The difference gives information about I and S linkages. Figure 1.10.e. shows the pulse sequence for the TRAPDOR experiment

The MQMAS Sequence: High resolution NMR spectra of half integer quadrupolar nuclei can be collected through the Multiple Quantum MAS (MQMAS) NMR technique[40]. With MQMAS, the second-order quadrupolar line broadening can be eliminated. The coherence pathway and pulse sequence of one of the most widely performed MQMAS experiments are shown in Figure 1.10.f. First, the MQ transition is excited by a single, high power rf-pulse, after which the MQ-coherence is allowed to evolve for a time t_1. After the evolution time, a second pulse is applied which converts the MQ coherence into a zero coherence. A z-filter soft pulse is then applied, which converts the zero coherence to SQ coherence that can be observed during t_2. The signal is then acquired and the echo will form at a time t_2. Both of the first two hard pulses are non-selective and will excite all coherences to a varying degree. Selection of the coherences of interest is done by appropriate phase cycling of the second pulse. In a MQMAS NMR spectrum of spin 5/2 nucleus[41], the isotropic chemical shift (δ_{CS}^{iso}) can be calculated using Equation 1.13. where δ_{G1}^{obs} and δ_{G2}^{obs} are the observed chemical shift of the center of gravity in isotropic dimension and in anisotropic dimension, respectively.

$$\delta^{iso}{}_{CS} = 10/27\ \delta^{obs}{}_{G2} + 17/27\ \delta^{obs}{}_{G1} \qquad [1.13]$$

Also the slices parallel to the anisotropic dimension can provide the 1D NMR spectrum for each individual site, from which C_Q, η, and can be obtained by fitting the lineshape of the resonances.

The HETCOR Sequence: An extension of the CP experiment can be performed in two dimensions which is generally referred to as HETeronuclear CORrelation (HETCOR) experiment. In this experiment, a second dimension is introduced by incrementing the t_2, shown in Figure 1.11. HETCOR experiments allow for a global perspective of the connectivities of two different nuclei and correlates the chemical shifts of the spin *I* with those of spin *S*, as shown in Figure 1.11.b. The distance probed can be experimentally defined by adjusting the contact time, as polarization between close nuclei is more efficient than between those separated by a longer distances.

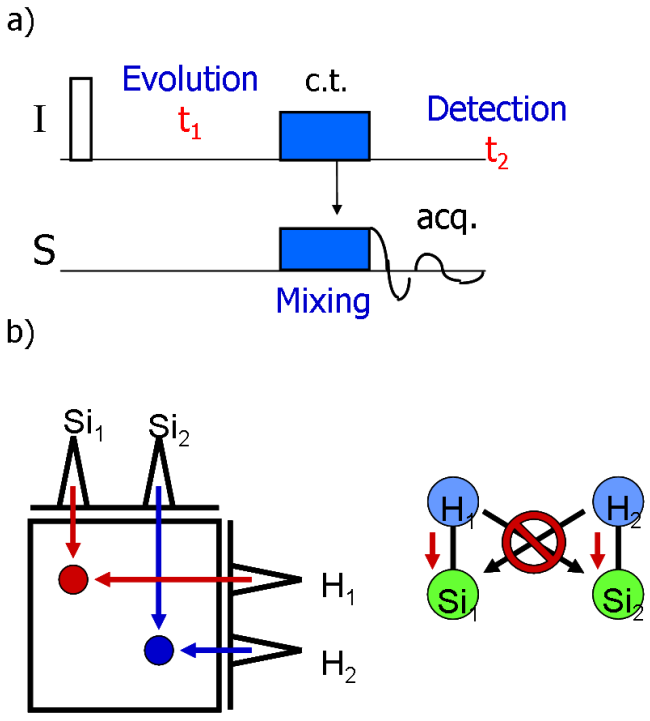

Figure 1.11. a) Diagram of the HETCOR experiment, b) illustration how the connectivities of two different nuclei can be studied.

1.4.1.3. NMR properties of the nuclei studied

^{29}Si MAS NMR: ^{29}Si has a spin I = ½ and a natural abundance of 4.7 %. It is not subject to quadrupolar peak broadening and distortion, so the dipole-dipole interactions and chemical shift anisotropy are the principle causes for peak broadening. ^{29}Si NMR spectroscopy provides direct information about the structure of zeolites from measurements of the isotropic chemical shifts, which are influenced most significantly by the coordination environment of the Si. Framework Si in zeolites are tetrahedrally coordinated and so there are five different possible environments of silicon atom. They are denoted as Si(nAl), where n (n≤4) signifies the number of aluminum atoms connected to silicon by oxygen. In general, substitution of each aluminum atom to the framework results in a shift towards low-field of 5 ppm[42,43]. Ranges of chemical shift for Si(nAl) building blocks are given in Figure 1.12. With the intensities of these five possible resonances, the Si/Al ratio can be calculated according to the "Lowenstein`s rule" (which stipulates that no Al-O-Al linkages can occur in the zeolite framework) with the following equation [44]:

$$\mathbf{Si / Al} = \sum_{x=0}^{4} I_{\mathrm{Si\,(OAl)x}} \Big/ \sum_{x=0}^{4} \mathbf{0.25} \times I_{\mathrm{Si\,(OAl)x}} \qquad [1.14]$$

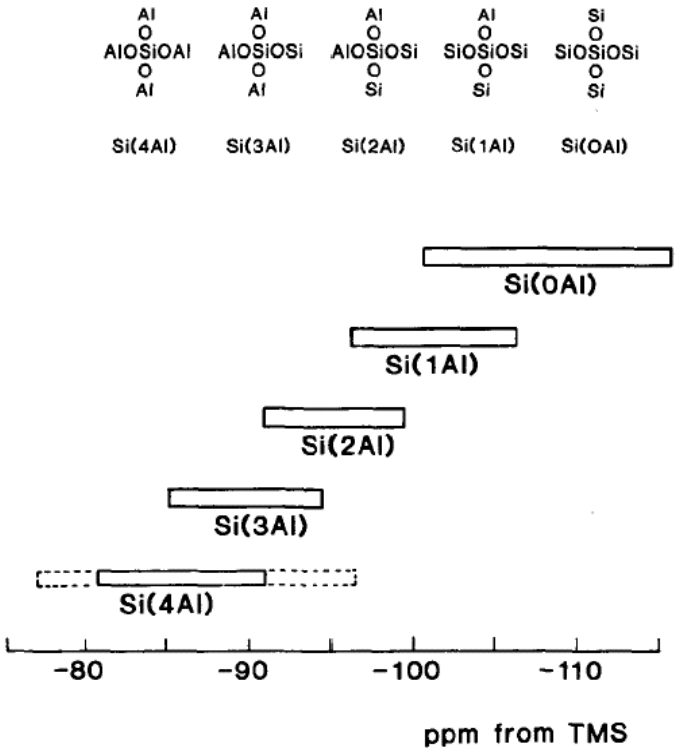

Figure 1.12. Possible environments for framework silicon tetrahedral and ^{29}Si NMR chemical shift ranges for Si(nAl) in pristine zeolites. Addition of each aluminum atom to silicon tetrahedral causes a shift of about 5 ppm to higher frequencies.

The ^{29}Si chemical shift values are directly related to the shielding of the ^{29}Si nucleus by the electronic structure of its immediate environment. Therefore, the chemical shift is influenced by the disposition and chemical nature of the adjacent atoms. In general, it is found that the chemical shifts become less negative with increasing Si-O bond length, decreasing T-O-T bond angle or with decreasing the electronegativity of the surrounding atom[43]. Therefore for the Si-N and Si-N-O compounds, the chemical shift ranges can be summarized as in Figure 1.13. According to the relevant literatures on nitrogen substituted mesoporous silicates[35,45], nitridated silicon environments have the following chemical shifts; $SiNO_3$ -90 ppm, SiN_2O_2 -72/-78 ppm, SiN_3O -63 ppm and SiN_4 -48 ppm. The terminal silicon nitrogen sites such $SiNH_2$ has a chemical shift of -43 ppm.

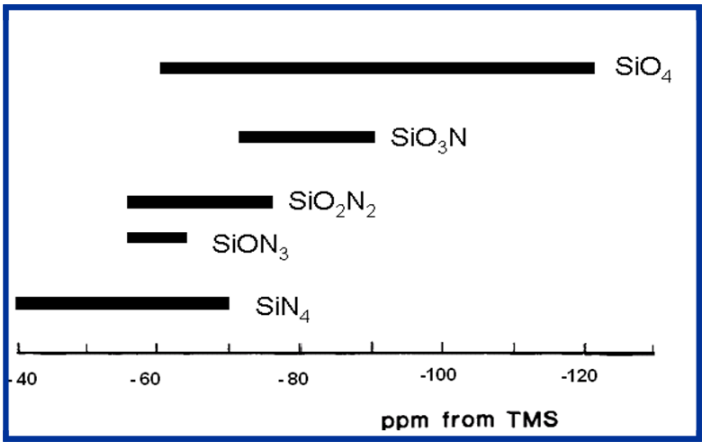

Figure 1.13. [29]Si MAS NMR chemical shift ranges for various Si-N units of silicon nitrides and silicon oxynitrides (adapted from reference 43). Substitution of each nitrogen atom to silicon tetrahedra causes a shift to higher frequencies.

[27]Al MAS NMR: [27]Al has a spin I= 5/2 and, thus, has a nuclear quadrupole moment arising from a non-spherical distribution of nuclear electrical charge that interacts with the electrical field gradients at the nucleus. Therefore, [27]Al MAS NMR studies of zeolites are always hindered by the large quadrupole coupling constants of the [27]Al nucleus. In [27]Al NMR, usually only the central transition is observed because the other allowed transitions are too broad and shifted too far from the resonance to be observed directly. An accurate value of the chemical shift can not be simply extracted as the isotropic shift is the sum of chemical shift and quadrupole induced shift. Spinning side bands can also occur as a result of quadrupole interactions which should be removed by spinning faster than the strength of the interaction, typically 10-12 kHz[43]. Despite these limitations [27]Al is a very favorable nucleus for NMR spectroscopy because of its high natural abundance (100%) and often quite fast relaxation times allowing good spectra to be acquired in very short experiment times. [27]Al spectra show distinct chemical shift ranges for tetrahedral, pentacoordinate and octahedral environments so aluminum framework and extraframework can be separated from each other. Aluminum tetrahedral framework atoms typically resonate at 60-50 ppm, whereas five and six coordinate extraframework species resonate at 25 to 30 and to 13 to -17 ppm, respectively [43].

[1]H MAS NMR: [1]H NMR is mainly used to investigate acidity and the defect sites in the zeolite framework, created during the synthesis, dehydration or catalytic reactions.

Although the H-H distances in dehydrated zeolites are relatively large and homonuclear interactions are not dominant, strong heteronuclear interactions and a narrow range of chemical shifts may cause problems. ^{1}H NMR chemical shifts for environments found in zeolites can be assigned as follows [6]; (a) 1.2 – 2.3 ppm, was ascribed to non hydrogen bonded (non-acidic) silanols on the surface of zeolite and the defect sites, (b) 1.2 – 3.6 ppm due to hydroxyl groups attached to extra-framework Al, (c) 3.0 – 5.0 ppm assigned as Bronsted acid sites, (d) 2.5 – 12 ppm due to hydrogen bonded silanols, (e) 4.6 – 5.0 ppm assigned as water, (f) 6.0 – 8.1 ppm due to (NH_4^+) and protonated amines.

^{14}N MAS NMR: ^{14}N is one of the few quadrupolar nuclei with an integer spin. It has a low γ with a natural abundance of 99.63 %. For half integer nuclei the central transition is unaffected by first-order quadrupole broadening but is broadened by the second order effects. Since ^{14}N has no ½ , -½ transition state all transitions suffer from both first and second order quadrupole broadening and it has a very large C_Q which results in NMR spectra that are typically beyond detection. The values for C_Q for ^{14}N compounds fall in the range of 0-8 MHz. C_Q value for protonated amine group in glycine is 1.18 MHz, while the C_Q for a NH group in N-acetyl-$_D$,L-valine is 3.2 MHz [43].

^{11}B MAS NMR: ^{11}B is a quadrupolar nucleus with a spin of 3/2 which can cause significant broadening of the NMR resonances of compounds with asymmetrical boron environments. However, the nucleus has a high natural abundance, and sensitivity and relatively fast relaxation delays, therefore, providing faster spectra. Boron containing compounds can typically contain tetrahedral BO_4 or trigonal BO_3 configurations. The former has a relatively narrow single resonance with δ_{iso} of 2 to -4 ppm and a C_Q of 0 to 0.5 MHz, whereas, the latter has larger C_Q around 2.5 MHz and δ_{iso} values ranging from 12 to 19 ppm[43].

1.4.2. Powder Diffraction and Rietveld Analysis

Since zeolites are crystalline powders, the simplest way to obtain structural information is the X-ray powder diffraction method. The position of the peaks, the relative intensities and width of the peaks and the background of X-ray diffraction data provides useful information about the zeolite structure. The peak positions in a powder

pattern are determined by the geometry of the unit cell. The relative intensities of the peaks are determined by the type and position of the various atoms within the unit cell and the widths of the peaks give an indication of the crystalline quality of the sample. They are dependent on the intrinsic instrumental peak width, crystalline size and the amount of stress or strain in the material. The background in a powder pattern indicates whether or not an amorphous phase/ material is present in the sample. The X-ray Powder Diffraction method is the simplest method to check the structural changes in modified zeolites. Changes in the relative intensities of the peaks confirm a structural modification, changes in the positions indicate that the unit cell has deformed. In general, non-framework species have a pronounced effect on the low angle region of the pattern. For example, a calcined material tends to have higher relative intensities in this region than the as synthesized or loaded sample[46]. The high angle region is usually less sensitive to presence or absence of electron density in the channels and cages and more sensitive to distortions of the framework.

Structure determination from powder diffraction is very important but can be complicated as the peaks get closer and begin to overlap with each other. The Rietveld method is a powerful method for determination of the average structure of a material including atomic positions and site occupancies. The full profile of the powder diffraction pattern can be refined based on a structural model. Initial estimates of the cell parameters, space group, as well as experimental parameters, such as wavelength should be known for the refinement process. The three important characteristics of the diffraction pattern that are modeled during Rietveld refinement are the position, intensity and profile (or shape) of each reflection[47]. Therefore, typically the background, scale factor, unit cell parameters and peak profiles are refined first. After the best possible fit is obtained from the starting model, structural parameters such as atomic coordinated, occupancies and motion, all of which affect the intensity of the diffracted peaks can be refined. During the refinement all parameters are continually varied until the best possible fit is obtained between the calculated and experimental patterns.

1.4.3. Pair Distribution Function (PDF) Analysis

Pair Distribution Function (PDF) analysis was initially used for analysis of glasses, liquids and disordered solids. In the last decade, application to systems with greater crystallinity has become possible due to several advances in experimental measurements. PDF is a total scattering technique where both Bragg and Diffuse scatterings are treated. Data from throughout the reciprocal space over a wide range of Q (scattering vector) values are utilized and the Fourier analysis of the total scattering data is known as the atomic pair distribution function (PDF) analysis. Since the total scattering pattern is used, the PDF is sensitive to chemical short range order, giving the probability of finding an atom at a given distance r from another atom. In other words, it can be understood as a bond length distribution.

PDF is obtained from the powder diffraction data via a sine Fourier transform of the normalized scattering intensity (function) $S(Q)$:

$$\begin{aligned} G(r) &= 4\pi r[\rho(r) - \rho_0] \\ &= \frac{2}{\pi}\int_0^\infty Q[S(Q) - 1]\sin(Qr)\,\mathrm{d}Q \end{aligned} \qquad [1.15]$$

where $\rho(r)$ is the microscopic pair density, ρ_0 is the average number density and Q is the magnitude of the scattering vector. For elastic scattering $Q = 4\pi \sin(\theta)/\lambda$ with 2θ being the scattering angle and λ is the wavelength of the radiation used. The resolution obtained in the $G(r)$ is dependent on the volume or reciprocal space measured. Therefore, $S(Q)$ must be measured to a high value of Q.

PDF has recently been used in limited applications to study modified mesoporous silica and zeolites with metal clusters. As mentioned in the previous sections on characterization techniques, detailed structural and atomic information for zeolites and mesoporous silica is usually obtained from X-ray Diffraction and Solid State NMR analysis. In these studies, PDF has been used to study the disordered zeolite structures and nature of the metal clusters present in the mesoporous system [48-51]. Martinez- Inesta

et al. studied the disordered zeolite beta by PDF analysis and showed that the PDF method is a viable technique to analyze the local structure of disordered zeolites (Figure 1.14).

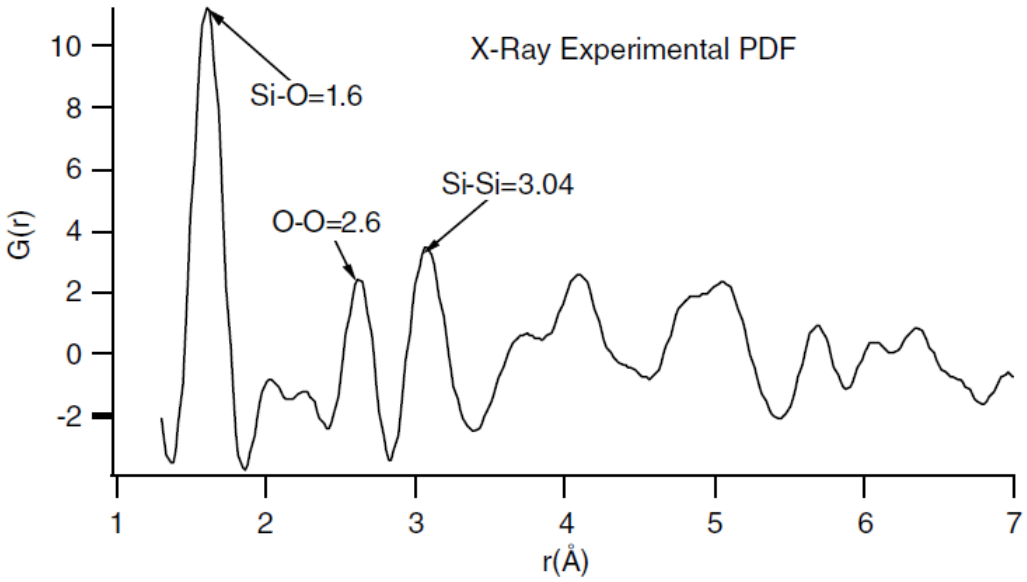

Figure 1.14. Pair distribution function of zeolite beta. Si-O, O-O and Si-Si bond distances are shown by the arrows.

1.5. Probing the basicity of zeolites

As briefly discussed in the previous sections, in pristine zeolites the basicity is ascribed to the framework oxygen atom that bridges the silicon and aluminum tetrahedra and the basicity increases with the number of aluminum atoms in the lattice and as the size of the exchangeable cation increases. Studying the basicity of zeolites requires understanding the roles of these two sites by using catalytic test reactions or with probe molecules that are used to investigate the basicity of the material.

Several methods, both theoretical and experimental, have been developed to measure the basicity of zeolites as well as a methodology based on the catalyst activity using reactants of different acidity[52-55]. The theoretical Sanderson electronegativity equalization method has been used to get average values of the negative charge over oxygen atoms that are based on the zeolite chemical composition where as the effect of

the crystalline structure has been quantified by electronegativity equalization method[56,57]. The DFT calculations performed have been mostly on methylation of bridging oxygen and disproportionation of N_2O_4 on basic zeolites to study the role of metal cations and bridging oxygens on basicity[54,55].

The experimental methods for studying the basicity of zeolites are either with use of catalytic test reactions or based on the use of probe molecules and studying their interaction with zeolite basic sites via an instrumental technique such as infrared (IR) or NMR spectroscopy which are based on the shifts in the data for the probe molecules[52,53,58]. Among the tested molecules, chloroform and, above all, pyrrole have been the subject of several publications[52,53]. The most used method to characterize zeolite basicity uses pyrrole as an IR probe molecule and is based on the shift to lower frequencies of the pyrrole N–H stretching band when the framework basicity increases Pyrrole is an amphoteric molecule which can interact with zeolite basic sites forming hydrogen bonds between the N–H group and framework oxygen atoms, and with cationic acid sites by donation of charge from its aromatic five-membered heterocycle. Hydrogen bonding is clearly shown by the shift of the IR N–H stretching frequency.

NMR is also commonly used to study the probe molecules interacting basic zeolites. The N-H and C-H groups of pyrrole and chloroform, respectively, form hydrogen bonds with framework oxygen atoms producing a displacement to low fields of the ^{1}H NMR resonances in an extent which depends on the zeolite basicity. For other chlorocarbons such as $CHCF_2Cl$, the shift in the ^{1}H MAS NMR resonance provides clear evidence for hydrogen bonding to basic zeolite framework sites. ^{13}C NMR has also been used to study the methoxy groups formed on reaction of a halocarbon or methanol with the zeolite framework, providing alternative method for investigating the basicity of the different zeolite framework.

Another probe molecule introduced by Liu *et al.* was boric acid trimethly ester (BATE)[59]. The group studied the different basic sites of zeolite Y by using BATE as an adsorption probe detected by IR spectroscopy. BATE is a typical Lewis acid with planar geometry, strong interaction with surface oxygen anions converts its planar structure into a pyramidal one. This makes it possible to study the changes in the symmetry of the

molecule due to the interactions with the basic sites in zeolites, by ^{11}B MAS NMR. In this study I will use BATE to investigate the basic properties of nitrogen substituted zeolites.

1.6. Objectives and Outline

The objective of this work is to synthesize nitrogen substituted zeolites with good crystallinity and porosity, investigate the changes in local structure and crystallinity of the treated material and study the substitution reaction mechanism. The overall methodology used on this dissertation is summarized in Figure 1.15. The outlines for the following chapters in the thesis are as follows;

- Chapter 2 contains the discussion on the optimization of the reaction conditions and the effect of composition of the starting material on nitrogen substitution reaction.
- In Chapter 3 I will be discussing the ^{29}Si MAS NMR data of nitrogen substituted zeolite Y with varying aluminum content and cation form which are prepared at different reaction conditions as well as Pair Distribution Function (PDF) Analysis of the treated zeolites .
- Chapter 4 will contain ^{27} Al MAS data of the same treated zeolites discussed in chapter three.
- In Chapter 5, we will be focusing on the basic properties of nitrogen substituted zeolites by using probe molecules and solid state MAS NMR.

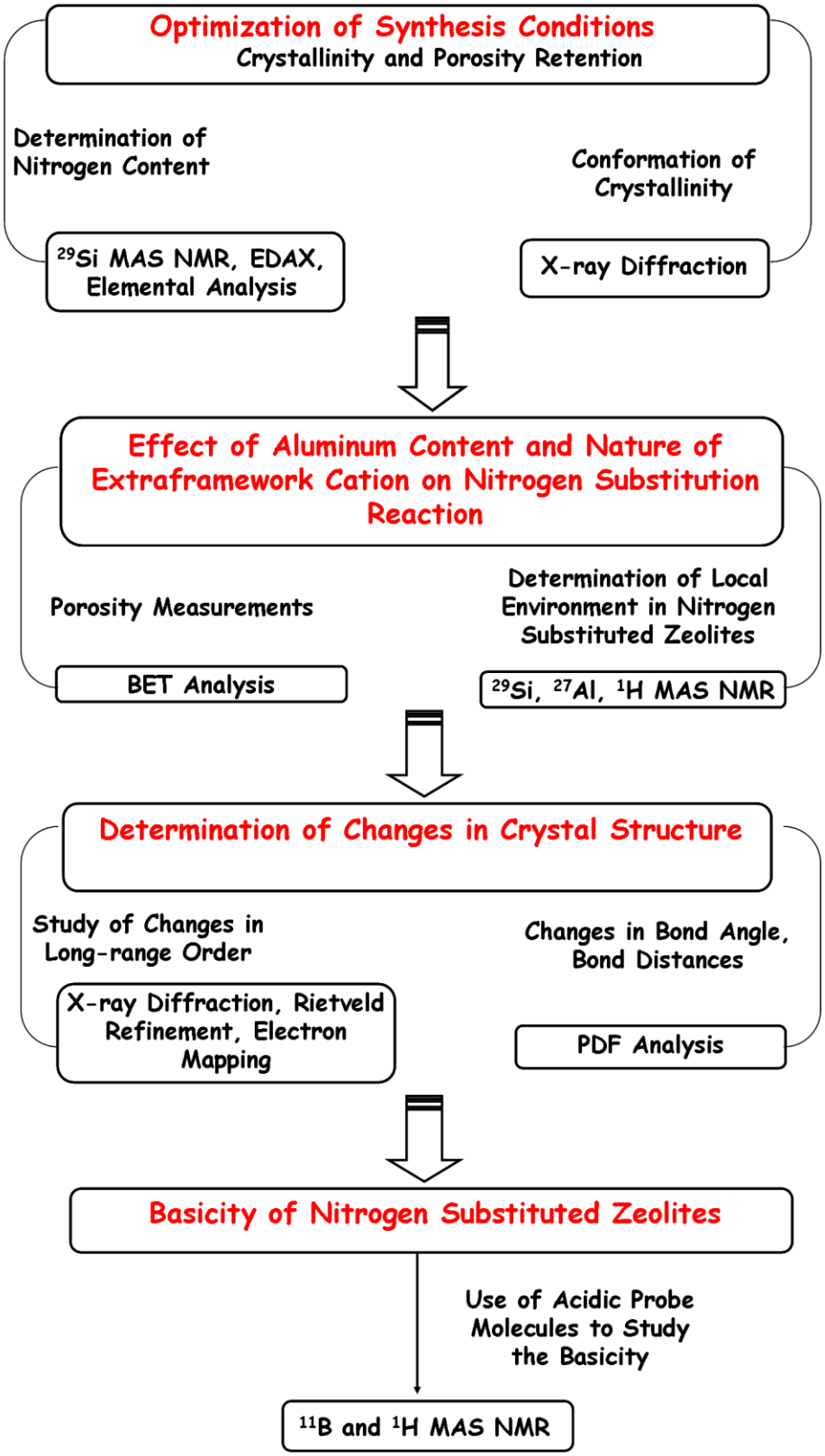

Figure 1.15. Summary of the experimental methodology used in this thesis to study the nitrogen substituted zeolites.

1.7. References

(1) Weitkamp, J.; Hunger, M.; Rymsa, U. *Microporous and Mesoporous Materials* **2001**, *48*, 255.

(2) Zhang, X.; Lai, E. S. M.; Martin-Aranda, R.; Yeung, K. L. *Appl. Catal., A* **2004**, *261*, 109.

(3) Han, A.-J.; He, H.-Y.; Guo, J.; Yu, H.; Huang, Y.-F.; Long, Y.-C. *Microporous Mesoporous Mater.* **2005**, *79*, 177.

(4) Xiong, J.; Ding, Y.; Zhu, H.; Yan, L.; Liu, X.; Lin, L. *J. Phys. Chem. B* **2003**, *107*, 1366.

(5) Astala, R.; Auerbach, S. M. *J. Am. Chem. Soc.* **2004**, *126*, 1843.

(6) S. M. Auerbach, K. A. C., P. K. Dutta *Handbook of Zeolite Science and Technology*; Marcel Dekker Inc., 2003.

(7) Wan, K.; Liu, Q.; Zhang, C. M.; Wang, J. C. *Bulletin of the Chemical Society of Japan* **2004**, *77*, 1409.

(8) Weitkamp, J. *Solid State Ionics* **2000**, *131*, 175.

(9) D.H., O. *Atlas of Zeolite Framework Types*; Elsevier, 2001.

(10) D.W., B. *Zeolite Molecular Sieves:Structure, Chemistry, and Use*; John Wiley&Sons,Inc., 1974.

(11) Lohse, U.; Altrichter, B.; Fricke, R.; Pilz, W.; Schreier, E.; Garkisch, C.; Jancke, K. *Journal of the Chemical Society-Faraday Transactions* **1997**, *93*, 505.

(12) Beck, J. S.; Vartuli, J. C.; Roth, W. J.; Leonowicz, M. E.; Kresge, C. T.; Schmitt, K. D.; Chu, C. T. W.; Olson, D. H.; Sheppard, E. W.; McCullen, S. B.; Higgins, J. B.; Schlenker, J. L. *Journal of the American Chemical Society* **1992**, *114*, 10834.

(13) Hu, W.; Luo, Q.; Su, Y. C.; Chen, L.; Yue, Y.; Ye, C. H.; Deng, F. *Microporous and Mesoporous Materials* **2006**, *92*, 22.

(14) Zhao, X. S.; Lu, G. Q.; Hu, X. *Microporous and Mesoporous Materials* **2000**, *41*, 37.

(15) Jentys, A.; Pham, N. H.; Vinek, H. *Journal of the Chemical Society-Faraday Transactions* **1996**, *92*, 3287.

(16) Shi, L.; Zou, Y.; He, H. Y. *Chemistry Letters* **2001**, 1164.

(17) Wouters, B. H.; Chen, T. H.; Dewilde, M.; Grobet, P. J. *Microporous and Mesoporous Materials* **2001**, *44*, 453.

(18) A. Auroux, A. B., E. Brunner, F. Fajula, E. Garrone, A. Jentys, J. A. Lercher, H. Pfeifer *Acidity and Basicity*; Springer: Heidelberg, 2008; Vol. 6.

(19) Barthomeuf, D. *Microporous Mesoporous Mater.* **2003**, *66*, 1.

(20) Ernst, S.; Hartmann, M.; Sauerbeck, S.; Bongers, T. *Appl. Catal., A* **2000**, *200*, 117.

(21) Suppes, G. J.; Dasari, M. A.; Doskocil, E. J.; Mankidy, P. J.; Goff, M. J. *Applied Catalysis a-General* **2004**, *257*, 213.

(22) Chheda, J. N.; Dumesic, J. A. *Catalysis Today* **2007**, *123*, 59.

(23) van Bokhoven, J. A.; van der Eerden, A. M. J.; Koningsberger, D. C. *Journal of the American Chemical Society* **2003**, *125*, 7435.

(24) van Bokhoven, J. A.; Koningsberger, D. C.; Kunkeler, P.; van Bekkum, H.; Kentgens, A. P. M. *J. Am. Chem. Soc.* **2000**, *122*, 12842.

(25) Jiao, J.; Ray, S. S.; Wang, W.; Weitkamp, J.; Hunger, M. *Z. Anorg. Allg. Chem.* **2005**, *631*, 484.

(26) Jiao, J.; Altwasser, S.; Wang, W.; Weitkamp, J.; Hunger, M. *J. Phys. Chem. B* **2004**, *108*, 14305.

(27) Hattori, H. *Chemical Reviews* **1995**, *95*, 537.

(28) Weitkamp, J.; Hunger, M.; Rymsa, U. *Microporous Mesoporous Mater.* **2001**, *48*, 255.

(29) Zhang, X. F.; Lai, E. S. M.; Martin-Aranda, R.; Yeung, K. L. *Applied Catalysis a-General* **2004**, *261*, 109.

(30) Climent, M. J.; Corma, A.; Fornes, V.; Frau, A.; GuilLopez, R.; Iborra, S.; Primo, J. *Journal of Catalysis* **1996**, *163*, 392.

(31) Wiame, H. M.; Cellier, C. M.; Grange, P. *Journal of Physical Chemistry B* **2000**, *104*, 591.

(32) Xia, Y.; Mokaya, R. *J. Phys. Chem. C* **2008**, *112*, 1455.

(33) El Haskouri, J.; Cabrera, S.; Sapina, F.; Latorre, J.; Guillem, C.; Beltran-Porter, A.; Beltran-Porter, D.; Marcos, M. D.; Amoros, P. *Advanced Materials* **2001**, *13*, 192.

(34) Xiong, J. M.; Ding, Y. J.; Zhu, H. J.; Yan, L.; Liu, X. M.; Lin, L. W. *Journal of Physical Chemistry B* **2003**, *107*, 1366.

(35) Zhang, C.; Liu, Q.; Xu, Z. *J. Non-Cryst. Solids* **2005**, *351*, 1377.

(36) Narasimharao, K.; Hartmann, M.; Thiel, H. H.; Ernst, S. *Microporous and Mesoporous Materials* **2006**, *90*, 377.

(37) Zhang, C.; Xu, Z.; Wan, K.; Liu, Q. *Appl. Catal., A* **2004**, *258*, 55.

(38) Chino, N.; Okubo, T. *Microporous Mesoporous Mater.* **2005**, *87*, 15.

(39) Grey, C. P.; Vega, A. J. *Journal of the American Chemical Society* **1995**, *117*, 8232.

(40) Iuga, D.; Morais, C.; Gan, Z. H.; Neuville, D. R.; Cormier, L.; Massiot, D. *Journal of the American Chemical Soceity* **2005**, *127*, 11540.

(41) Millot, Y.; Man, P. P. *Solid State Nuclear Magnetic Resonance* **2002**, *21*, 21.

(42) Klinowski, J. *Annual Review of Materials Science* **1988**, *18*, 189.

(43) Mackenzie, K. J. D.; Smith, M. E. *Multinuclear Solid-State NMR of Inorganic Materials*; Pergamon Material Series, 2002; Vol. 6.

(44) Loewenstein, W. *Am. Mineral.* **1954**, *39*, 92.

(45) Zhang, C.; Xu, Z.; Liu, Q. *J. Wuhan Univ. Technol., Mater. Sci. Ed.* **2005**, *20*, 32.

(46) Ciraolo, M. F.; Hanson, J. C.; Grey, C. P. *Microporous Mesoporous Mater.* **2001**, *49*, 111.

(47) Young, R. A. *Int. Union Crystallogr. Monogr. Crystallogr.* **1993**, *5*, 1.

(48) Abeykoon, A. M. M.; Donner, W.; Brunelli, M.; Castro-Colin, M.; Jacobson, A. J.; Moss, S. C. *J Am Chem Soc* **2009**, *131*, 13230.

(49) Narkhede, V. V.; Gies, H. *Chemistry of Materials* **2009**, *21*, 4339.

(50) Martinez-Inesta, M. M.; Peral, I.; Proffen, T.; Lobo, R. F. *Microporous and Mesoporous Materials* **2005**, *77*, 55.

(51) Martinez-Inesta, M. A. M.; Lobo, R. F. *Journal of Physical Chemistry C* **2007**, *111*, 8573.

(52) Sanchez-Sanchez, M.; Blasco, T. *Chemical Communications* **2000**, 491.

(53) Sanchez-Sanchez, M.; Blasco, T.; Corma, A. *J. Phys. Chem. C* **2008**, *112*, 16961.

(54) Mignon, P.; Geerlings, P.; Schoonheydt, R. *Journal of Physical Chemistry B* **2006**, *110*, 24947.

(55) Mignon, P.; Pidko, E. A.; Van Santen, R. A.; Geerlings, P.; Schoonheydt, R. A. *Chemistry-a European Journal* **2008**, *14*, 5168.

(56) Sanderson, R. T. *Journal of the American Chemical Society* **1983**, *105*, 2259.

(57) Varekova, R. S.; Jirouskova, Z.; Vanek, J.; Suchomel, S.; Koca, J. *International Journal of Molecular Sciences* **2007**, *8*, 572.

(58) Yang, C.; Wang, J.; Xu, Q. H. *Microporous Materials* **1997**, *11*, 261.

(59) Liu, J.; Ying, P. L.; Xin, Q.; Li, C. *Zeolites* **1997**, *19*, 197.

Chapter 2

Optimization of Nitrogen Substitution Reaction: Synthesis of Mesoporous Oxynitrides and Nitrogen-Substituted Zeolites

Abstract

We examine the effect of synthesis conditions and the nature of starting material on the degree of nitrogen substitution, retention of crystallinity and microporosity during ammonia treatment of mesoporous silicates and zeolites. The objective is to find a reproducible optimal synthesis protocol to prepare nitrogen substituted zeolites and mesoporous materials and choose the optimum structure as starting material for higher nitrogen substitution efficiency yet higher crytsallinity and porosity. We have investigated the effects of several synthesis parameters using different synthesis protocols. The most important parameter in the synthesis is the ammonia flow rate; which should be kept as high as possible. Higher reaction temperatures and times also give higher nitrogen substitution level, however, can result in decrease in crystallinity and porosity. The presence of nitrogen and substitution level in the treated materials is investigated by ^{29}Si MAS NMR spectroscopy and the changes in the crystallinity of the treated materials are studied by X-ray Diffraction.

2.1. Introduction

Nitrogen- substituted zeolites, amorphous silicates, and aluminophosphates are typically prepared by high-temperature treatment of the parent compound with ammonia or another amine. Ammonia is by far the most common because of cost and safety concerns, but other alkyl amines such as methyl amine and ethyl amine have been used[1-3]. However, it is extraordinarily difficult to synthesize zeolites and mesoporous silicates with nitrogen substitutions without significant damage to the framework structure, and published syntheses tend to be difficult to reproduce. Much of this can be attributed to the vast array of synthesis conditions employed in different laboratories throughout the world and the lack of thorough understanding of the sensitivity of the substitution reaction to those conditions. The temperature treatment conditions used in the literature vary from as low as 200^{o}C using alkylamines[1,2] to as high as 1100^{o}C using ammonia[3,4]. Flow rates are similarly varied: from static conditions (for alkylamines) to flow rates of tens[5-7], hundreds[3], or even thousands[4] of cubic centimeters per minute. Many of these syntheses are unlikely to produce nitrogen-substituted materials that are structurally similar to their parent materials. In most cases, any method employing a temperature of less than 500^{o}C, regardless of the aminating agent, is unlikely to produce substitution because of the strength of the Si-O bond compared to that of the Si-N bond. Batch (non flow) processes are unlikely to be able to remove water produced by the reaction, as are processes employing low mean fluid velocities.

The changes in the crystal structure and order of the synthesized materials are characterized by X-ray Diffraction methods. The local structure of both pristine and treated mesoporous silicas and zeolites is studied with ^{29}Si MAS NMR because of its resolving power and ability to show clearly the nature of the silicon environments in the pristine material and also the changes in the local environment after nitrogen substitution reaction. As briefly summarized in the first chapter section 1.4.1.3, the ^{29}Si chemical shifts of the Si-O units are sensitive to the coordination number and systematic variations of tetrahedral Si chemical shifts can be used for identification of different silicate species[8]. Silicate structures may be regarded as built up of tetrahedral units with varying degrees of polymerization. These can be described in terms of a “Q” notation where Q denotes a

silicon bonded to four oxygen atoms. A superscript n, where n=0 to 4 is used to indicate the number of other Q units attached to the unit in question. Thus, Q^0 denotes silicon bonded through oxygen to no other network-forming elements where as Q^4 denotes a silicon bonded through oxygen to four other silicons (Figure 2.1). The ^{29}Si chemical shift becomes increasingly negative with each additional Si-O-Si linkage, due to increased electronic shielding of central Si. Q^0 units in monosilicates have typical shifts of about -65 ppm, changing in steps of about 10 ppm for each additional bonded Si tetrahedra up to about -110 ppm for the SiQ^4 units.

This chapter covers the experimental methodology to obtain a reproducible and effective synthesis method for nitrogen substitution of zeolities and mesoporous silicates. Nitrogen substitution reaction is initially tested on mesoporous silicates having different silicon site defects and then performed on zeolites with different aluminum content and extraframework cations. With this protocol we test the effect of crystal structure and the elemental composition of the parent compound on nitrogen substitution efficiency. The effects of several treatment parameters, such as reaction temperature, reaction time, ammonia flow rate on the crystallinity, microporosity, and level of substitution ammonia treated materials are also studied in order to find the optimum conditions for reproducible results.

The detail comparison of the Si/Al ratio and the presence of protons versus sodiums (as extraframework cations) will be discussed in the following chapter with a detail discussion on their ^{29}Si MAS NMR data with complementary methods X-ray Diffraction, Pair Distribution Function (PDF), Energy-Dispersive X-ray spectroscopy (EDX) Analysis and BET surface area analysis methods.

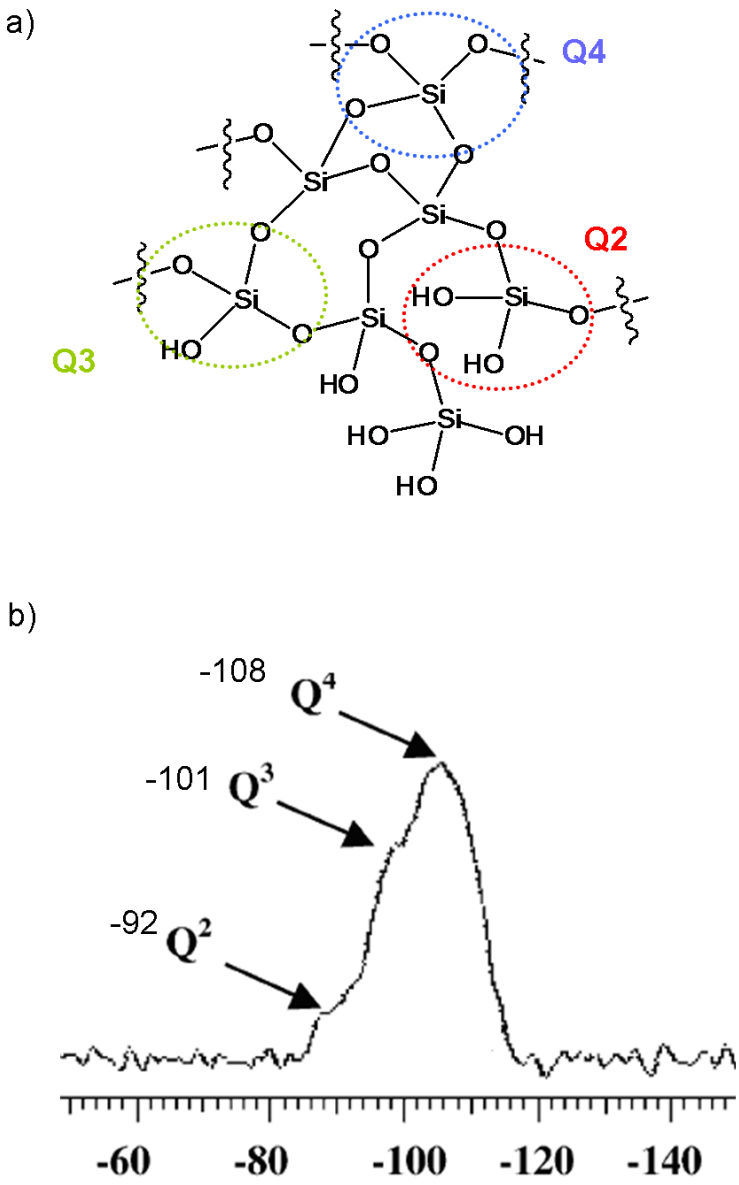

Figure 2.1. a) Possible silicon environments in mesoporous silicates, Q^4 denotes a silicon bonded through oxygen to four other silicons, Q^3 and Q^2 has one and two terminal OH groups, respectively b) ^{29}Si NMR chemical shifts of different silicon sites, addition of each terminal OH group to silicon tetrahedral results in a shift of ~ 10 ppm to higher frequency in ^{29}Si NMR.

2.2. Experimental

2.2.1. Materials

The ammonia treatment reaction was first applied and tested on mesoporous MCM-41 and SBA-15. The optimization of the reaction conditions and detailed characterization studies were then studied with zeolite Y. The siliceous MCM-41 sample was synthesized using tetraethyl orthosilicate (TEOS, Aldrich), sodium hydroxide (Aldrich), cetyltrimethlyammonium bromide (CTAB, Aldrich) and deionized water according to the following procedure[9]. First, CTAB template was dissolved in sodium hydroxide solution under stirring and then TEOS was added slowly under stirring. The mixture was transferred into autoclave and heated at 150^{o}C for 48 hours. The material was recovered by filtration and the template was removed by heating in nitrogen to 550^{o}C for 1 hour and then heating in air for 6 hours. Mesoporous SBA-15 was synthesized as follows[10]; Pluronics (P123, PEO20PPO70PEO20, from BASF) was dissolved in a misture of water and HCl at 40^{o}C. Then, TEOS was slowly added under stirring and the mixture was maintained at 40^{o}C, still stirring. The solution containing the precipitate was then aged at 90^{o}C for 2 days. The product was filtered, dried in an oven for 1 day at 100^{o}C and calcined in air at 500^{o}C for 10 hours. For zeolite precursors, commercial NH_4Y, Si/Al = 6 (CBV 712), zeolite H-beta with Si/Al ratio of 180 (CP811C-300) and zeolite NH_4 beta, Si/Al= 19 (CP814C) from Zeolyst were used as starting materials. The Si/Al values quoted here are provided by the manufacturer, and represent the overall Si/Al ratio, not necessarily the Si/Al ratio of the framework.

2.2.2. Experimental Set Up

Samples to be substituted with nitrogen were treated by flowing anhydrous ammonia at high temperatures in a fused quartz tube within a tube furnace. The anhydrous ammonia was further dried at room temperature with a glass moisture trap which uses calcium sulfate at room temperature to remove all traces of water. The desiccant was changed and regenerated after each run. The actual temperature at the

sample was measured with a thermocouple which was placed with the sample placed in a quartz boat. Nitrogen substitution reaction was achieved as follows. Approximately 0.3 g of material was placed in a quartz boat, packed loosely and as a thin surface covering the alumina boat so as to allow rapid removal of water produced by the reaction. This boat was placed in a tube furnace with flowing nitrogen gas and heated at 0.2°C per minute to 110°C. This temperature was held for 2 h, and the furnace was then heated at 0.5°C per minute to 400°C. That temperature was held for 8 h to ensure the zeolite pores were devoid of water, which is important both to prevent dealumination before ammonia is added and to drive the reaction forward after ammonia is added, as the ammonia addition reaction is highly endothermic. The furnace was then heated at 1.5°C per minute to the reaction temperature of 550-850°C. The gas was changed from nitrogen to ammonia either at the beginning of the ramp (500°C) or at the end of the ramp after the reaction temperature had been reached (RxnT). The oven was maintained at this temperature for 8-48 h, after which the flow gas was replaced again with nitrogen. The oven was then cooled to room temperature with a ramp of 5°C per minute. A diagram of the treatment steps is included in Figure 2.2.

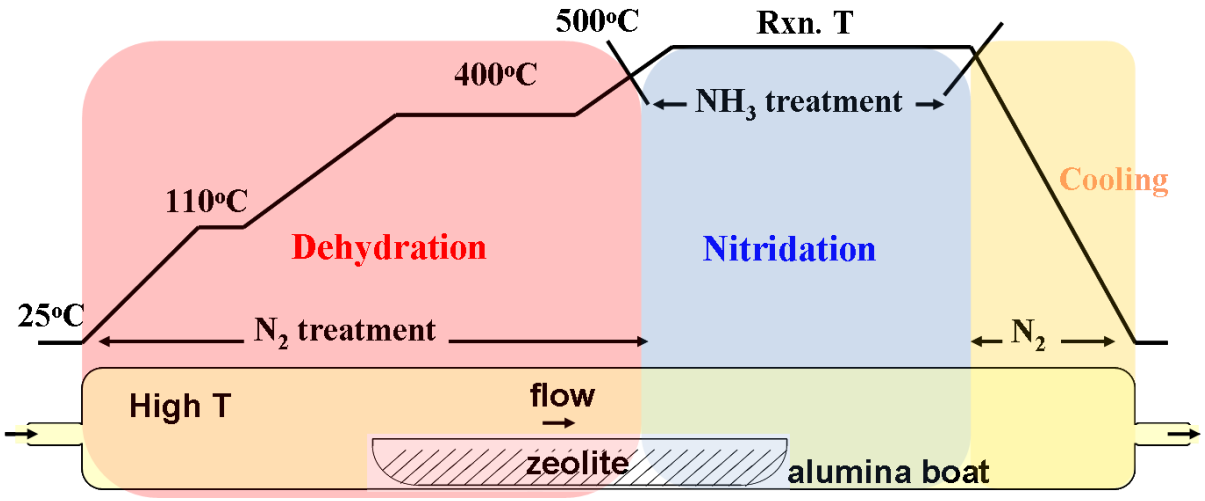

Figure 2.2. Treatment steps for nitrogen substitution reaction. The parent zeolite is first dehydrated in nitrogen environment, prior to ammonia flow. The ammonia flow starts at 500oC till the end of nitridation reaction. The sample is then cooled down slowly under nitrogen.

2.2.3. Characterization

The ^{29}Si MAS NMR analysis was performed on a Varian 360 MHz spectrometer with a 4 mm probe using 14 kHz MAS and a ^{29}Si 90° pulse of 4.5 μs. Pulse delay of 30 s was used for the ^{29}Si MAS NMR experiments and ^{29}Si chemical shift was referenced to tetramethylsilane (TMS) at 0 ppm. All the dehydrated/nitrided samples were packed into NMR rotors under dried nitrogen atmosphere in a glove box.

For the samples prepared and characterized at University of Massachusetts Amherst (UMASS), ^{29}Si MAS NMR spectra were collected using a Bruker DSX300 spectrometer with a 7.05 T magnet using a 4 mm probe. A spinning speed of 3 kHz, π/2 pulse length of 7 μs and a recycle delay of 30s was employed in all spectra. Chemical shifts are with respect to TMS at 0 ppm.

The chemical shift calculations and spectral fitting for ^{29}Si MAS NMR were performed by our collaborators at UMASS.

Powder X-ray diffraction patterns were collected on a Rigaku diffractometer using Cr K-α radiation (wavelength 0.229 nm).

2.3. Results and Discussion

2.3.1. Nitrogen Substitution of Mesoporous Silica: MCM-41 and SBA-15

The nitrogen substitution reaction was initially studied on mesoporous MCM-41 and SBA-15, as previous studies have shown that the crystalline zeolites do not react with ammonia easily as amorphous oxides and the substitution reaction starts with the defect sites in the structure[11]. The samples were treated at 1050^{o}C as the initial experiments with lower temperature treatment did not show any sign of nitrogen in the structure. Ammonia flow rate of 100cm^{3}/min was used for 8 hours of reaction time. The characterization of the treated material was performed by X-ray Diffraction and ^{29}Si MAS NMR.

The crystal structure of the as synthesized and nitrogen substituted materials were initially studied with X-ray Diffraction. Low-angle XRD is commonly used to investigate the ordering of mesoporous materials. The diffraction pattern of the synthesized untreated

MCM-41 exhibited three clear reflections namely (100), (110) and (200) reflection (Figure 2.2.) in agreement with previous studies. In the literature, these reflections have been reported as characteristic of a 2D hexagonal ordered structure for MCM-41 [12]. From the diffraction pattern of the ammonia treated sample it is found that the (100) reflection moves to higher 2θ values, showing a decrease in the d value (interatomic spacing) after nitridation at high temperature. The (110) and (200) reflections disappear with the reaction, a sign of a decrease in the structural ordering of MCM-41 after nitridation. The diffraction patterns of as synthesized SBA-15 show a hexagonally ordered structure similar to that of MCM-41. However, the reaction with NH_3 at 1050^oC causes a collapse of pore structure which results in a totally amorphous phase as shown in Figure 2.3.

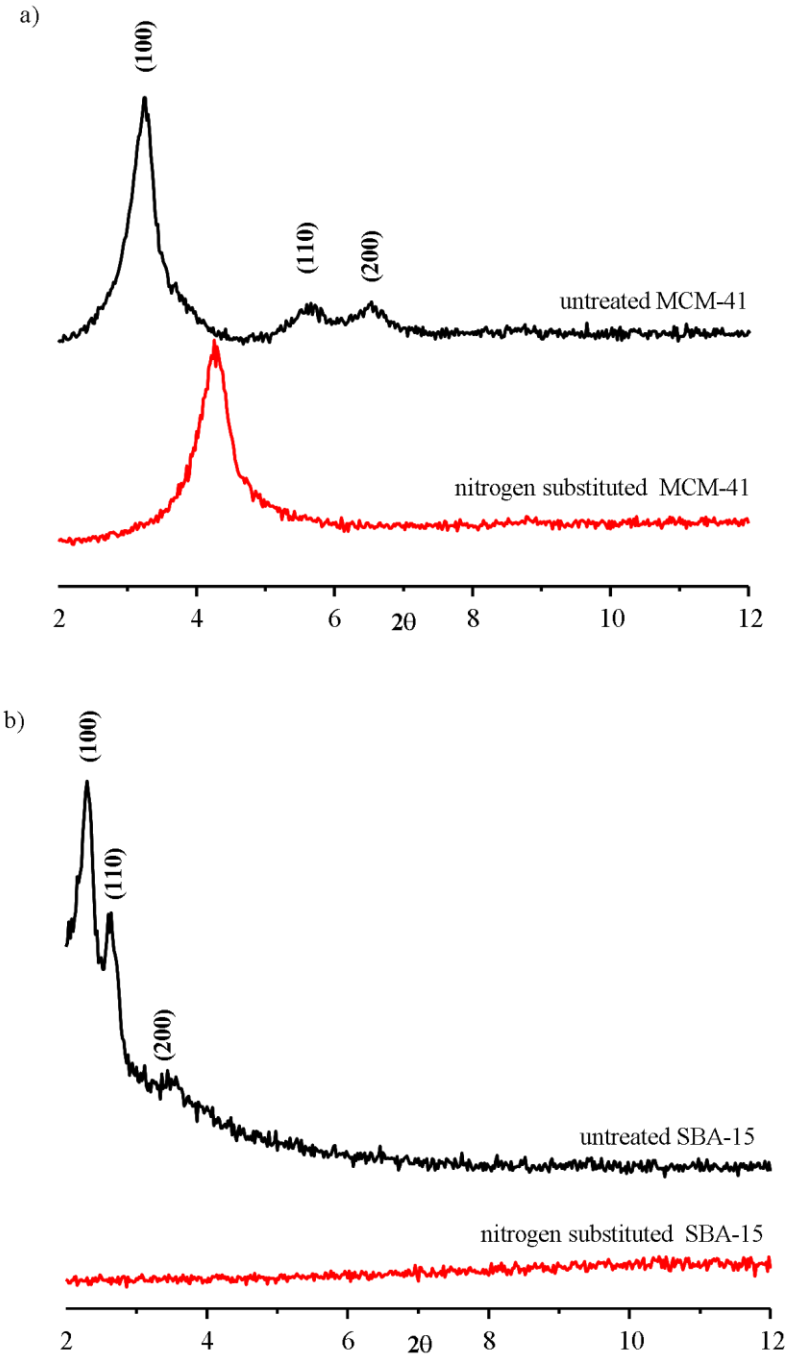

Figure 2.3. Comparison of XRD patterns (CrKα) for untreated and nitrogen substituted a) MCM-41 b) SBA-15. All the reflections are indexed. The nitrogen substitution reactions were performed at 1050^{o}C for 8 hours under ammonia flow.

The framework of pristine mesoporous MCM-41 includes surface silicon sites with varying OH groups in the silicon tetrahedra. Mesoporous MCM-41 is composed of

mostly Q^4, Q^3 and Q^2 silicon environments where as SBA-15 involves fewer defects sites and composed of mostly silicon Q^4 and Q^3 sites. As stated in the introduction part, the ^{29}Si NMR chemical shift values show a shift about 7 to 9 ppm shift to higher frequency as the number of OH groups increase (Figure 2.1).

According to the relevant literatures on MCM-41[9] nitrogen incorporated silicon environments have the following chemical shifts; $SiNO_3$ -90 ppm, SiN_2O_2 -72/-78 ppm, SiN_3O -63 ppm and SiN_4 -48 ppm. The terminal silicon nitrogen sites such as Si2NH and $SiNH_2$ have a chemical shift of -43 ppm.

Figure 2.4.a shows the ^{29}Si MAS NMR spectra of ammonia treated and non-treated MCM-41 and SBA-15. The NMR spectrum of the pristine MCM-41 indicates the presence of a large number of SiQ^3 groups with terminal silanols at around -99 ppm as well as SiQ^4 sites with a peak at around -109 ppm. After ammonia treatment, a number of Si(O,N) subunits with a variety of O:N ratio have formed. The ^{29}Si NMR data unambiguously confirm the changes in composition that accompany the nitridation process of the network of the MCM-41 sample. On the other hand, the reaction has clearly not gone to completion, because some SiOH, and SiQ^4 groups are still present. With the comparison of the changes in relative intensity of these two sites, it is clearly seen that the defect silanol groups been substituted by first, forming terminal $SiNH_2$ groups. As the reaction proceeds, nitrogen substitution within the framework silicon sites and increase in the nitrogen substitution degree takes place. Following ^{29}Si chemical shifts assignments in literature, the silicon peaks observed in ^{29}Si MAS NMR of nitridated MCM-41 can be tentatively assigned as follows; -109 and -99 ppm nitrogen free SiQ^4 and SiQ^3 sites, -89 ppm $SiNH_2$/SiNHSi, -65,-50, -45 ppm are 2N, 3N and 4N substituted silicon environments, respectively. As seen in the figure the silicon peaks for the treated MCM-41 are not well resolved suggesting the presence of different silicon sites and poor crystallinity which is also confirmed by X-ray Diffraction. Therefore it is not straight forward to assign the exact nature of the sites by single pulse ^{29}Si MAS NMR.

Figure 2.4.b shows ^{29}Si MAS NMR data for both pristine and ammonia treated SBA-15. It is seen that the nitrogen substitution reaction on mesoporous SBA-15 with the same reaction conditions as MCM-41 discussed above, was not achieved effectively. The ^{29}Si NMR spectra of the pristine material involves mostly the SiQ^4 peak with less defect

sites and SBA-15 in known to be hydrothermally more stable than MCM-15. However, as seen in X-ray diffraction data, the hexagonally ordered SBA-15 structure has completely collapsed resulting in a total amorphous material and the silicon sites are poorly nitrogen substituted resulting in a broad component spreading from -50 to -100 ppm in the ^{29}Si MAS NMR spectrum.

Ammonia treatment of mesoporous silicates did not show any nitrogen substitution under 1050^{o}C. The treatment at this temperature shows high nitrogen substitution for MCM-41 mesoporous silicate where as mesoporous SBA-15 was poorly nitridated. The framework of the two materials was affected by high temperature treatment which resulted in highly disordered as well as amorphous structure. The ^{29}Si NMR experiments performed on nitrogen substituted MCM-41 has given broad overlapping peaks as a sign of distribution of different silicon environments and disorder in the structure. The comparison of the ^{29}Si NMR data of pristine material with the nitridated material has shown that the nitrogen substitution reaction starts with the terminal silanol groups and the mesoprous silicate with more defect sites in the structure has higher nitrogen substitution degree in the framework.

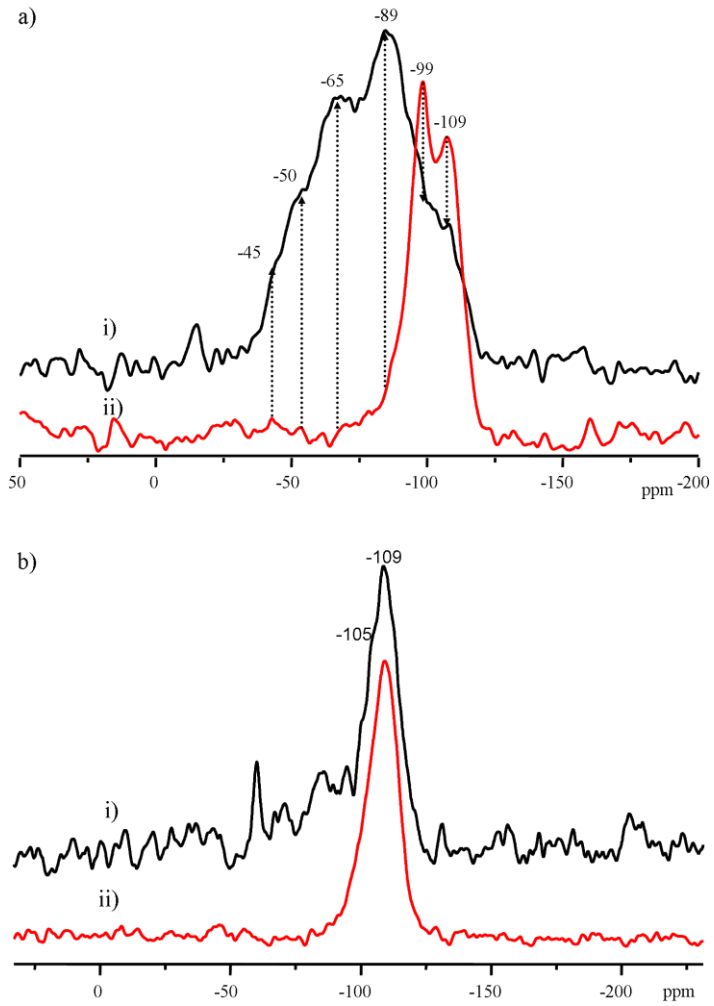

Figure 2.4. ^{29}Si NMR of i) nitrogen substituted, ii) pristine a) MCM-41 b) SBA-15 mesoporous silicates. The nitrogen substitution reactions were performed at 1050^{o}C for 8 hours under ammonia flow. ^{29}Si NMR peak positions are noted on the figure. The dashed arrows show the formation of new nitrogen substituted silicon environments.

2.3.2. Nitrogen Substitution of Zeolite Beta

The nitrogen substitution reaction on aluminosilicates was initially tested on zeolite beta which has a highly disordered framework as compared to other zeolite families (Chapter 1). The nitridation reaction was applied to two different zeolite beta samples with different aluminum contents (Si/Al ratio of 180 and 19) and extraframework cations (H^+ and NH_4^+ form). The samples were treated with ammonia flow of approximately 600 cm^3/min at 850 ^{o}C for 24 hours.

The ^{29}Si MAS NMR of untreated samples shows two distinct peaks at about -112 and -91 ppm for both of the zeolites which can be assigned as Si(0Al)Q^4 site and Si(0Al)Q^2 site, respectively. The presence of a -90ppm peak suggests the presence of defects sites in the structure consistent with reported structure[6]. Comparing the aluminum content of the two parent compounds, the NH_4Y beta sample should have Si(1Al)Q^4 sites in the framework, which are seen as a shoulder at around -105 ppm in the ^{29}Si NMR spectrum (Figure 2.5).

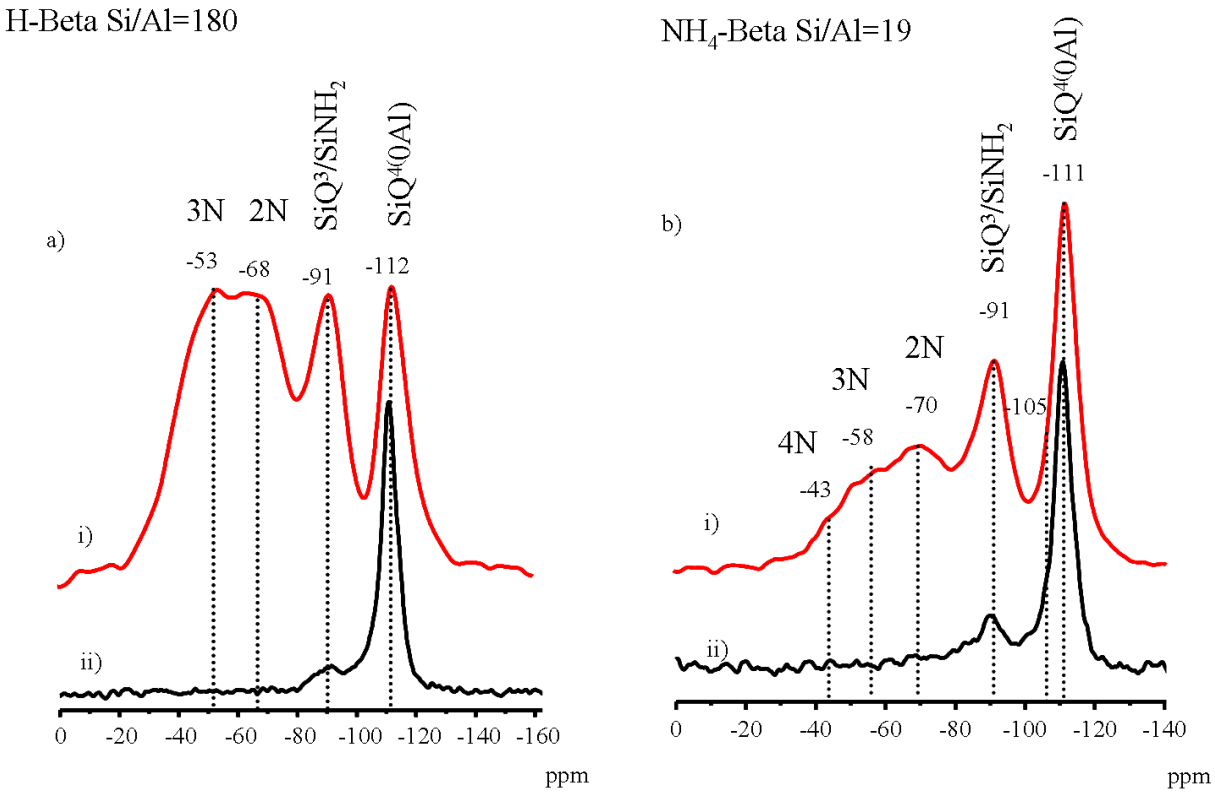

Figure 2.5. ^{29}Si NMR of i) nitrogen substituted, ii) pristine a) H-beta zeolite with Si/Al ratio of 180 b) NH_4-beta zeolite with Si/Al ratio of 19. The nitrogen substitution reactions were performed at 850^{o}C for 24 hours under ammonia flow. The chemical shift values and corresponding silicon environments are assigned.

Figure 2.5 shows ^{29}Si NMR data for nitrogen substituted H-Beta and NH_4-Beta zeolites. It is clearly seen with the ammonia treatment, both samples have been nitrogen

substituted forming 1N, 2N, 3N and 4N substituted silicon sites. However, the reaction is not complete as a $Si(0Al)Q^4$ site is still present as seen by ^{29}Si NMR peak. There is an obvious decrease in the relative intensity differences of the -90 and -110 peaks suggesting that not only the defect silanol sites but also framework Si-O-Si linkages have gone to nitridation. This argument is also consistent with the proposed nitridation mechanism, as at early stages of the reaction, the nitrogen substitution starts with terminal groups and as reaction proceeds bridging Si-NH-Si bonds form. The peak at -90 ppm in ^{29}Si NMR spectra can be assigned as both unsubstituted $SiQ^2$and $SiNH_2$ as both sites appear at almost similar chemical shifts. The presence SiOH groups can be a sign of the following reaction during ammonia treatment which further yields to framework Si-NH-Si sites.

$$\equiv Si - O - Si\equiv + NH_3 \rightarrow \equiv Si - NH_2 + \equiv Si - OH \qquad (1.1)$$

The presence of overlapping peaks and overall a broad component within -80 to -40 ppm region in ^{29}Si NMR is the result of distribution of different silicon environments that are nitrogen substituted and also a possible disorder in the structure as a result of high temperature ammonia treatment. This is also confirmed by X-ray diffraction analysis of nitrogen substituted samples. Figure 2.6 shows the comparison of diffraction data for the untreated and ammonia treated beta zeolites. As seen in the figure, for both of the beta samples, the intensity of the reflections decreases with nitrogen substitution proving an increase in the disorder of nitrogen substituted zeolite framework.

An important difference that is observed in the silicon NMR data of nitrogen substituted samples is that the pristine H-Beta zeolite has shown more reactivity to ammonia treatment yielding higher nitrogen substitution degree than the NH_4 form. Comparing the relative intensities of the different peaks in the spectra it can be concluded that the H-beta sample has uniform distribution of the nitrogen substituted sites. Considering the difference in the aluminum content of the two samples, this suggests that either the nitrogen substitution is favored for a Si-O-Si linkage rather than Si-O-Al or the H-Beta zeolite more easily have gone to dealumination during the treatment increasing the degree of nitrogen substitution to framework silica at the defect sites that are formed. The effect aluminum content and extraframework cations on the nitridation mechanism

are further studied on zeolite Y and will be discussed in the following chapters more detailed.

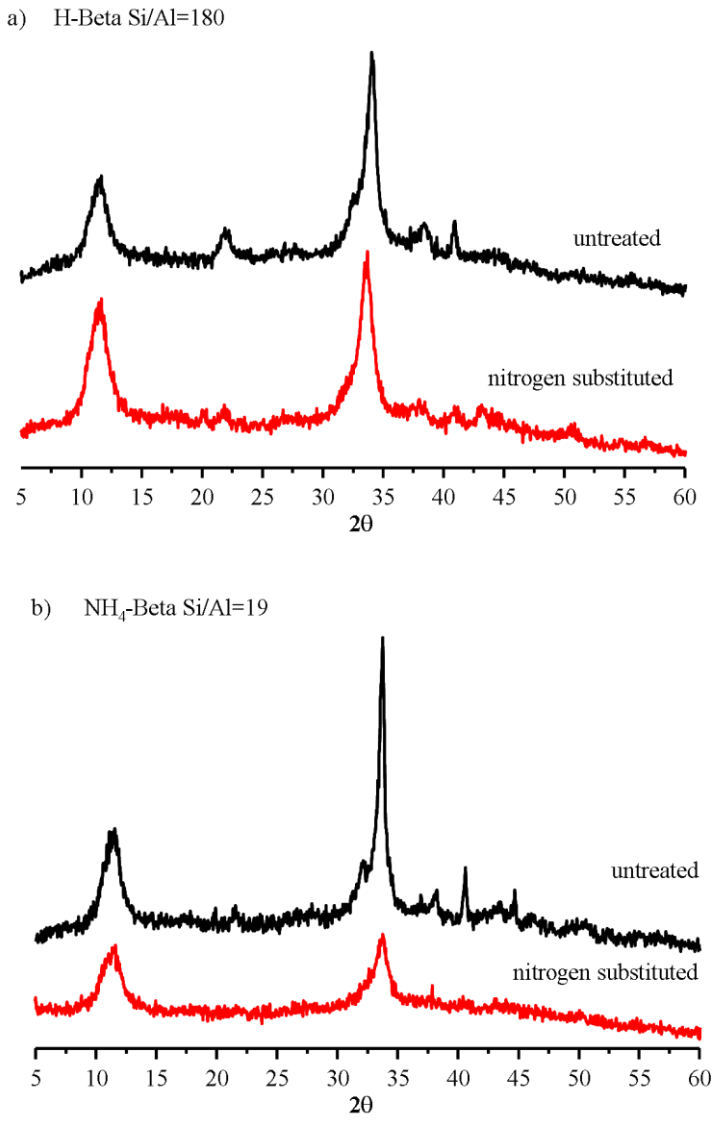

Figure 2.6. Comparison of XRD patterns (CrKα) for untreated and nitrogen substituted a) H-beta zeolite with Si/Al ratio of 180 b) NH_4-beta zeolite with Si/Al ratio of 19. The nitrogen substitution reactions were performed at 850^{o}C for 24 hours under ammonia flow.

2.3.3. Nitrogen Substitution of Zeolite Y: Optimization of Synthesis Conditions

As summarized in this chapter, all the preliminary nitrogen substitution reactions on mesoporous and highly disordered zeolitic parent compounds resulted in one or more new peaks appearing in the ^{29}Si MAS NMR spectrum. However, in order to obtain an optimum solid base catalyst, the degree of crystallinity, the presence and volume of micropores is crucial as much as the nitrogen substitution degree. These however, do not only depend on the only the nature of the parent compound, but also depends on the synthesis conditions.

Further experiments on the effect of aluminum content, extraframework cation, and synthesis conditions on the nitridation efficiency were performed on zeolite Y because of its high symmetry, order, pore size and aluminum content. We conducted several syntheses under varied conditions, -reaction temperature, time and ammonia flow rate- to test the effects of several experimental parameters on the final properties of the material. Samples from each synthesis procedure were analyzed by X-ray diffraction, high-resolution physical adsorption, and ^{29}Si MAS NMR spectroscopy to look for changes in crystallinity, microporosity, and chemical environment (due to substitution), respectively. In this chapter only the ^{29}Si NMR data will be presented.

2.3.3.1. Effect of Ammonia Introduction Temperature

Figure 2.7 shows the effect of ammonia introduction temperature on the structure of zeolite Y studied by ^{29}Si MAS NMR and X-ray Diffraction. From the X-ray diffraction data it is clearly seen that there is a significant loss in the crystallinity of the sample heated up under nitrogen environment. Most of the reflections disappeared and the intensities of the reflections are decreased due to the disorder in the framework. On the other hand the nitrogen substituted zeolite sample heated under ammonia environment still shows high cystallinity.

The effect of ammonia introduction temperature can also be observed by comparing the ^{29}Si MAS NMR data of zeolite samples heated under ammonia and nitrogen environments (Figure 2.7). ^{29}Si MAS spectrum of nitrogen substituted NaY

zeolite heated under nitrogen environment shows broader and overlapping silicon resonances in the -70 to -120 ppm range as an indication of higher structural deformation and distribution of different silicon environments. This is also consistent with the diffraction data and proves the presence of disorder and defects sites in the zeolite framework.

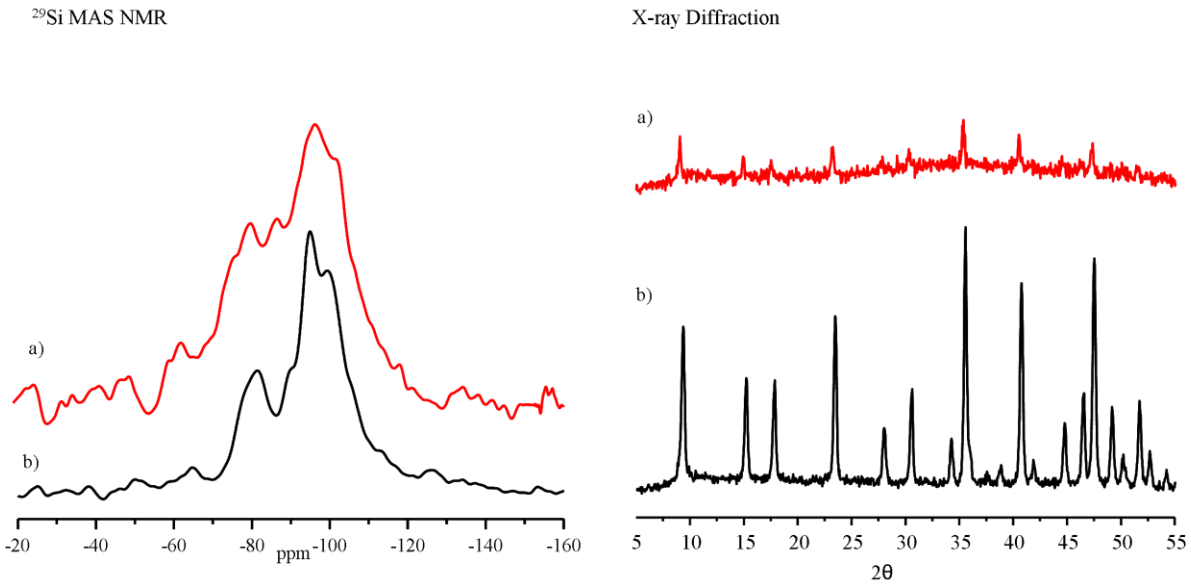

Figure 2.7. The effect of ammonia introduction temperature on crystal structure of nitrogen substituted NaY. ^{29}MAS NMR and X-ray diffraction data for a) sample heated up under nitrogen environment b) sample heated up under ammonia environment. The nitrogen substitution reactions were performed at 850^{o}C for 12 hours under ammonia flow.

Although the temperature, at which ammonia is introduced to the zeolite, may seem to be relatively unimportant in terms of the level of substitution, experiments have shown that it does have an affect on the crystallinity of the product nitrogen substituted zeolite. Introducing ammonia at the actual reaction temperature (for instance 850^{o}C as it is found as the optimum temperature in terms of both crystallinity and nitrogen substitution efficiency) produces higher deformation in the crystal structure, if the reaction temperature is high. The loss in the crystallinity is more pronounced for the

parent compounds with high aluminum content and proton form, which has lower hydtrothermal stability. The same effect is not observed for the samples where the ammonia flow starts at 500^{o}C before the actual reaction temperature. This indicates that the ammonia atmosphere is probably an important factor in preserving the framework structure of zeolites during nitridation at high temperatures. It is suspected that high temperatures in the absence of ammonia cause minor structural deformations as the Si-O and Al-O bonds are thermally excited. When ammonia is present, the same phenomena can also result in substitution in addition to dealumination and/or structural distortion, suggesting that the presence of ammonia either prevents the formation of defects or heals some of them as they form. For this reason, we recommend introducing ammonia before the furnace reaches the reaction temperature, preferably 500^{o}C.

2.3.3.2. Effect of Flow Rate

The effect of ammonia flow rate was studied keeping the reaction temperature and time at an optimum value and varying the gas flow rate. As seen in Figure 2.8.a switching from a flow rate of approximately 70 to 600 to 2000 cm^3/min while leaving the temperature at 850^{o}C and the treatment time at 8 h produces drastic effects. Significantly less nitrogen substitution is evident in the ^{29}Si spectrum for the sample treated with an ammonia flow of 70 cm^3/min. In contrast, the higher flow rates (600 and 2000 cm^3/min) produce more substitution. This great sensitivity to flow rate suggests that thermodynamic limitations (nitridation is highly endothermic) are overcome at higher flow rates by keeping NH_3 concentration high, and H_2O concentration low. With the proposed nitrogen substitution mechanisms (section 1.3.4), we know that water is produced especially at early stages of the reaction. The produced water can then react with the material instead of NH_3, leading to formation of silanol groups of bronsted acid sites decreasing the nitrogen substitution efficiency. Therefore, the NH_3 flow rate seems to be the most important parameter. For all the samples discussed in the following chapters an ammonia flow rate of 2000 cm^3/min was used to keep the nitrogen substitution level high.

2.3.3.3. Effect of Treatment Time

The effect of reaction time (time for ammonia flow at reaction temperature) is shown for three different values in Figure 2.8. The effect on the ^{29}Si MAS NMR spectrum is minimal for short times (4-8 h), but at longer times (24 h) the bulk of the NMR signal is shifted to less negative chemical shifts, indicating more double and triple nitrogen substitutions. These higher substitutions come at the expense of overall crystallinity and microporosity. Long hold times, especially 48 h, shows a marked difference in the cystallinity, surface area and micropore volume suggesting partial collapse of the zeolite structure. These will be discussed in the following chapter. The level of substitution seems to be higher at longer times, which is logical, but the general breadth of the peaks in the NMR spectrum also suggests the presence of amorphous material.

2.3.3.4. Effect of Ammonia Treatment Temperature

Increasing the temperature produces more nitrogen substitution over framework oxygen, as seen in the ^{29}Si MAS NMR spectra (Figure 2.8.c). However, as discussed earlier in this chapter, high temperatures can result in loss of crystallinity and order in the structure depending on the thermal stability of the parent compound. Our studies have shown that most of zeolite parent compounds cannot tolerate ammonia treatment above 900^{o}C and result in an amorphous structure. Reaction temperature of 850^{o}C gives high nitrogen content as well as satisfactory crystallinity and microporosity as we will be discussing in the following chapter. Therefore it is taken as the optimum temperature for nitridation reaction.

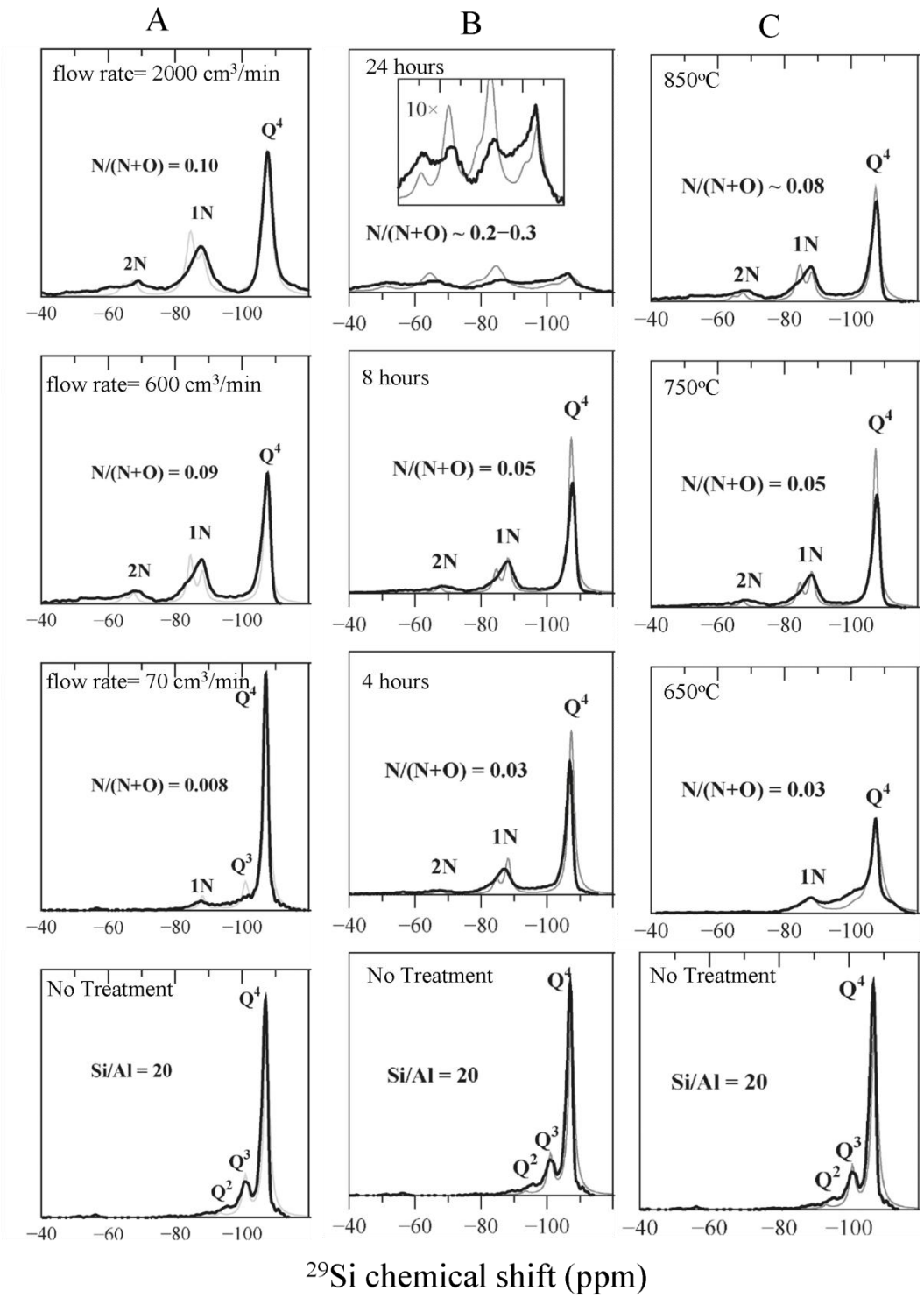

Figure 2.8. ^{29}Si MAS NMR of nitrogen substituted zeolite Y treated at different A) ammonia flow rate, B) reaction hour, C) reaction temperature. Possible silicon environments are assigned on the data. N/(N+O) values are the nitrogen substitution ratios calculated from ^{29}Si NMR data.

2.4. Conclusion

We examined the effect of synthesis conditions (reaction temperature, time and ammonia flow rate) and nature of the starting material on the nitrogen substitution reaction of mesoporous and zeolitic materials. Of all the synthesis parameters, ammonia flow rate seemed to be the most important parameter and presence of ammonia in the environment and high flow rate was crucial to obtain higher nitrogen substitution level and maintaining the crystallinity of the treated materials. The presence of ammonia or the absence of water which was produced during the reaction heals defects and/or prevent them from causing dealumination (for the zeolite parent compounds). High reaction temperatures increases the nitrogen substitution degree but at the same time causing crystallinity and order losses depending on the thermal stability of starting materials that are used. For all the materials used, increasing the ammonia exposure time also results in higher nitridation levels.

As a test for the effect of nature of the starting material, mesoporous MCM-41/SBA-15 and zeolite beta/zeolite Y were tested for their nitridation efficiency for the formation of solid base catalysts. Samples with high defect sites showed higher nitrogen content and nitrogen substitution degree per tetrahedra even at relatively low ammonia flow rates and low reaction times. However, ^{29}Si MAS NMR data on the samples showed high disorder and distribution of different silicon environments which might effect the catalytical activity of the treated material. Zeolie Y having higher structural symmetry and order was found to be a better candidate for solid base catalysts formed by nitrogen substitution reaction.

2.5. References

(1) Guo, J.; Han, A.-J.; Yu, H.; Dong, J.-p.; He, H.; Long, Y.-C. *Microporous Mesoporous Mater.* **2006**, *94*, 166.

(2) Han, A.-J.; He, H.-Y.; Guo, J.; Yu, H.; Huang, Y.-F.; Long, Y.-C. *Microporous Mesoporous Mater.* **2005**, *79*, 177.

(3) Zhang, C.; Xu, Z.; Wan, K.; Liu, Q. *Appl. Catal., A* **2004**, *258*, 55.

(4) Wakihara, T.; Saito, Y.; Tatami, J.; Kometa, K.; Meguro, T.; Mackenzie, K. J. D.; Takagi, S.; Yokouchi, M. *J. Ceram. Soc. Jpn.* **2008**, *116*, 980.

(5) Ernst, S.; Hartmann, M.; Sauerbeck, S.; Bongers, T. *Appl. Catal., A* **2000**, *200*, 117.

(6) Narasimharao, K.; Hartmann, M.; Thiel, H. H.; Ernst, S. *Microporous and Mesoporous Materials* **2006**, *90*, 377.

(7) Guan, X.; Li, N.; Wu, G.; Chen, J.; Zhang, F.; Guan, N. *J. Mol. Catal. A Chem.* **2006**, *248*, 220.

(8) Mackenzie, K. J. D.; Smith, M. E. *Multinuclear Solid-State NMR of Inorganic Materials*; Pergamon Material Series, 2002; Vol. 6.

(9) Zhang, C.; Liu, Q.; Xu, Z. *J. Non-Cryst. Solids* **2005**, *351*, 1377.

(10) Chino, N.; Okubo, T. *Microporous Mesoporous Mater.* **2005**, *87*, 15.

(11) Weitkamp, J.; Hunger, M.; Rymsa, U. *Microporous Mesoporous Mater.* **2001**, *48*, 255.

(12) Zhang, C.; Xu, Z.; Liu, Q. *J. Wuhan Univ. Technol., Mater. Sci. Ed.* **2005**, *20*, 32.

Chapter 3

The Search for Microporous, Basic Catalysts: A Joint Characterization Study of Nitrogen Substituted Zeolites by X-ray Diffraction, Pair Distribution Function Analysis and ^{29}Si MAS NMR

Abstract

Nitrogen substituted zeolites with high crystallinity and microporosity are obtained by nitrogen substitution for oxygen in zeolite Y. The substitution reaction is performed under ammonia flow by varying the temperature and reaction time. We examine the effect of aluminum content and charge-compensating cation ($H^+/Na^+/NH_4^+$) on the degree of nitrogen substitution and on the preference for substitution of Si–O–Al vs. Si–O–Si linkages in the FAU zeolite structure. ^{29}Si and ^{1}H/^{29}Si cross polarization (CP) MAS NMR spectroscopy have been used to probe the different local environments of the nitrogen-substituted zeolites. X-ray Diffraction, Pair Distribution Function Analysis (PDF), Energy dispersive X-ray spectroscopy (EDX) measurements and BET surface analysis have been applied to study the changes in the long range order, bond angle and bond distances, elemental composition and porosity of treated materials. The results show that high levels of nitrogen substitution can be achieved while maintaining porosity, particularly for NaY and low-aluminum HY materials, without significant loss in crystallinity. The nitrogen substitution in the zeolite framework causes a decrease of the unit cell parameter. Experiments performed at lower temperatures (750–800^{o}C) show a preference for substitution at Si–OH–Al sites.

Quantum calculations are also performed by our collaborators at University of Massachusetts, Amherst, to calculate the nitrogen substitution energies and ^{29}Si chemical shifts of different nitrogen environments in the zeolite framework, allowing to compute

the nitrogen doping levels as controlled by temperature, reaction time, and aluminum content in the zeolites studied.

3.1. Introduction

Zeolites and other microporous silicates are widely used as acidic catalysts for size and shape selective catalytic reactions[1-3]. Much effort has been expended to identify microporous materials that can replace liquid basic catalysts, since microporous basic catalysts are non-corrosive, easily separated from the reaction mixture, and readily regenerated after the reaction[4-6]. Furthermore, the high surface area and shape selectivity of such materials can be used to tune selectivities in base-catalyzed reactions[7-10]. Such reactions are particularly important in light of recent interest in biomass conversion to produce fuels from renewable feedstocks[11].

As introduced in the first chapter, zeolitic materials have been made with some of the bridging oxygen atoms in Si–O–Si and/or Si–O–Al linkages replaced by NH_2 groups or by NH groups, in a process named nitridation[12,13] with treating the material with amines at high temperatures. Crystalline zeolites are more difficult to nitride as they contain fewer silanol groups as defect sites, and it has been claimed by some authors that the nitrogen substitution reaction starts from these defect sites[14,15]. Furthermore, ammonia treatment of zeolites at high temperatures can result in loss of crystallinity.

In this section, synthesis, detailed characterization and the nature of both framework sites and zeolite structure in heavily nitrogen-doped zeolite Y is presented. Despite the difficulties with working with zeolitic frameworks mentioned above, I establish conclusively the formation of zeolites with framework nitrogen and minimal loss of zeolite structure. In particular, I present the synthesis and detailed characterization of nitrided zeolite Y with high levels of nitrogen substitution, high crystallinity, and high porosity. This is established by combining X-ray Diffraction, PDF, ^{29}Si MAS NMR, and EDX analysis to determine the signatures of various nitrogen environments.

The structural properties of nitrided zeolites and mesoporous materials have previously been investigated by various analytical methods. Powder X-ray diffraction has been used to study the changes in the crystallinity of the material after the reaction[9,16];

Fourier transform infrared (FT-IR) and FT-Raman spectroscopy methods have been used to characterize the nitrogen-substituted surface groups and unreacted defect silanol groups[16-18]; and elemental analysis has been employed to determine nitrogen content[17,18]. However, few studies have focused on characterizing these materials by ^{29}Si solid state Magic Angle Spinning (MAS) Nuclear Magnetic Resonance (NMR) spectroscopy[4,18,19], and no experimental NMR study has yet to (a) demonstrate high nitridation levels, and (b) consider how aluminum in the framework may influence the NMR spectrum of the nitrided zeolite.

^{29}Si NMR provides a method with which to study the nitrogen substitution level in the zeolite framework. Previous ^{29}Si NMR experimental studies on nitrogen substituted zeolites and mesoporous materials have already discussed in the previous chapter (Chapter 2). The recent quantum mechanical calculations on the ^{29}Si NMR chemical shifts[20] have shown that the substitution of nitrogen for oxygen in the zeolite framework results in an even larger shift to less negative values of chemical shift, providing a sensitive method to study the degree of nitridation. The assignment of resonances in both silicon oxynitrides and zeolites is, however, complicated by the presence of possible terminal amine/hydroxyl groups and the effect of framework aluminum on the nitrogen shifts.

Theoretical calculations performed earlier provide information on the changes in bond lengths and bond angles in zeolites with doping of methylene and amine groups in SOD zeolites[21,22]. By using density functional theory-based electron structure calculations on silicate zeolitic frameworks doped with methylene and amine groups, Astala *et al.* showed that, Si-X-Si angle increases with the electronegativity of X (X= C, N, and O)[21]. They also reported that this effects the overall cell parameter of the structure as the Si-C-Si and Si-N-Si angles in doped sodalites are substantially smaller than the corresponding Si-O-Si angle in untreated zeolite SOD. Here we have studied the change in the crystal structure and long range order of the nitrogen substituted zeolites by high energy X-Ray Diffraction Analysis and Pair Distribution Function (PDF) Analysis. X-ray diffraction technique provides information on the changes in the long range order for the nitrogen substituted zeolites while Pair Distribution Function (PDF) analysis gives the probability of finding any two atoms as a function of interatomic distance[23,24]. The combination of

these two methods gives information about the changes in the crystal structure, bond distances and bond angles due nitrogen substitution in the zeolite framework, as a complementary technique to ^{29}Si NMR studies. We have obtained consistent results with theoretical calculations for the changes in bond length and bond angles in nitrogen substituted zeolites.

In this chapter, I present a detailed microscopic picture showing the effects of Si/Al ratio, H^+ vs. Na^+ extra-framework cations, and temperature on reactivity, degree of nitrogen substitution, and framework stability. It is shown that the highest levels of nitridation and crystallinity are obtained by using zeolites with low aluminum content. I first present X-ray diffraction, nitrogen content analysis, and adsorption data, followed by a discussion of PDF analysis results on the nitrogen substitutes zeolites treated at different reaction conditions. The single pulse (SP) and cross polarization (CP) ^{29}Si MAS NMR data of the treated zeolites with different aluminum content and extraframework cation will then be covered in detail, allowing me to study a wide range of different nitrogen substituted silicon environments, discuss the nitrogen substitution mechanism and explore the preferential substitution of NH/NH_2 in Si–O–Al vs. Si–O–Si positions. In the end, it is found out that, high levels of nitrogen substitution can be achieved while maintaining porosity, particularly for NaY and low-aluminum HY materials, without significant loss in crystallinity. Experiments performed at lower temperatures (750–800^{o}C) show a preference for substitution at Si–OH–Al sites where as for higher and longer temperature treatment Si-O-Si linkages go through nitrogen substitution as much as the aluminum sites.

3.2. Experimental

3.2.1. Synthesis

Commercial HY, Si/Al=15 (CBV 720, Lot #72004N00868); NH_4Y, Si/Al = 2.55 (CBV 300, Lot #300001021451); NaY, Si/Al = 2.55 (CBV 100, Lot #100031042531); and HY, Si/Al = 2.55 (CBV 400, Lot #400054002618) from Zeolyst (Valley Forge, PA) were used as starting materials. The Si/Al values quoted here are provided by the

manufacturer, and represent the overall Si/Al ratio, not necessarily the Si/Al ratio of the framework. Both dehydration and nitridation were accomplished in an alumina boat which was inserted into a quartz tube furnace with dimensions of 3.8 cm diameter and 72 cm in length. Dehydration of the samples prior to the nitridation was conducted under nitrogen flow. The temperature was slowly ramped to 110°C at 0.1°C/min, held at that temperature for 2 h, then slowly ramped to 400°C at 0.5°C/min, and held at that temperature for 10 h. Following this dehydration step, several samples were prepared by heating the samples in flowing nitrogen to 550°C, then initiating a high ammonia flow rate of approximately 2000 cm^3/min. The temperature was then raised to the final nitridation temperature. Subsequently, the samples were cooled down to room temperature under nitrogen flow and stored in a nitrogen glove box until needed for the characterization experiments. Since the temperatures quoted correspond to those measured with a thermocouple outside the quartz tube, we also determined the temperature near the center of the tube using the same flow rates and only a 5°C difference between the measured and actual sample temperatures was found in our experimental setup.

The samples for the characterization experiments were all prepared in a glove box with dry nitrogen atmosphere. The following nomenclature is used to label the samples: The first label "Nit" indicates that zeolites are nitrided. The type of the zeolite (e.g., HY, NaY) and Si/Al ratio is then given, which is followed by the nitridation temperature in °C and the treatment duration in hours. For example, the label "Nit.HY Si/Al=15.850.24" refers to a nitrided, HY zeolite with Si/Al ratio of 15 and treated at 850 °C for 24 h.

3.2.2. Characterization

Powder X-ray diffraction patterns were collected on a Rigaku diffractometer using Cr K-α radiation (wavelength 0.229 nm). The 2θ values were converted with respect to Cu K-α (wavelength 0.154 nm) for ease of comparison. Elemental analyses of the nitrided samples for nitrogen content were carried out by Galbraith Laboratories, Inc. by a combustion reaction using a Perkin Elmer 240 Elemental Analyzer (PerkinElmer; Waltham, MA). The Kjeldahl method, performed at Galbraith Laboratories

(Knoxville, TN), was also used to check the accuracy of different methods for nitrogen elemental analysis. Energy dispersive X-ray spectroscopy (EDX) measurements were carried out on a LEO–1550 field emission scanning electron microscope (SEM) operating at an accelerating voltage of 20 kV. Adsorption analyses were performed by using a Micromeritics ASAP 2010 surface analyzer (Micromeridics Corp.; Norcross, GA).

The ^{29}Si MAS NMR analysis was performed on a Varian 360 MHz spectrometer with a 4 mm probe using 14 and 8 kHz MAS for the single pulse (SP) and ^{1}H-^{29}Si CP experiments, respectively. The ^{29}Si and ^{1}H 90° pulses were 2.4 and 4.5 μs, respectively. The RF field strengths for ^{1}H-^{29}Si CP experiments are ~42 and ~100 khz for ^{29}Si and ^{1}H, respectively. Contact times of 0.1 to 10 ms were used in the CP experiments. Pulse delays of 30 s were used for the ^{29}Si MAS NMR experiments. The spin-lattice relaxation times (T_1) measured on select samples (Nit-HY-15-850-24 and Nit-NaY-2.55-850-24) were approximately 15s for every silicon site (i.e., no differences in T_1 values were determine for the different environments). Thus, as pulse delays of 30 s was considered sufficient to ensure qualitatively reliable intensities. The ^{29}Si chemical shifts were referenced to tetramethylsilane (TMS) at 0 ppm. All the dehydrated/nitrided samples were packed into NMR rotors under dried nitrogen atmosphere in a glove box.

The Si/Al ratios of the pristine materials were calculated from the SP ^{29}Si NMR data, according to "Loewenstein's rule"[25] (which stipulates that no Al–O–Al linkages can occur in the zeolite framework), with the Equation (1.13).

PDF analysis presented in this chapter was performed at the high energy beamline 11-ID-B at the Advanced Photon Source (APS) at Argonne National Laboratory, IL, USA. A wavelength of 0.2127 Å (60 keV) and a General Electric amorphous silicon area detector were used. A CeO_2 standard was employed to calibrate the sample-to-detector distance and the tilt of the image plate (IP) to the beam path. Samples were packed into Kapton capillaries and data were obtained from the powder sample in transmission geometry. The IP data were integrated and converted to intensity readings versus 2θ with the Fit2D software. The PDF data were generated using the PDFgetX2 program.

3.2.3. Quantum Mechanical Calculations

A small fragment of the FAU framework containing 14 tetrahedral (Si, Al) atoms is studied. The cluster contains two central tetrahedral atoms and one oxygen atom that are three or more coordination shells away from the terminating hydrogen atoms. The cluster is terminated with hydroxide groups, the hydrogen atoms of which are placed along the cleaved Si–O bond at approximately 0.86 Å from the oxygen. All terminal OH groups and any silicon atoms bound to two or more OH groups are fixed at their crystallographic coordinates during geometry optimization; this is necessary to ensure the final geometry is representative of FAU zeolite. A version of this cluster in which one silicon atom has been replaced by aluminum (with the compensating hydrogen atom) is shown in Figure 3.1. Hydrogen atoms are placed on the nitrogen or oxygen atom nearest the central silicon atom to avoid edge effects. Sodium ions are placed near positions SI, SI', SII, and/or SIII in each cluster, and they were then allowed to relax. This is a crude approximation, as the real material would show a distribution of different cation arrangements. However, the change in the chemical shift when sodium ions are absent entirely (instead, the entire cluster has a negative change) is very small, indicating the effects of ion placement are less significant than other sources of error in the calculation.

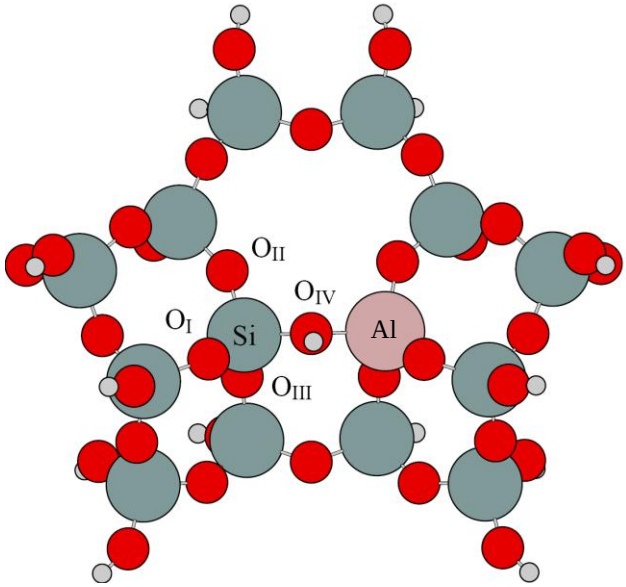

Figure 3.1. Zeolite cluster used in the calculations. A faujasite framework containing 14 tetrahedral (Si, Al) atoms with two central tetrahedral atoms and one oxygen atom that are three or more coordination shells away from the terminating hydrogen atoms is used. Red spheres represent oxygen atoms, silicon and aluminum atoms are represented by blue and purple spheres, respectively.

3.3. Results and Discussion

3.3.1. X-ray Diffraction Analysis

The powder XRD patterns of the zeolites nitrided at different temperatures for different times are shown in Figure 3.2. The nitrided HY (Si/Al = 15), NaY (Si/Al = 2.55) and HY (Si/Al = 2.55) samples all maintain a faujasite (FAU) structure with only slight decreases in crystallinity, particularly for NaY heated at high temperatures. Noticeable decreases in the intensities of some of the reflections (e.g., 220 and 711) occur as the reaction proceeds, indicating that structural changes have occurred. In contrast, the NH_4Y (Si/Al = 2.55) sample shows a much more pronounced loss of crystallinity after ammonia treatment. NH_4Y reacts to form HY during the dehydration process, and HY is known to be unstable above 500 °C due to dehydroxylation of the Si–O(H)–Al linkages to form Lewis acid sites[26,27]. This process occurs at much lower temperatures in the presence of water or steam[28]. In contrast, NaY zeolites are stable at higher temperatures. Thus, the

difference in the framework stabilities following nitridation is attributed to the greater concentration of Si–O(H)–Al linkages in the NH_4Y sample as compared to the HY (Si/Al = 15) sample, the rupture of these linkages due to the elevated temperature (and water released due to nitridation) presumably competing with the nitridation mechanism. The HY sample (Si/Al = 2.55) contains a significant concentration of extra-framework aluminum atoms resulting in a lower aluminum content for the framework (Si/Al ratio of 6.1). This is consistent with the enhanced stability of this zeolite.

High Resolution X-ray Diffraction Analysis were also performed (not shown) on the nitrogen substituted zeolite samples discussed above, at high energy beamlines, 11-BM at the Advanced Photon Source (APS), Argonne National Laboratory and X-7B, National Synchrotron Light Source (NSLS), Brookhaven National Laboratory. The High Resolution X-ray Diffraction data of the zeolite samples treated at different reactions conditions show that, as the ammonia flow temperature increases, a noticeable shift is observed in the reflection positions towards higher 2θ values. Preliminary results on the Reitveld refinement of the data reveal that while the space group remains the same, the cell parameter of the zeolite treated at high temperature decreases, compared with the cell parameter of the parent zeolite. This suggests possible nitrogen substitution in the zeolite framework with the ammonia treatment.

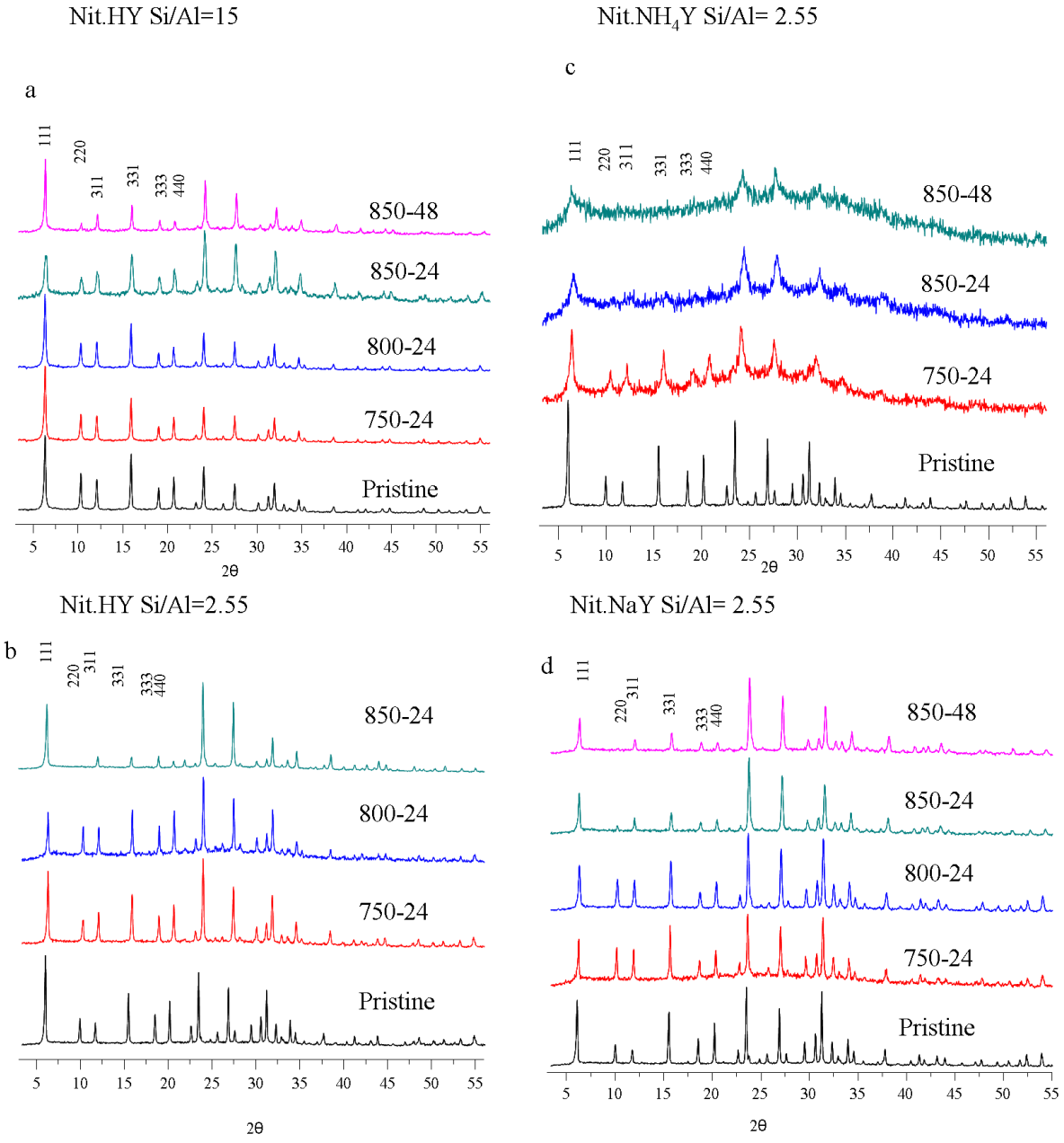

Figure 3.2. (a, b, c, d) powder XRD patterns for nitrogen substituted zeolite HY Si/Al ratio of 15 and 2.5, NH4Y and NaY, respectively (Cu K-α). The first six reflections of the faujasite cell are indexed.

3.3.2. Nitrogen Content and Porosity

The results of nitrogen adsorption (measurement of the micropore volume and BET surface area, Table 3.1) all indicate that no severe structural damage has occurred during the high temperature treatment for the nitrided HY (Si/Al = 15 and Si/Al = 2.55) and NaY samples. The two HY zeolites with high and low aluminum content maintain a higher microporosity than the other samples, losing only 25 percent of their porosity upon nitrogen treatment at all temperatures studied. In contrast, nitrided NaY and NH_4Y zeolites show a 50–80 percent decrease in their micropore volumes, respectively, the larger loss in pore volume correlated with the loss in framework crystallinity as shown by XRD for NH_4Y (Figure 3.2).

Nitrogen content analyses by both elemental analysis and by EDX measurements demonstrate that high concentrations of nitrogen are present, more than 30 percent of the weight of the material being replaced by nitrogen in the HY zeolites at the highest temperature studied (850°C; Table 3.1), based on the EDX results. However, there are noticeable inconsistencies between the results of the two methods, with the combustion results showing noticeably lower nitrogen contents than those derived from EDX.

The EDX nitrogen contents were calculated from the changes in the ratios of the Si and O intensities of the K-edges of the treated and the untreated zeolites, as shown in Figure 3.3 for nitrogen substituted zeolite Y samples treated at high temperatures and long reaction times. The Si intensity provides a standard with which to compare between the different samples. Unfortunately, I was unable to obtain a standard material containing a known Si:Al:O:N ratio to help in these analyses, introducing a source of error. A more significant cause of the lower numbers obtained from combustion analysis is that the combustion reaction may not go to completion. A second source of error is the possible adsorption of water in the zeolites before the analysis, which is difficult to prevent since the chemical analyses are performed by a third party (Galbraith Laboratories). Any water absorption, which can be quite large if the zeolites are fully hydrated, will lead to higher than expected oxygen content in the materials. In order to check the reliability of the elemental analysis, we analyzed the nitrogen content of four batches of the same Nit.NH_4Y.2.55.850.48 sample by both combustion and Kjeldahl

methods. Four different combustion analysis runs of the same sample gave nitrogen content results in the 7 to 14 weight percent range, whereas the same number of Kjeldahl method analyses indicated 15 to 20 weight percent nitrogen, suggesting that neither method is reliable. In contrast, EDX indicated that there is approximately 31 percent by weight nitrogen (68.2 mol % nitrogen of the total anion (O + N) content) in this material. This is much closer to the nitrogen contents estimated based on the ^{29}Si NMR results. We note that elemental analysis, and weight gain in a TGA experiment (which also relies on a combustion reaction) represent the standard methods for characterizing nitrogen content of these materials[9], providing further motivation for our detailed ^{29}Si NMR analyses of these materials.

Apart from the quantitative information on nitrogen content of the treated materials, EDX analysis results can be used to obtain qualitative information on the elemental composition of the zeolitic structure. As seen in Figure 3.3. all the samples have nitrogen either in the framework or as an extraframework cation after the ammonia treatment and the changes in the relative intensities of N and O peaks shows framework oxygen is being substituted by nitrogen. If we compare these relative changes within oxygen and nitrogen K edge intensities for different zeolites, zeolite HY with low aluminum content and NH_4Y zeolite have gone through higher nitrogen substitution level which is consistent with ^{29}Si MAS NMR results. Although ^{29}Si MAS NMR data of sample Nit.HY.Si/Al=2.55. 850.24 shows high level of nitrogen substitution degree, the intensity of nitrogen K-edge peak is not that pronounced in the EDX data compared to the oxygen K-edge peak. One explanation for this might be the presence of adsorbed water in the treated sample due to the poor sample preparation for EDX analysis. Looking at the EDX data of the pristine sample, the oxygen intensity is higher comparing to other samples which can be explained by the presence of adsorbed water. Interestingly, the EDX analyses of both HY high aluminum and NH_4Y samples reveal a small amount of sodium. This is probably due to the presence of residual sodium cations located at the SI position, due to incomplete ion-exchange[29].

Finally, it should be noted that all the nitrogen determination measurements measure the total nitrogen content in the materials, not only the framework nitrogen content.

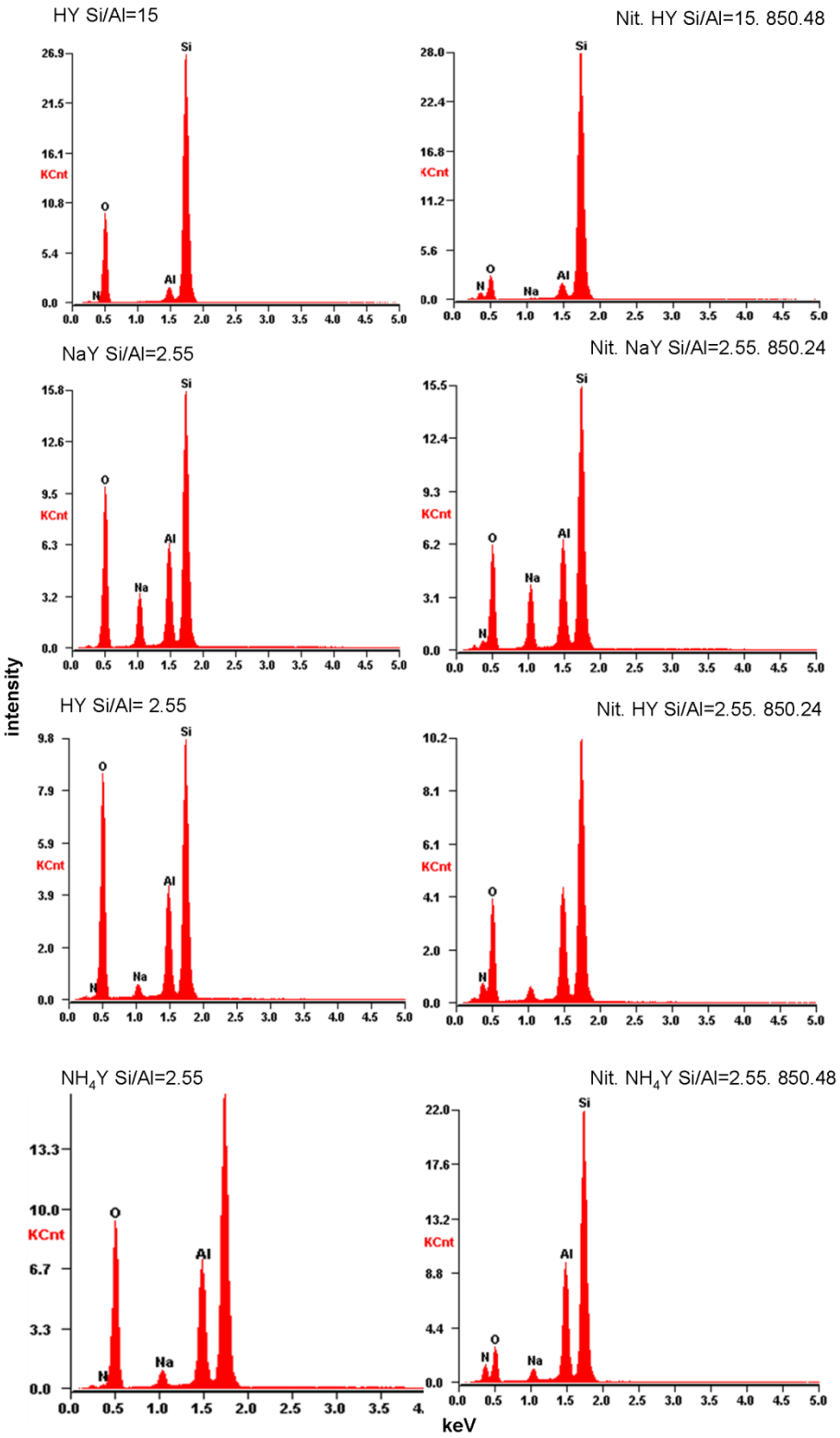

Figure 3.3. EDX analysis of pristine and nitrogen substituted zeolite Y with different aluminum content and extraframework cations.

Table 3.1. Nitrogen content and surface area analysis for nitrided zeolites.

Nitrided Zeolite	Nitrogen Content				Adsorption		
	Elemental Analysis	EDX[a]		^{29}Si NMR			Micropore volume
	% w/w[a]	% w/w	% mole	Expt.	BET Surface Area (m^2/g)	C_{BET}	(cm^3/g)
Nit.HY.Si/Al=15.750.24		12.8	27.3	9.7	634.6	−62.7	0.23
Nit.HY.Si/Al=15.800.24		21.7	46.1	25.9	597.1	−65.2	0.21
Nit.HY.Si/Al=15.850.24	11.8	26.1	54.9	45.2	658.4	−69.6	0.22
Nit.HY.Si/Al=15.850.48	13.9	34.7	73.2	46.6	665.7	−75.5	0.21
HYSi/Al = 15 pure Si/Al = 42 (from ^{29}Si NMR)					857.6	−59.7	0.32
Nit.NaY.750.24		5.6	13.3	5.3	348.2	−45.2	0.17
Nit.NaY.800.24		7.2	16.7	6.8	348.7	−47.2	0.16
Nit.NaY.850.24	5.4	15.6	36.9	35	193.6	−54.7	0.08
Nit.NaY.850.48	9.2			42	331.9	−49.7	0.15
NaYSi/Al = 2.5 pure Si/Al=2.65(from ^{29}Si NMR)					655.7	−45.6	0.31
Nit.HY.Si/Al=2.55.750.24		9.4	25.0	19	475.3	−47.8	0.22
Nit.HY.Si/Al=2.55.800.24		10.5	22.1	19			
Nit.HY.Si/Al=2.55.850.24	10.2	29.8	65.1	53	427.8	−51.2	
HY Si/Al = 2.55 pure Si/Al = 6.1 (from ^{29}Si NMR)					638.0	−47.5	0.29
Nit.NH_4Y.750.24	7.4	16.4	34.9		291.9	−80.8	0.08
Nit.NH_4Y.850.24		22.3	49.2		178.1	−252.6	0.03
Nit.NH_4Y.850.48	8.4–10.5	31.3	68.2		152.3	−198.4	0.02
NH_4Y Si/Al = 2.5 pure Si/Al = 4.2 (from ^{29}Si NMR)					1110.3	−64.5	0.40

[a] For the elemental and EDX analyses, we report the percent of nitrogen of the total weight of the sample (% w/w), for ease of comparison with data for comparable materials reported in the literature. To allow comparison with the ^{29}Si NMR data, the EDX data have also been converted into percent nitrogen substitution by moles (N/(O+N)), calculated by using the molecular formula of the anhydrous zeolite.

3.3.3. Pair Distribution Analysis of Nitrogen Substituted Zeolites

Figure 3.4 shows the possible bond distance and bond angle values for some of the main structural units of faujasite type zeolites. The T-O bond distances of the parent zeolites are in the order of 1.6 to 1.7 Å (Al-O bond lengths longer than Si-O bond length) and the T-O-T bond angle is approximately 107.7^{o}. The T-T and O-O bond distances depend on the T-O-T bond angle and the former is about 3.09 Å whereas the latter is 2.6 to 2.7 Å.

The PDF data contains real space information about the distances between pairs of atoms. The first strong correlations in the X-ray PDFs of the pristine zeolites, shown in Figure 3.5 at about 1.60-1.70 A˚, are due to the overlapping T–O bonds within the $(Si,Al)O_4$ tetrahedra. The lineshape of the first peak for parent HY zeolite with Si/Al ratio of 15 (Figure 3.5.a), is narrower comparing to the lineshape of the same peak for the other zeolites. This is due to narrower distribution of different bond lengths as the HY zeolite with Si/Al ratio 15 has lower aluminum content and therefore it has fewer Al-O bonds than the other zeolites.

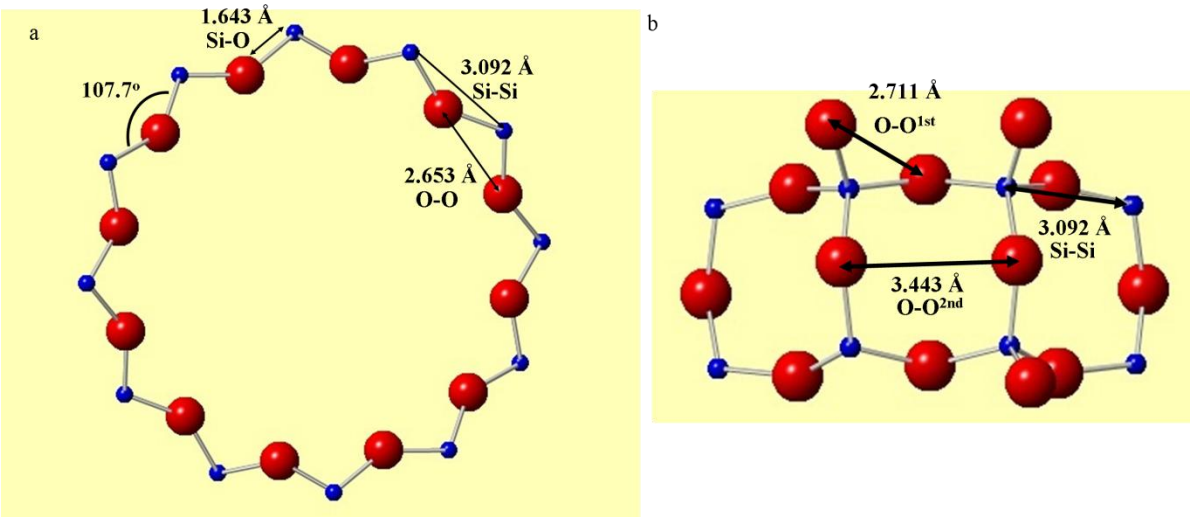

Figure 3.4. Possible bond distances and bond angles in faujasite framework (blue spheres represent Si or Al atoms and red spheres represent O). a) 12-ring window of the supercage b) 4-ring windows of the hexagonal prism of faujasite structure.

The X-Ray PDF data on the ammonia treated zeolites show that as the treatment temperature increases, the position of the first strong peak (peak at 1.60A˚) shifts to higher distances as an indication of Si-N bond formation. This clearly shows that the Si-N distance of the 1st shell is longer than Si-O bond distance, consistent with the theoretical calculation results. This shift is more obvious (from 1.64Å to 1.70 Å) for the NH_4Y zeolite sample treated at 850^{o}C for 24h (Figure 3.5.c) which has a higher nitrogen content as proven by ^{29}Si MAS NMR (Figure 3.8.c) which will be discussed in the following section. For the nitrogen substituted NH_4Y zeolite sample, the relative intensity of 1.64 Å peak increases as the nitrogen content increases. This shows a more uniform bond distance distribution (mostly for Si-N bonds) as a result of higher nitrogen substitution degree of the silicon tetrahedra.

The second strong peak in the X-ray PDFs of the both pristine and ammonia treated zeolites, is the 3.06 Å peak which is correlated to the Si-Si/Si-Al bond distance. As the ammonia treatment temperature increases the peak shifts to lower distance values for all the zeolite types. As indicated above the Si-Si/Si-Al bond distance depends on the T-O-T bond angle, therefore it can be concluded that as the nitrogen substitution degree of the zeolite increases, the T-O-T bond angle decreases. This also explains the decrease in the cell parameter observed by the refinement of the HR-XRD data. The illustration of the changes in the bond lengths and bond angles of the zeolite framework due to the nitrogen substitution is given in Figure 3.6.

The change in the Si-Si/Si-Al bond distance is more pronounced for the NH_4Y zeolite sample treated at 850^{o}C for 24h which has one of the highest nitrogen content (Figure 3.5.c). It is also seen that the intensity of the peak increases and the peak lineshape gets broader due to distribution of different bond distances. It should be noted that the sample is not totally nitridated but still has some Si-O-Si or Si-O-Al linkages in the framework.

Although the PDF peak intensities are low, changes are still observable for the O-O bond distances (peak at 2.6 Å in Figure 3.4.a) of the same tetrahedra and O-O distances for the oxygens in the second coordination shell (peak at 3.4 Å in Figure 3.4.b), with the changes in ammonia treatment temperature. As the reaction temperature increases, the peaks get broader due to distribution of O-O, O-N and N-N bond distances.

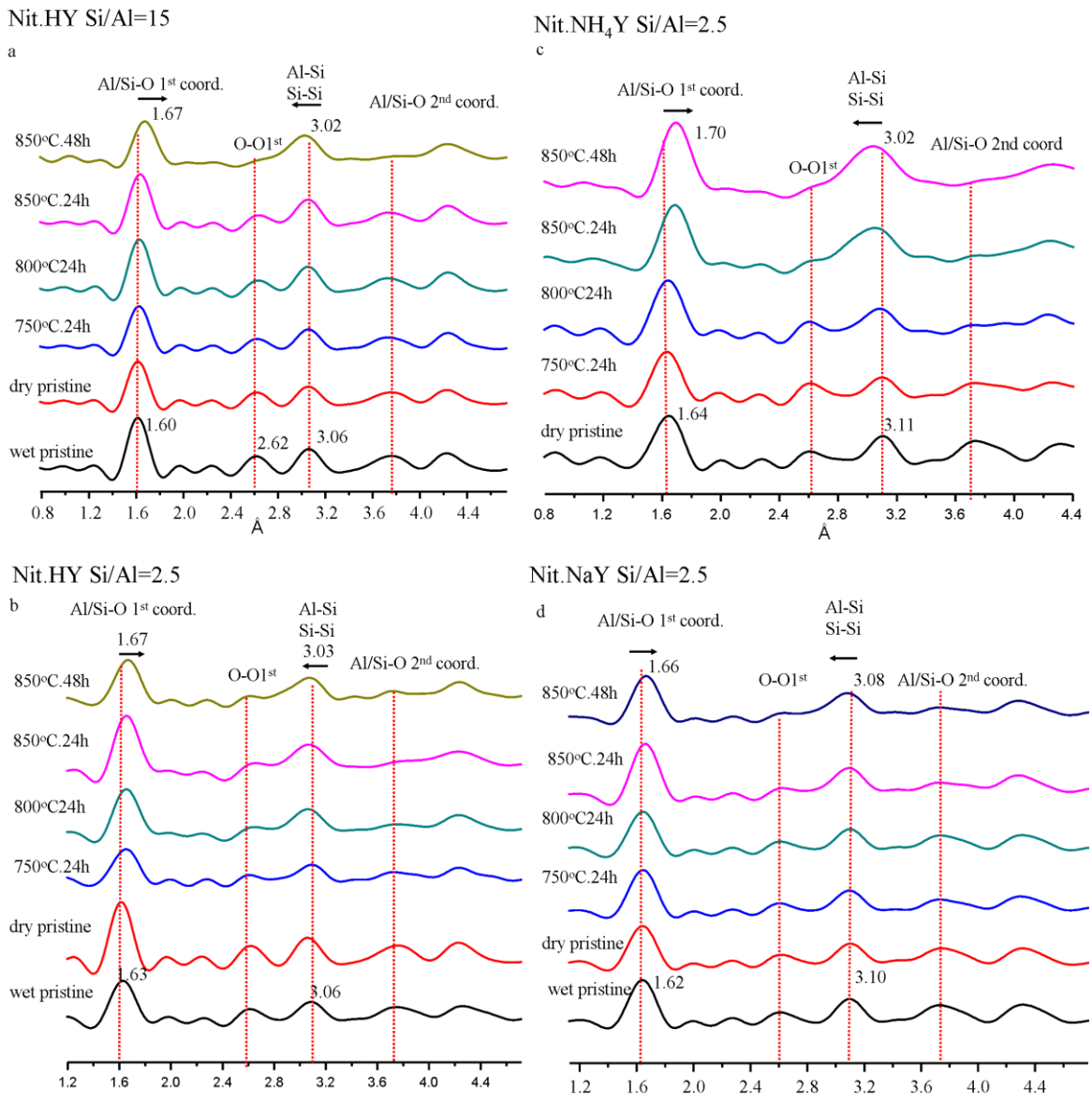

Figure 3.5. PDF`s for pristine and nitrogen substituted zeolite Y with different aluminum content and extrframework cation. The substitution reaction was performed at different reaction conditions. Arrows indicate the shifts in positions of peaks for Al/Si-O and Si-O-Si/Si-O-Al bond distances.

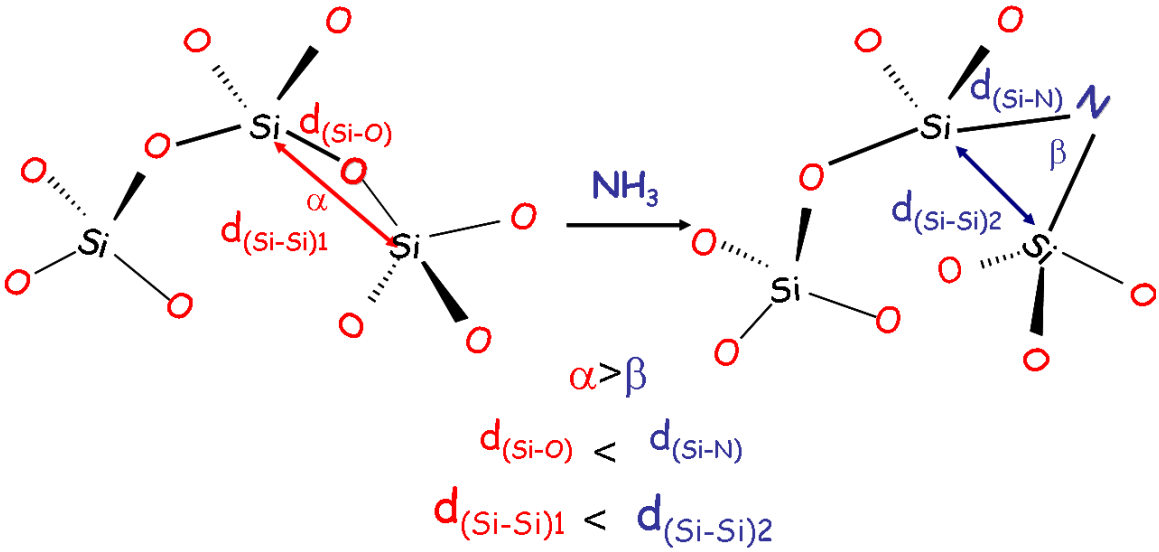

Figure 3.6. The illustration of the changes in the bond lengths and bond angles of the zeolite framework with the nitrogen substitution reaction. α and β are Si-O-Si and Si-N-Si bond angles, respectively. "d" represent the bond distance.

3.3.4. Structural Characterization by ^{29}Si MAS NMR Spectroscopy

3.3.4.1. Calculated Chemical Shifts and Energies

The ^{29}Si chemical shifts of each cluster and the energy changes due to the addition of ammonia and loss of water are presented in Table 3.2. The reaction energies listed are changes in the electronic energy only; no correction for zero-point energy, thermal energy, or entropy has been applied. These corrections are likely small compared to the reaction energies considered. There are three trends in energy that are roughly additive. Substitution of the OH group of a Brønsted acid site with NH_2 is endothermic by about 35 kJ/mol, while substitution of oxygen with NH between two silicon atoms is endothermic by about 100 kJ/mol. Substitution between silicon and aluminum but *not* at an acid site costs 120 kJ/mol or more. This suggests that substitution at acid sites should be preferred thermodynamically over substitution elsewhere. However, kinetic limitations are also likely under the conditions of the reaction, so this is taken as a first hypothesis only.

Table 3.2. Electronic energy differences (V) between FAU clusters and the ^{29}Si chemical shifts of each cluster.

species	ΔV [kJ/mol]	$\delta_{TMS}(^{29}Si)$ [ppm] calcd
siliceous sites		
≡Si−O−**Si**≡	0	−107.4
≡Si−NH−**Si**≡	99.5	−84.6
≡Si−NH−**Si**−NH−Si≡	210.0	−64.6
sites on the surface		
≡**Si**−OH	0	−94.6
≡**Si**−NH_2	30.1	−78.7
sites with a single aluminum atom nearby		
≡Al−OH−**Si**≡	0	−101.3
≡Al−NH_2−**Si**≡	32.3	−88.2
≡Al−NH_2−**Si**−NH−Si≡	140.4	−67.7
sites with two aluminum atoms nearby		
≡Al−OH−**Si**−OH−Al≡	0	−93.7
≡Al−NH_2−**Si**−OH−Al≡	35.7	−81.5
≡Al−NH_2−**Si**−NH_2−Al≡	70.5	−67.1
sites with three aluminum atoms nearby		
(≡Al−OH−)$_3$**Si**−	0	−85.5
(≡Al−OH−)$_2$**Si**−NH_2−Al≡	34.8	−67.1
≡Al−OH−**Si**(−NH_2−Al≡)$_2$	65.1	−51.7
(≡Al−NH_2−)$_3$**Si**−	104.0	−45.5

Several trends are evident in the ^{29}Si chemical shift. The chemical shift increases by 5–7 ppm as the number of nearby aluminum atoms increases. This is similar to the trend observed experimentally. Substitution at a Brønsted acid (OH) site by an NH_2 group changes the chemical shift by 12–15 ppm toward TMS (reaction pathway c in Figure 3.7). Substitution between two silicon atoms changes the chemical shift by 20–22 ppm, regardless of the presence of aluminum near one of the *other* oxygen atoms (reaction pathway e in Figure 3.7.). It should be noted that the change in chemical shift gets smaller as the number of nitrogens added per silicon gets larger, presumably due to changes in Si–O–Si and Si–N–Si bond angles. Such strain effects are amplified by the finite cluster size and artificial termination.

As given in Figure 3.7, for nitrogen substitution reaction, there are various possible reaction pathways leading to formation of different silicon and aluminum environment with varying nitrogen substitution degree. Substitution can take place

through a terminal silanol group forming terminal amines (reaction pathway a in Figure 3.7) or it can go through a Si-O-Si linkage of a silicon tehrahedra with no aluminum connection, forming Si-NH-Si environment (reaction pathway b in Figure 3.7). The nitrogen substitution is also possible through Si-O-Si linkage where silicon atoms are connected to at least one aluminum atom (reaction pathway d in Figure 3.7) As the substitution reaction proceeds, the number of nitrogen atoms connecting to framework tetrahedral may increase leading to 2N, 3N and 4N environments. The presence of all these different environments and substitution mechanism will be studied by various solid state NMR techniques and discussed throughout this thesis.

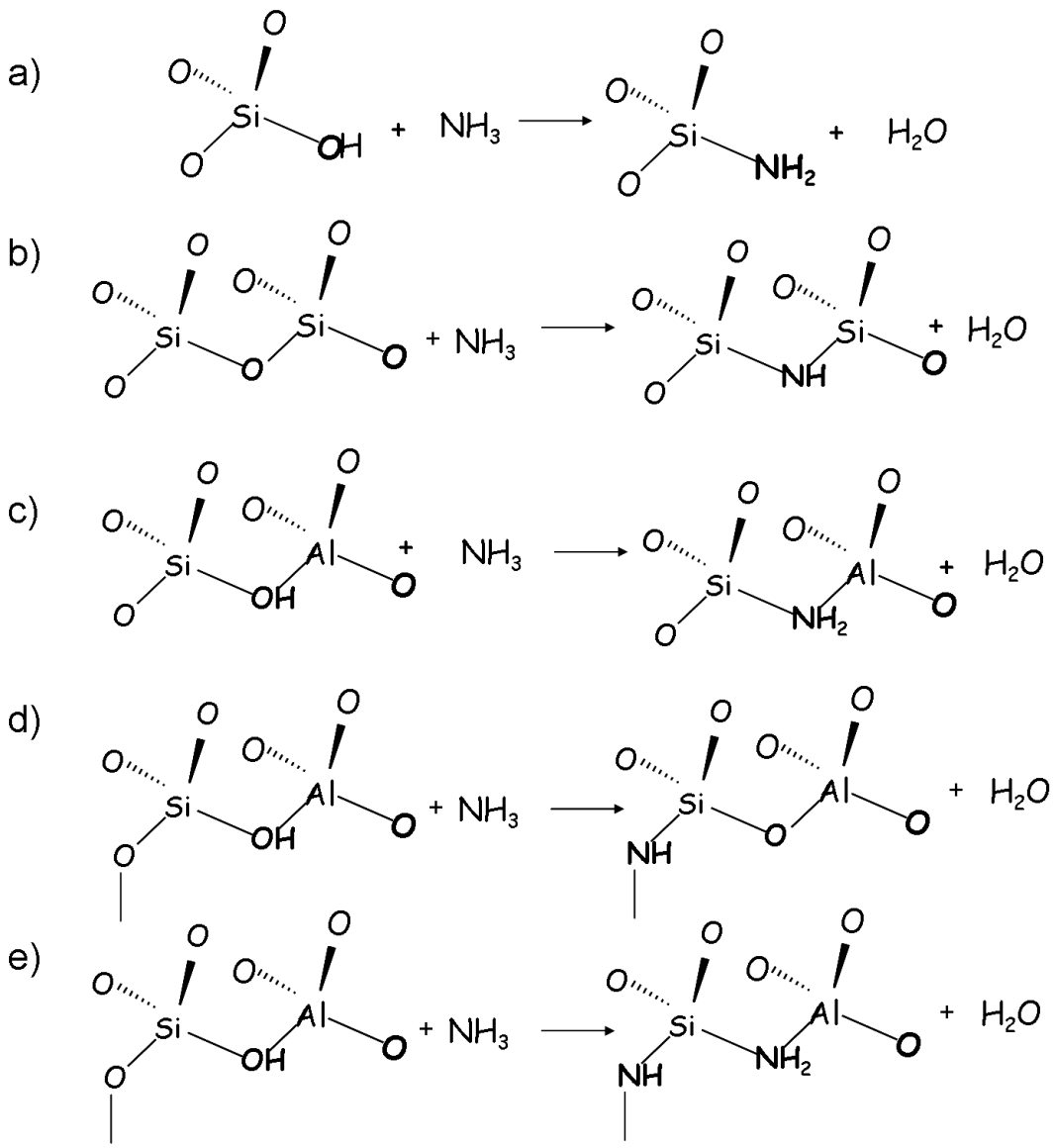

Figure 3.7. Possible reaction pathways of nitrogen substitution in zeolites. a) is nitrogen substitution to a silanol group forming terminal amines. b, c, d, and e are nitrogen substitutions to bridging Si-O-Si or Si-O-Al linkages.

3.3.4.2. ^{29}Si NMR of Starting Materials

The spectrum of the HY zeolite with a nominal Si/Al elemental ratio of 2.55 is dominated by the $Si(OSi)_4$ and $Si(OAl)(OSi)_3$ resonances at −107 and −102 ppm, respectively. A noticeably higher Si/Al ratio of 6.1 for the zeolite framework than implied based on the Si/Al elemental ratio was extracted from the intensities of the

different $Si(OAl)_x(OSi)_{4-x}$ resonances with Equation (1.13), indicating that significant dealumination has occurred. A similar phenomenon is observed for zeolite HY with a Si/Al elemental ratio of 15. Its spectrum is dominated by the $Si(OSi)_4$ resonance at around −107 ppm, yielding a Si/Al ratio of 42 for the framework. ^{27}Al MAS NMR of these samples (will be covered in the following chapter) contains signals at approximately 6 and 30 ppm, due to extra-framework 6- and 5-coordinate aluminum species, respectively. The significant concentration of extra-framework aluminum atoms is ascribed to a combination of the instability of the HY framework in the presence of moisture and the method used to prepare the lower aluminum content zeolites . The ^{29}Si MAS NMR spectra of NaY and NH_4Y (Si/Al ratio = 2.55) are dominated by resonances at around −102 and −95 ppm, which are assigned to $Si(OAl)(OSi)_3$ and $Si(OAl)_2(OSi)_2$ sites, respectively (Figure 3.8). Analysis of the ^{29}Si NMR spectra of these materials indicates that the dealumination is minimal, and a Si/Al ratio of 2.65 is obtained. The Si/Al ratios of the framework of the four zeolites used in this study are summarized in Table 3.1.

3.3.4.3. ^{29}Si NMR of Nit. HY (Si/Al = 15)

Nitrided low-aluminum HY shows considerable nitrogen substitution following ammonia flow at high temperatures (Figure 3.8.a). Slightly sharper line widths of the ^{29}Si resonances, as compared to the spectra of the other nitrided Y zeolites, are seen. This is attributed to the presence of fewer local silicon environments containing aluminum in the first coordination shells, and thus a smaller range of local environments. As seen in Figure 3.8.a, a new, asymmetric ^{29}Si resonance at approximately −86 ppm is observed along with a very weak resonance at around −66 ppm following ammonia treatment at 750°C. The resonance at −102 ppm due to the $Si(OHAl)(OSi)_3$ environment has almost completely disappeared, indicating that the these new resonances are due to nitrided silicon environments near both 0 and 1 aluminum atoms. On the basis of published literature, the −86 and −66 ppm peaks are assigned to $Si(NHSi)(OSi)_3$ / $Si(NH_2Al)(OSi)_3$ (1N) and $Si(NHSi)_2(OSi)_2$ / $Si(NH_2Al)(NHSi)(OSi)_2$ (2N) resonances, respectively. The loss of the $Si(OHAl)(OSi)_3$ resonance suggests that there is some preferential substitution

of terminal silanol groups and Si–OH–Al linkages, which is consistent with the lower energies associated with these reactions.

Upon increasing the temperature to 800°C, the intensity of the 1N (−86 ppm) resonance has increased and the −66 ppm (2N) resonance becomes more pronounced. A new peak at around −53 ppm, assigned to silicon near three NH/NH_2 groups (3N), is also observed. The −108 ppm $Si(OSi)_4$ resonance decreases in intensity, broadens, and shifts to −105 ppm. This shift and broadening is ascribed to distortion of the bond angles and bond lengths of the $Si(OSi)_4$ groups due to the nitridation of nearby sites (and/or the formation of defects). Upon reaching the maximum treatment temperature of 850 °C, a broad shoulder appears at around −43 ppm, the intensity of the high frequency peaks growing with reaction time. Given the almost complete disappearance of the 0N resonances in Nit.HY Si/Al=15.850.48, where the spectrum of the starting material is dominated by this resonance, the 1–4N resonances in this sample material are likely dominated by environments that do not contain any aluminum in their local coordination shells. Thus, the resonances at −86, −66, −53, and −43 ppm are assigned as $Si(NHSi)_x(OSi)_{4-x}$, with x = 1, 2, 3, and 4, respectively. Close examination of the resonances reveals that weaker resonances are hidden under the dominant resonances, which are assigned to environments containing aluminum and possibly NH_2 groups. In particular, the 1N resonance in the Nit.HYSi/Al=15.750.24 spectrum shows noticeable asymmetry, which are ascribed to different local environments such as $Si(NHSi)(OSi)_3$ and $Si(NH_2Al)(OSi)_3$.

$^1H/^{29}Si$ CP MAS NMR spectroscopy was performed to investigate the proximity of the hydrogen and silicon atoms. The CP enhancements, obtained by comparing the intensities of the resonances obtained in the CP spectra acquired at short contact times (ct = 0.1, 0.2, and 0.5 ms) with those seen in the single pulse experiments, are −66 ppm (2N) > −86 ppm (1N) >> −107 ppm for Nit.HYSi/Al=15.800.24 (Figure 3.9.a). CP enhancements, particularly at short contact times, reflect silicon environments near a larger number of protons, since the larger the number of protons in the group, the stronger the ^{29}Si-^1H dipolar interaction and the faster the transfer of magnetization from the ^1H to ^{29}Si nuclei. This is consistent with the argument that the higher frequency resonances are due to silicon near increasingly larger numbers of nitrogen, since the

substituted nitrogen will be present in the form of an NH group (or NH_2 for Si–NH_2–Al linkages), confirming our spectral assignments. $^{1}H/^{29}Si$ CP MAS NMR experiments on the other nitrided HY-15 nitrided samples are in agreement with this conclusion. Although a peak at around −43 ppm has been assigned as Si_2NH and $Si(NH)_2$ by other authors[19], I assign this broad shoulder on the basis on the CP results to a combination of $Si(NHSi)_4$ sites and possibly terminal sites that contain four nearby nitrogen atoms.

Given the different errors associated with the various elemental analysis methods, a more reproducible and reliable method is required for establishing framework nitridation level. To this end, the percent nitrogen substitution was calculated from the single pulse ^{29}Si MAS NMR spectra (Table 3.1) by determining the intensity of each $Si(NH_yT)_x(OSi)_{4-x}$ resonance by spectral deconvolution as follows. It is assumed that the resonances centered at −107, −86, −66, −53, and −43 ppm correspond to x = 0, 1, 2, 3, and 4 nitrogen substitutions near one silicon atom, respectively, and that any overlap between spectral regions of the $Si(NH_yT)_x(OSi)_{4-x}$ resonances is accounted for in the peak deconvolution. The relative numbers of framework nitrogen and oxygen atoms are obtained by multiplying the intensity of each resonance by x and $4 - x$, respectively. This calculation implicitly assumes that nitridation of Si–O–Al, Si–O(H)–Al, and Si–O–Si bonds occurs randomly, the need for this assumption arising from the fact that we do not see the T sites occupied by aluminum. Note that a preference for Si–O(H)–Al or Si–O–Al substitution will result in an underestimation of the nitrogen content of the framework with this method, since the number of substitution sites per silicon atom is higher when aluminum atoms are present. The numbers based on NMR are intermediate between those estimated based on nitrogen elemental analysis and EDX. However, nitrogen contents based on the NMR spectrum reflect the nitrogen content of the *framework*, and the higher nitrogen content seen by EDX may reflect a higher nitridation level of the extraframework aluminum species. This will probably be more significant for samples nitrided at lower temperatures, since they should, kinetically, be easier to nitride than the framework. This method will also underestimate the nitrogen content if there are significant numbers of terminal Si–NH_2 groups, which may also account for some of the differences between the two methods, particularly at the highest temperature.

Nit.HY with Si/Al = 2.55: Upon nitridation at 750 °C, (Figure 3.7.b) the ^{29}Si MAS NMR spectrum of HY contains two new resonances at around −83 ppm (1N) and −66 ppm (2N), which are noticeably broader than the 1N and 2N resonances seen in the lower aluminum HY sample. The $Si(OHAl)(OSi)_3$ site (–102 ppm) has almost completely disappeared, indicating that (a) preferential attack of the Si–O(H)–Al sites has occurred, and (b) that many of the new silicon sites must contain aluminum atoms in the first cation coordination shell, accounting for the additional broadening of these resonances. Distinct resonances are observed in the ^{29}Si NMR of Nit.HY Si/Al=2.55.800.24, the chemical shift ranges due to 1N and 2N containing at least two different resonances at −86 and −81 ppm (1N) and −68 and −63 ppm (2N). Since substitution of aluminum for silicon in the SiO_2 framework causes a shift of approximately 5 ppm per aluminum atom, and lower frequency resonances (−86 and −68 ppm) are the dominant resonances in low aluminum HY zeolite, it is possible that the high frequency resonances arise from silicon near aluminum atoms, e.g., environments such as $Si(OAl)(NHSi)(OSi)_2$. However, since the bond angles of the Si–N–Al linkages are strained due to the rest of the zeolite framework, and the calculations (Table 3.2) indicate that Si–NH_2–Al environments resonate at a lower frequency than Si–NH–Si bonds, the assignment of the higher frequency shoulder remains ambiguous. Terminal sites such as $Si(OSi)_3NH_2$ or terminal sites with even higher nitrogen contents may also be present, producing even further peak broadening. The nitrogen substitution levels calculated by NMR (Table 3.1), as for the lower aluminum content material, fall in between those estimated based on nitrogen elemental analysis and based on EDX.

Upon increasing the reaction temperature to 850°C, almost no sign of the $Si(OSi)_3$ and $Si(OHAl)(OSi)_3$ resonances from the pristine material are seen, and the spectrum is dominated by the 2N resonance at −66 ppm. The weak shoulder around −44 ppm is assigned to the 4N environments $Si(NHSi)_4$, $Si(NH_2Al)(NHSi)_2(OSi)$, and $Si(NH_2Al)_2(NHSi)(OSi)$. The surface substitutions cannot account for this peak. Essentially all of the tetrahedral sites are substituted by at least one nitrogen atom without significant change in the crystal structure of the zeolite (Figure 3.2.b). This is consistent with the EDX elemental analysis, which indicates that 65.1 percent of the oxygen atoms have been replaced by nitrogen atoms (Table 3.1). Sharper resonances, particularly for

the 2N and 3N environments, are seen at higher temperatures. This is probably because at higher reaction temperatures, all Brønsted acid sites have been substituted and only Si–O–Si linkages (and non-protonated Si–O–Al linkages) remain. For example, the Nit.HY SI/Al=2.55.800.24 sample is dominated by the $Si(OSi)_4$ resonance, which on nitridation at 850ºC, (where this signal has completely disappeared) will only produce $Si(OSi)_{4-x}(NHSi)_x$ resonances. $^1H/^{29}Si$ CP MAS NMR results are also consistent with these assignments (Figure 3.9.b). The −66 ppm and −52 ppm resonances have enhanced peak intensities even at short contact times (0.1 to 0.5 ms), confirming that these sites are near more protons.

Nit.NH_4Y with Si/Al ratio = 2.55: The spectrum of NH_4Y zeolite following treatment at 750 °C (Figure 3.8.c) is similar to that of HY with an Si/Al ratio of 2.55, and the resonances can be similarly assigned. What is significant, however, is the dramatic decrease in the intensity of the resonances due to the $Si(OHAl)(OSi)_3$ and $Si(OHAl)_2(OSi)_2$ sites in the ^{29}Si MAS NMR, the resonance due to the residual $Si(OSi)_4$ sites dominating the spectrum. This appears to suggest a strong preference for nitridation of the environments containing aluminum. In this higher aluminum content zeolite, the nitridation is accompanied by a significant loss of crystallinity, as seen by XRD (Figure 3.2.c) and via the loss in micropore volume (Table 3.1). This dealumination will generate terminal defects in form of silanols, which should be easily nitrided. The loss of crystallinity and the variety of different nitrided species most likely contribute to the very broad resonances seen in this system, which are particularly pronounced following nitridation at 850°C for 24 and 48 h. The $^1H/^{29}Si$ CP MAS NMR data of nitrided NH_4Y also indicate that the environments corresponding to −52 and −43 ppm are highly protonated (Figure 3.9.c). Given the breadth of these spectra, I did not attempt to deconvolute the line shapes and use the ^{29}Si NMR spectra to extract the nitrogen content.

Nit.NaY with Si/Al ratio = 2.55: Although the NaY zeolite used herein has the same Si/Al ratio as the NH_4Y zeolite, NaY shows the least nitrogen substitution of all the zeolites treated with ammonia at high temperatures (Figure 3.8.d). Only negligible substitution is seen at 750 °C, and only the formation of a weak resonance at around −80 ppm is observed. This is consistent with the energy calculations, since the substitution between silicon and aluminum but *not* at an acid site costs more than

120 kJ/mol (compared to 100 kJ/mol for substitution at a Si–O–Si site). The sample prepared at 800°C for 24 h is still dominated by the 0N (SiO_4) resonances of the pristine zeolite, but now the new (1N) resonance at −81 ppm, with a shoulder around −78 ppm, is clearly resolved. The chemical shifts of these 1N resonances are less negative than the 1N resonances in the HY samples with lower aluminum content, which is ascribed to the presence of more aluminum atoms in the local silicon coordination shell. Some differences between the chemical shifts will also arise due to the replacement of H^+ by Na^+. For example, the 1N silicon resonance for H^+ zeolite shows a chemical shift within the range of −88 to −81 ppm, whereas the same site for Na^+ zeolite has a shift of approximately −78 ppm.

On increasing the temperature to 850°C, new sites with resonances at −63 and −53 ppm are observed, but the reaction does not go to completion. Even the spectrum of the material prepared at 850°C for 48 h still contains the −95 ppm ($Si(OAl)_3(OSi)$) resonance from the pristine NaY zeolite. The intensities (relative to those in the untreated material) of non-nitrogen substituted sites are $Si(OAl)_3(OSi) > Si(OAl)_2(OSi)_2 > Si(OAl)(OSi)_3$. This suggests that nitridation is slightly biased toward Si–O–Si sites for zeolite NaY. This phenomenon appears to occur at all temperatures studied, a comparison of the relative intensities of the ^{29}Si resonances of nitrided NaY zeolite prepared at 750 and 800°C also suggesting that nitrogen substitution occurs preferentially at silicon oxide tetrahedra with lower numbers of nearby aluminum atoms. This is supported by the higher energy of Si–NH–Al substitutions relative to Si–NH–Si substitutions. ^{1}H-^{29}Si CP NMR (Figure 3.9.d) and CP kinetics for each resonance (not shown) show that the −53, −63, and −78 ppm sites are in closer proximity to more protons than the other sites, confirming that those resonances correspond to nitrogen substitution.

The nitrogen content values calculated by NMR are lower than those obtained by EDX analysis, as was the case for the other treated zeolites, for the materials treated at 750 and 800°C. However, for the material treated at 850°C, the NMR and EDX results are similar. We observe similar trends for the other high temperature treated zeolites. This may be related to the fact that EDX is more sensitive to the elemental composition closer to the surface than in the center of the particle (i.e., the first 0–0.75 mm), suggesting that the substitution at lower temperatures may be less uniform than the

substitution at high temperatures. We note that the slight tendency for substitution at Si–O–Si vs. Si–O–Al sites means that, in contrast to the HY samples, this NMR method will lead to a slight overestimation of the nitrogen content of the framework.

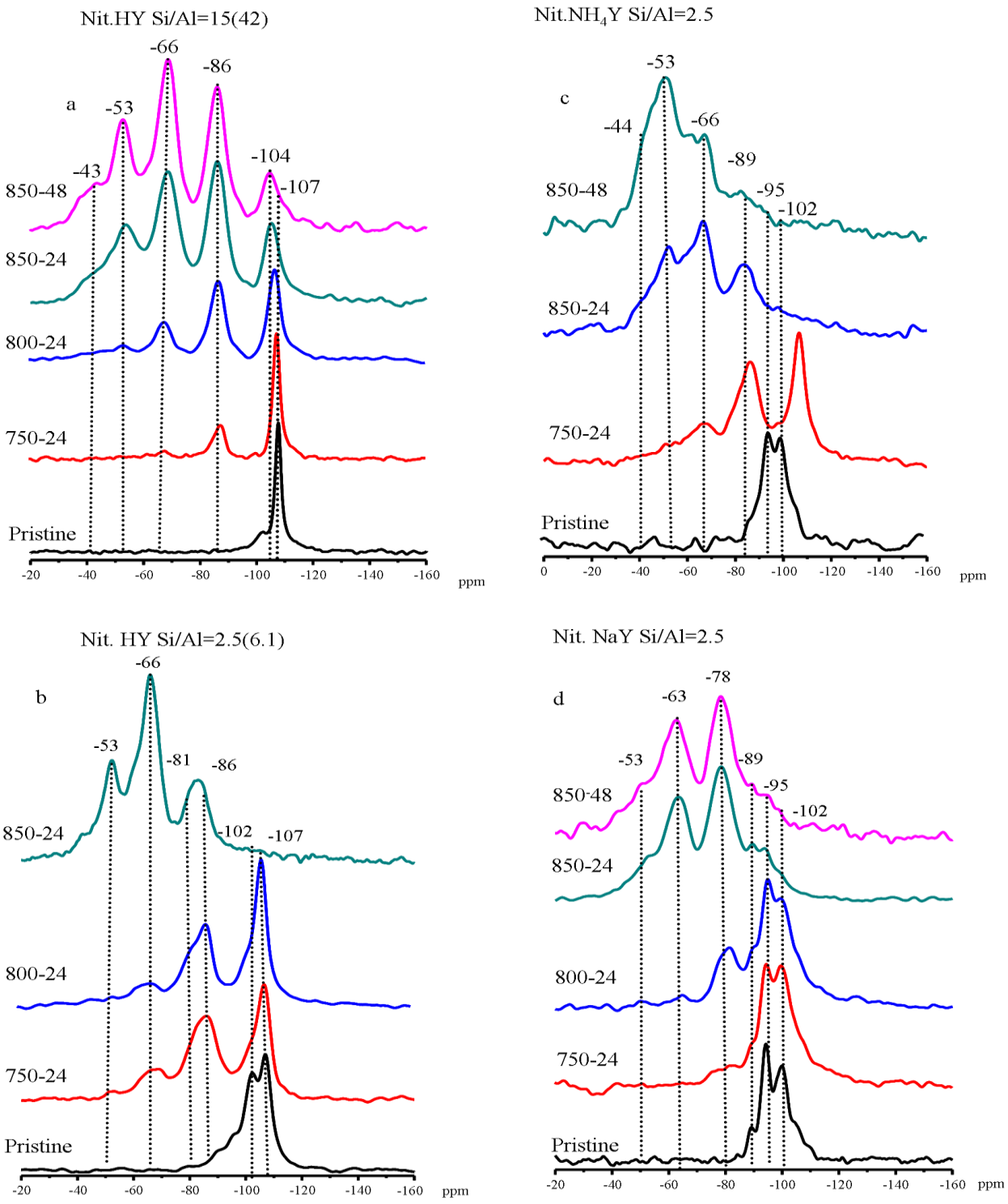

Figure 3.8. (a, b, c, d) ^{29}Si MAS NMR of nitrogen substituted zeolite HY Si/Al ratio of 15 and 2.5, NH4Y and NaY, respectively. The substitution reaction was performed at different reaction temperatures and reaction times. Dashed lines show the formation of new silicon environments.

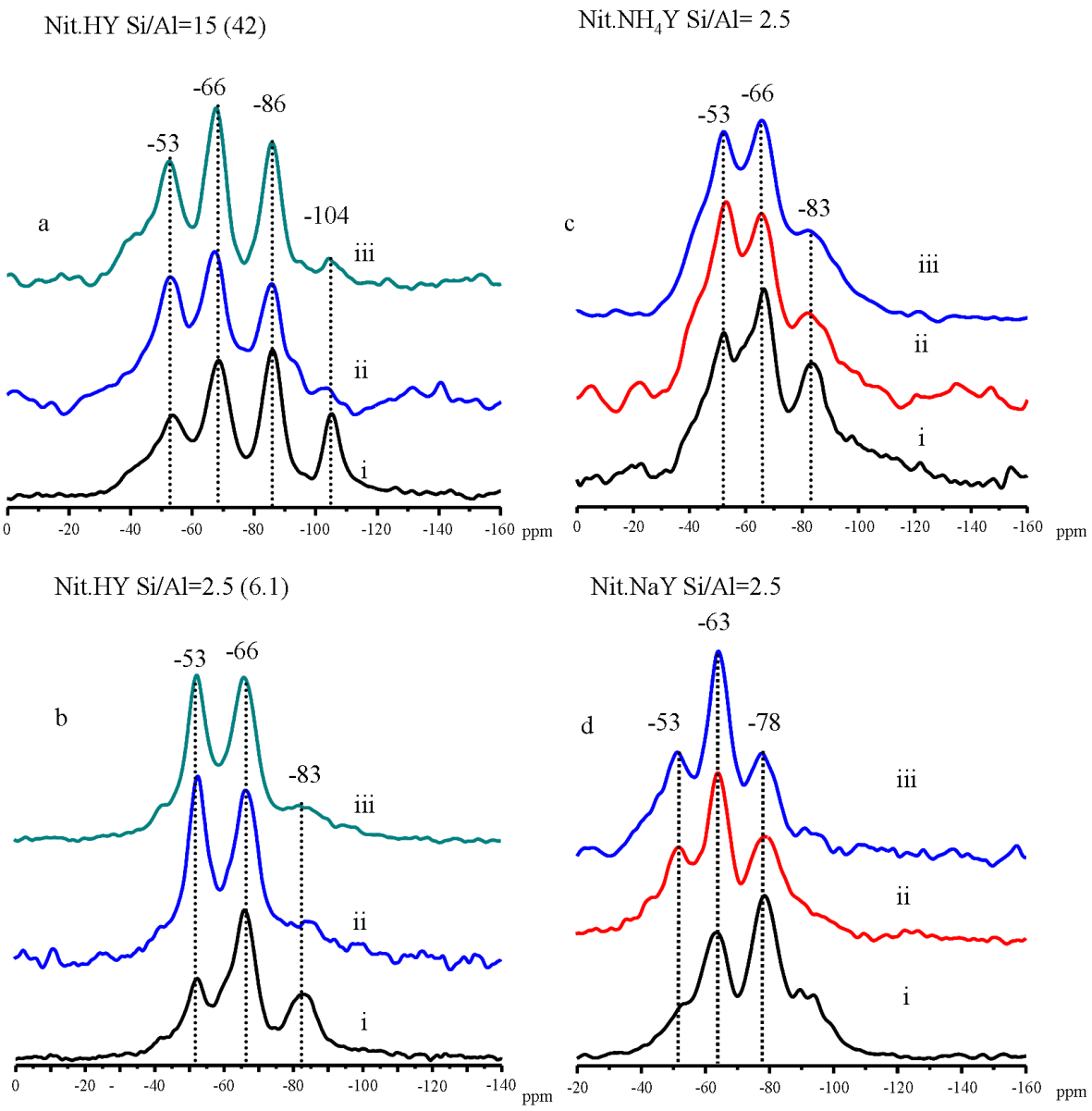

Figure 3.9. ^{29}Si SP and CP MAS NMR data for nitrogen substituted zeolite Y with different aluminum content and extraframework cation. Samples are prepared under ammonia at 850°C for 24 h. Dashed lines show the formation of new silicon environments. Ii is the single pulse experiment, ii and iii, CP experiment with contact times of 0.2 and 0.5 ms, respectively.

3.4. Conclusions

The effects of aluminum content and charge-compensating cation on the nitridation of zeolite Y using high-temperature ammonia have been studied using a combination of modeling, NMR spectroscopy, adsorption, and X-ray diffraction. The appearance and evolution of new silicon resonances in the ^{29}Si MAS NMR spectra and the results of nitrogen content measurements of samples prepared at various temperatures using various reaction durations show that the degree of substitution increases with increasing reaction temperature and time. The effects of reaction conditions such as ammonia flow rate will be discussed in detail in the following chapter. Zeolites with higher Si/Al ratios show more well-resolved and sharp ^{29}Si MAS NMR spectra and higher crystallinity after the reaction, whereas, protonated acidic zeolites with high aluminum content lose their crystallinity and microporosity during the ammonia treatment. In particular, although nitrided NH_4Y undergoes the highest nitrogen substitution under the same conditions as compared to the sodium and low aluminum acidic zeolites, it decomposes in the process and therefore will be less useful as a catalyst for reactions that require high surface areas and shape selectivity arising from porosity. The presence of sodium as a charge-compensating cation provides higher stability, but decreases the extent of the reaction.

The comparisons between measured and calculated ^{29}Si MAS NMR chemical shifts show good agreement, providing strong evidence that high levels of nitrogen substitution have been achieved. The calculations on small nitrogen-substituted zeolite clusters show that the nitridation reaction is energetically unfavorable, and that the expected energy of reaction for different silicon environments is Si–OH–Al < Si–O–Si < Si–O–Al. This preference is less pronounced or absent for higher reaction temperatures, in part because all of the Si–O(H)–Al sites have already reacted at these temperatures. Nitrogen substitution of NaY zeolite shows a lower degree of substitution than the treated HY zeolites at low temperatures. This is supported by the calculations, which show a higher energy of substitution for the Si–NH–Al connectivity relative to the Si–NH–Si and Si–NH_2–Al connectivities. Sodium Y substitutions are slightly biased toward reaction of Si–O–Si over Si–O–Al groups, as seen in the analysis of the change in

$Si(OSi)_{4-y}(OAl)_y$ resonances with temperature and in the simulations of the experimental data.

The PDF analysis on the pristine and ammonia treated zeolite samples provide information about the changes in the bond lengths and bond angles with nitrogen substitution of the zeolite framework. The results show that the Si-N distance in the 1st shell is longer than Si-O bond distance and Si-Si/Al bond distance of the Si-O/N-Si/Al linkage decreases, as an indication of a decrease in bond angle and they are in agreement with the theoretical calculations.

Adsorption isotherms show that the crystalline samples maintain substantial microporosity post-treatment, although some pore-blocking/loss of crystallinity has clearly occurred. This shows that low-aluminum zeolites in particular can be treated with ammonia to produce crystalline, microporous, nitrogen-substituted zeolites. These materials are expected to behave as relatively strong solid base catalysts. The basicity of treated zeolites with different compositions will be discussed in the last chapter. Further characterization experiments are needed to investigate the detailed mechanisms of nitrogen substitution, as well as the nature of the nitrogen substituted environments in treated zeolites. In the following chapters a combination of ^{27}Al, ^{1}H MAS NMR and double resonance techniques will be used and the reaction mechanism for nitrogen substitution of zeolite Y will be discussed.

3.5. References

(1) S. M. Auerbach, K. A. C., P. K. Dutta *Handbook of Zeolite Science and Technology*; Marcel Dekker Inc., 2003.

(2) Weitkamp, J. *Solid State Ionics* **2000**, *131*, 175.

(3) Haw, J. F. *Phys. Chem. Chem. Phys.* **2002**, *4*, 5431.

(4) Wan, K.; Liu, Q.; Zhang, C.; Wang, J. *Bull. Chem. Soc. Jpn.* **2004**, *77*, 1409.

(5) Weitkamp, J.; Hunger, M.; Rymsa, U. *Microporous and Mesoporous Materials* **2001**, *48*, 255.

(6) Barthomeuf, D. *Microporous Mesoporous Mater.* **2003**, *66*, 1.

(7) Narasimharao, K.; Hartmann, M.; Thiel, H. H.; Ernst, S. *Microporous and Mesoporous Materials* **2006**, *90*, 377.

(8) Zhang, X.; Lai, E. S. M.; Martin-Aranda, R.; Yeung, K. L. *Appl. Catal., A* **2004**, *261*, 109.

(9) Ernst, S.; Hartmann, M.; Sauerbeck, S.; Bongers, T. *Appl. Catal., A* **2000**, *200*, 117.

(10) Zhang, X. F.; Lai, E. S. M.; Martin-Aranda, R.; Yeung, K. L. *Applied Catalysis a-General* **2004**, *261*, 109.

(11) Suppes, G. J.; Dasari, M. A.; Doskocil, E. J.; Mankidy, P. J.; Goff, M. J. *Applied Catalysis a-General* **2004**, *257*, 213.

(12) Yamamoto, K.; Sakata, Y.; Nohara, Y.; Takahashi, Y.; Tatsumi, T. *Science (Washington, DC, U. S.)* **2003**, *300*, 470.

(13) Kerr, G. T.; Shipman, G. F. *J. Phys. Chem.* **1968**, *72*, 3071.

(14) Chino, N.; Okubo, T. *Microporous Mesoporous Mater.* **2005**, *87*, 15.

(15) Xiong, J. M.; Ding, Y. J.; Zhu, H. J.; Yan, L.; Liu, X. M.; Lin, L. W. *Journal of Physical Chemistry B* **2003**, *107*, 1366.

(16) Han, A.-J.; He, H.-Y.; Guo, J.; Yu, H.; Huang, Y.-F.; Long, Y.-C. *Microporous Mesoporous Mater.* **2005**, *79*, 177.

(17) Zhang, C.; Xu, Z.; Liu, Q. *J. Wuhan Univ. Technol., Mater. Sci. Ed.* **2005**, *20*, 32.

(18) Zhang, C.; Liu, Q.; Xu, Z. *J. Non-Cryst. Solids* **2005**, *351*, 1377.

(19) El Haskouri, J.; Cabrera, S.; Sapina, F.; Latorre, J.; Guillem, C.; Beltran-Porter, A.; Beltran-Porter, D.; Marcos, M. D.; Amoros, P. *Advanced Materials* **2001**, *13*, 192.

(20) Hammond, K. D.; Dogan, F.; Tompsett, G. A.; Agarwal, V.; Conner, W. C.; Grey, C. P.; Auerbach, S. M. *J. Am. Chem. Soc.* **2008**, *130*, 14912.

(21) Astala, R.; Auerbach, S. M. *J. Am. Chem. Soc.* **2004**, *126*, 1843.

(22) Lesthaeghe, D.; Van Speybroeck, V.; Marin, G. B.; Waroquier, M. *J. Phys. Chem. B* **2005**, *109*, 7952.

(23) Martinez-Inesta, M. M.; Peral, I.; Proffen, T.; Lobo, R. F. *Microporous and Mesoporous Materials* **2005**, *77*, 55.

(24) Proffen, T.; Billinge, S. J. L.; Egami, T.; Louca, D. *Zeitschrift Fur Kristallographie* **2003**, *218*, 132.

(25) Loewenstein, W. *Am. Mineral.* **1954**, *39*, 92.

(26) Kao, H.-M.; Grey, C. P. *J. Phys. Chem.* **1996**, *100*, 5105.

(27) Luz, Z.; Vega, A. J. *J. Phys. Chem.* **1987**, *91*, 374.

(28) Wouters, B. H.; Chen, T.; Grobet, P. J. *J. Phys. Chem. B* **2001**, *105*, 1135.

(29) Ciraolo, M. F.; Hanson, J. C.; Norby, P.; Grey, C. P. *J. Phys. Chem. B* **2001**, *105*, 2604.

Chapter 4

Investigation of the Structural Changes and Reaction Mechanism of Nitrogen Substituted Zeolite Y by Multinuclear NMR Spectroscopy

Abstract

Multinuclear Solid State Nuclear Magnetic Resonance Spectroscopy is used to study the changes in the local structure and the mechanism of nitrogen substitution on zeolite Y. The reaction is performed on NaY and HY types of zeolites with different aluminum content. ^{27}Al Single Pulse and Multiple Quantum Magic Angle Spinning NMR studies performed on zeolite samples prepared at variable reaction conditions show signs of dealumination of the framework in the early stages of the substitution reaction in proton type of zeolites, whereas, the NaY zeolite is thermally more stable. As the reaction proceeds with increasing temperature and time the nitrogen substitution then continues over the siliceous framework. Even for the high nitrogen content zeolites, ^{27}Al NMR data shows low nitrogen substitution levels for framework aluminum tetrahedra suggesting preferential substitution towards Si-O-Si linkage for high reaction temperatures and reaction times. The nature of the proton sites and expected basic groups in the nitrogen substituted zeolites is investigated by ^{1}H MAS NMR spectroscopy. The data is consistent with other the MAS NMR experiments showing an increase in the formation and intensity of NH/NH_2 sites as the reaction temperature and time increases [1].

4.1. Introduction

Basic zeolites can be obtained by modification of the zeolite framework by substitution of nitrogen with framework oxygen[1-6]. Using this approach, the Lewis basicity of the framework may increase owing to the lower electronegativity of nitrogen with respect to oxygen[7]. The substitution reaction can be performed by treating the dehydrated pristine zeolite with ammonia at high temperatures[1,3]. Our characterization results, discussed in the previous chapter, have shown that high levels of nitrogen substitution can be achieved while maintaining porosity, particularly for NaY and low-aluminum HY materials, without significant loss in the crystallinity[1,6]. Experiments performed at lower temperatures (750–800 °C) showed a preferential attack at Si–OH–Al sites as shown by ^{29}Si MAS NMR which are also consistent with DFT studies on the energy changes with substitution of nitrogen to different bridging oxygens[8]. However, a number of issues remain, which include the overall mechanism and nature of the sites at the end of substitution reactions, which have not been clearly investigated. Here we will present additional solid state NMR experiments to study the local environments of nitrogen substituted zeolites and reaction mechanisms.

Nuclear Magnetic Resonance spectroscopy has been widely used and it is an attractive technique to characterize zeolitic structures as they are composed of all spin active nuclei such as ^{1}H, ^{27}Al, ^{29}Si and ^{23}Na[9-11]. NMR is a sensitive method for the investigation of local structure of both framework and extraframework atoms and has an advantage of studying the acid sites, catalytic actives centers and binding sites within the pores of zeolite catalysts[11-14]. As presented in previous chapters, ^{29}Si MAS NMR spectroscopy is extremely useful to study the changes in the local environments of silicate tetrahedra during nitrogen substitution reactions within the zeolite framework. We have shown that the substitution of nitrogen for oxygen results in a shift of 15-20 ppm to higher frequencies for each nitrogen addition in ^{29}Si NMR spectra, providing a sensitive method to study the degree of nitridation as well as the nature of newly formed groups[1].

The application of ^{27}Al MAS NMR to nitrogen doped zeolites can be used as an effective probe to confirm the changes that occurred on the aluminum sites (Si-O-Al

bridges) after the nitridation treatment and provide information on the selectivity of nitrogen substitution to Si-O-Si over Si-O-Al linkages. ^{27}Al MAS NMR has been widely used to study the coordination state and distribution of aluminum atoms both at framework and extrframework positions in untreated dehydrated and steamed zeolites[9,15,16].

Aluminum has a half integer (spin 5/2) nuclear spin possessing an electric quadrupolar moment which interacts with Electric Field Gradient (EFG) at the nucleus. The EFG depends on the geometry and the electric charge distribution around the aluminum atoms and therefore the information derived from the data can be used as a probe for local aluminum environment in the material. Since the spectral resolution of the central transition of ^{27}Al NMR resonance is affected by the 2ndorder quadrupolar interaction (Figure 1.8), the interpretation is not straight forward. An accurate value of the chemical shift can not generally be extracted directly from the spectrum as the isotropic shift is the sum of chemical shift and quadrupole induced shift. Thus, the use of Multiple Quantum MAS NMR (MQMAS) (Section 1.4.1.2) is useful for the detection of isotropic resonances (δ_{iso}), for obtaining well resolved spectra and also obtaining the quadrupolar coupling constant (C_Q) and asymmetry parameter (η), which reflect the electron distribution surrounding the aluminum site [10-12].

In pristine zeolites, ^{27}Al MAS NMR spectra show distinct chemical shift ranges for tetrahedral, pentacoordinate and octahedral environments, thus the framework and extraframework aluminum can be distinguished from each other. Aluminum tetrahedral framework atoms typically resonate at 50-60 ppm, whereas five and six coordinate extraframework species resonate at 25 to 30, and -17 to 13 ppm, respectively[12,15,16]. However, for the steam-dealuminated zeolites there have been debates on the nature of the 30 ppm resonance. Double rotation (DOR) ^{27}Al NMR studies at different magnetic fields showed that the nature of the Al species depends on the method of dealumination. Fyfe *et al* studied aluminum environments in the ultrastable Y zeolite catalyst formed by steaming HY zeolite and observed a broad ^{27}Al MAS NMR line shape covering the 100 − -50 ppm region with peak maximums at 58, 30 and -3 ppm at 9.4 Tesla[17,18]. They repeated the experiments at higher fields (18.8 MHz), where they obtained clearly resolved sharper peaks at 61, 30 and 1 ppm with a shoulder at 54 ppm which were

assigned as 4-coordinate, 5-coordinate, 6-coordinate and distorted 4-coordinate aluminum environments respectively. Thus, either distorted tetrahedral aluminum sites or five coordinated sites can be attributed to the 30 ppm resonance. M. Hunger and co-workers performed various studies on the effect of dehydration and dealumination on the local environment of aluminum sites in zeolites and studied the quadrupolar interactions by ^{27}Al MQMAS NMR[19]. The calculated C_Q values reported for nonhydrated NaY and HY zeolites 4-coordinate aluminum sites were 5 and 16 MHz, respectively whereas for hydrated HY zeolite it was reported as 2 MHz. For 5-coordinate and octahedral aluminum sites, which were observed in steamed zeolite Y, C_Q values of 7.5 and 0.5 MHz were reported, respectively.

^{27}Al MAS NMR studies of silicon aluminum oxynitride ceramics have shown the following chemical shift ranges for aluminum environments with varying nitrogen coordination: AlN_4, 114-105 ppm, AlN_3O 93 ppm, AlO_2N_2 and AlO_3N 89 and 75 ppm[12,20]. Thus, with nitrogen substitution of framework oxygen, the chemical shift of the aluminum sites is expected to move to higher frequencies.

^{1}H NMR is mainly used to investigate acidity and the defect sites in the zeolite framework created during the synthesis, dehydration or catalytic reactions[9,10,21]. In this study, ^{1}H MAS spectroscopy has been used to characterize the proton groups formed on nitrogen substitution of zeolite Y. Characterization of such groups is important to obtain information on both basic and acidic catalytic sites formed during the nitrogen substitution reaction. Therefore, ^{1}H MAS NMR is used to determine whether any N-H and N-H_2 groups are formed in the modified zeolite samples. ^{1}H/^{14}N and ^{1}H/^{27}Al transfer of populations in double resonance (TRAPDOR) MAS NMR experiments are also performed on the higher N-content materials to help in our assignments (section 1.4.1.2.). The TRAPDOR method probes the heteronuclear dipolar interactions and thus internuclear distances between two (or more) nuclei (e.g., ^{1}H-^{14}N, ^{1}H-^{27}Al), where one nucleus is quadrupolar[14,22]. This experiment is particularly useful when the quadrupolar nucleus is difficult to detect directly, which is typically the case for ^{14}N. The technique provides a very powerful tool for assigning linkages. If a TRAPDOR effect is observed, then the peak of the dipolar coupled species undergoes a decrease in intensity which can be checked from the difference spectra of the control and the double resonance

experiment (showing the proton sites in the vicinity of nitrogen or aluminum atoms). The TRAPDOR effect or the intensity of these difference spectra is affected by the quadrupolar coupling constant of the irradiated nuclei. Higher quadrupolar interactions result in lower intensity resonance peaks in the difference spectra under non-adiabatic conditions[22].

In this chapter, the structural changes and formation of new sites in the framework of nitrogen substituted zeolites are studied by using ^{27}Al MAS NMR and ^{1}H MAS NMR spectroscopy. The samples studied are the nitrogen substituted zeolites discussed in the previous chapter. Zeolite Y samples with different extraframework cation and aluminum content were treated under ammonia at varying reaction temperature and durations. ^{27}Al Single Pulse (SP) and Multiple Quantum MAS NMR spectroscopy were applied on these samples to study the local symmetry, the coordination state and nature of the aluminum species in the nitridated zeolites where as ^{1}H MAS NMR and ^{1}H/^{14}N and ^{1}H/^{27}Al TRAPDOR MAS NMR were used for characterization of both basic and acidic sites in highly nitrogen doped zeolite Y. The correlations between different protons environments and nitrogen silicon tetrahedra having different aluminum connections were studied by ^{1}H/^{29}Si HETCOR MAS NMR experiments.

4.2. Experimental

4.2.1. Materials

The synthesis of nitrogen substituted zeolites used in this study is described in the previous chapter in Section 3.2.1. The pristine dry zeolites were prepared by heating the samples first to 110^{o}C and keeping at the temperature for 3 hours under constant vacuum and then heating to 400^{o}C where they were kept under vacuum overnight. All the samples for the characterization experiments are loaded into NMR rotors in a glovebox. The following nomenclature is used to label the samples: The first label “Nit” indicates that zeolites are nitridated. The type of the zeolite (e.g., HY, NaY) and Si/Al ratio is then given, which is then followed by the nitridation temperature in ^{o}C and the last the treatment duration in hours.

4.2.2. Characterization

^{27}Al MAS NMR studies were carried out with a double resonance 4 mm probe with a spinning rate of 12 kHz on a 11.7 Tesla spectrometer. The spectra were referenced to a 1 M solution of $Al_2(SO_4)_3$ at 0 ppm. Single pulse experiments were performed with a pulse width of 0.5μs and a pulse delay of 2 μs. The ^{27}Al MQMAS NMR experiments were carried out using the 'z-filter' method (Figure 1.10). A standard triple quantum MAS pulse sequence with two hard pulses followed by a soft 90 degree solid pulse was applied. The experiment was performed at a 10 kHz spinning rate. The 2nd order quadrupolar parameters and isotropic chemical shift values are calculated by the simulation of the slices of the F_2 dimensions of 2D ^{27}Al MQMAS data and also by the calculations using the following formula:

$$\delta_{CS}^{iso} = \frac{10}{27}\delta_{G2}^{obs} + \frac{17}{27}\delta_{G1}^{obs} \qquad [4.1]$$

where δ_{G1}^{obs} and δ_{G2}^{obs} are the observed chemical shift of the center of gravity in isotropic dimension and in anisotropic dimensions, respectively. All the simulations were done with the WSolids NMR simulation package by K. Eichele.

^{1}H SP and Spin-Echo MAS NMR experiments are conducted on a Varian 500 MHz spectrometer with a 14 kHz spinning speed on a 4mm probe with 90^o pulse lengths of 2 μs. A pulse delay of 1s was used and the ^{1}H chemical shifts are referenced to tetramethylsilane (TMS) at 0 ppm. The spectra were normalized per unit weight of sample and keeping the acquisition number same for each experiment. All the dehydrated/nitrided samples were packed into NMR rotors under a dry nitrogen atmosphere in a glove box.

The RF field strengths used for ^{1}H/^{29}Si HETCOR experiments are ~42 and ~100 kHz for ^{29}Si and ^{1}H, respectively. Contact times of 0.1 to 10 ms were used in the experiments and the Hartmann-Hahn condition was set by using nitrogen substituted HY sample. The samples were spun at 10 kHz.

^{1}H/^{14}N and ^{1}H/^{27}Al TRAPDOR experiments were performed on a Varian 500 MHz spectrometer with a 5 kHz MAS frequency. We used a variant of the TRAPDOR experiment where ^{14}N or ^{27}Al irradiation was applied in both the evolution and refocusing

periods of the spin-echo experiments. RF field strengths for the ^{14}N and ^{27}Al nuclei of 46 and 56 kHz, respectively were used. Evolution periods of 200 and 800 μs, corresponding to 1 and 4 rotor periods, were used and a difference spectra was obtained by subtracting the TRAPDOR ($^{27}Al/^{14}N$) spectra from the control (i.e., the normal echo) spectra.

4.3. Results and Discussion

4.3.1. ^{27}Al MAS NMR

4.3.1.1. Effect of Temperature and Ammonia Flow on Zeolite Y Structure

Figure 4.1 and Figure 4.2 show the Single Pulse (SP) ^{27}Al MAS NMR data for the pristine and nitridated Y zeolites, with different aluminum contents and extraframework cations treated at different reaction conditions. The data includes a comparison of ^{27}Al NMR data for wet and dry pristine samples, showing the changes in the local environment of the aluminum sites in the pure material on dehydration. The pristine wet HY zeolites both with high aluminum and low aluminum content (Figures 4.1.a and 4.1.b) have a peak at around 0 ppm due to a 6-coordinate aluminum site indicating that the commercial HY zeolites are slightly dealuminated and contain extraframework aluminum sites. The dealumination was also supported by ^{29}Si NMR and the calculated Si/Al ratios from the data were higher than the reported values by the zeolite company (Chapter 2). ^{27}Al MAS NMR of both the pure and dry HY zeolite with low aluminum content (Si/Al=15) show a large quadrupolar broadening resulting from distortion of tethrahedral framework aluminum and formation of 5-coordinate extraframework $Al(OH)^{2+}$ species due to further dealumination caused by the dehydration process, as reported in previous studies[17,18,23] (Figure 4.1.i.a). Dehydrated HY zeolite with a higher aluminum content (Si/Al =2.5) also shows a similar trend and the formation of 5-coordinate extraframework species, but with less deformation and smaller quadrupolar broadening in ^{27}Al MAS NMR. This can be explained by a smaller amount of extraframework aluminum cations when compared to the lower aluminum content zeolite. The HY zeolites are synthesized from NH_4Y zeolites by removing the NH_3 with high temperature treatments. During this

thermal treatment, dealumination occurs which leads to the formation of extraframework cations. High silica (low aluminum content) zeolites are obtained by dealumination of higher aluminum content zeolites (generally by steaming the zeolite framework) and usually the extraframework cations are not totally washed away during the commercial synthesis. Therefore the product always contains extraframework aluminum cations. As seen in Figure 4.1.i.c, the pristine wet NH_4Y zeolite has none of these effects and only contains 4- coordinate framework aluminum which is seen as a peak around 60 ppm in ^{27}Al MAS NMR data. Similarly, the aluminum data for the pristine wet NaY zeolite shows only one environment for framework aluminum (4-coordinate) with peak maxima around 60 ppm. ^{27}Al MAS NMR shows no sign of dealumination for the dry NaY zeolite during the dehydration process (Figure 4.2.a). Compared to the wet sample, it shows line broadening due to the strong electric nuclear quadrupolar interactions, as the geometries of the tetrahedral sites deviate from ideal geometries upon dehydration.

Figures 4.1 and 4.2 show ^{27}Al and ^{29}Si MAS NMR data of nitrogen substituted zeolite Y treated under different reaction conditions. As discussed in the previous chapter, with ammonia flow over zeolite Y formation of new peaks and a gradual change in the intensity of these peaks is observed in the ^{29}Si MAS NMR spectra as the ammonia flow time and temperature increases. ^{27}Al MAS NMR also show a similar trend; with changing reaction conditions a gradual change is observed in terms of new peak formation, increase in the intensity of these new peaks and line broadening. This observation indicates possible nitrogen substitution of the zeolite framework either through Al-O-Si linkages or through Si-O-Si linkages adjacent to an aluminum tetrahedron. The observed line broadening is the result of a distribution of different aluminum environments, as well as an increase of the quadrupolar interaction arising from the changes in the structure as a result of either nitrogen substitution or dealumination of the framework due to high temperature treatment and formation of H_2O during the reaction (Reaction 1.4 and 1.8). As discussed in the Introduction (Section 1.3.1) the formation of water introduces a "steaming" effect causing the dealumination of the framework aluminum. This effect is clearly observed for the NH_4Y type of zeolite with a Si/Al ratio of 2.55. In the previous chapter, the comparison of ^{29}Si MAS NMR spectrum of pristine NH_4Y zeolite and the nitrogen substituted form at 750^{o}C (therefore with a low nitrogen substitution level)

shows that the former has mostly Q^4(1Al) species (framework silicons with no terminal group and only one aluminum neighbor) and Q^4(2Al) sites (framework silicons with no terminal group and only two aluminum neighbors) where as the latter has mostly Q^4(0Al) environments as a sign of dealumination in the framework due to nitridation temperature treatment (Figure 4.1). The ^{27}Al MAS NMR of the same sample also supports this interpretation as the spectrum shows the presence of 5- and 6-coordinate extraframework aluminum sites with peaks at about 36 and 0 ppm, respectively.

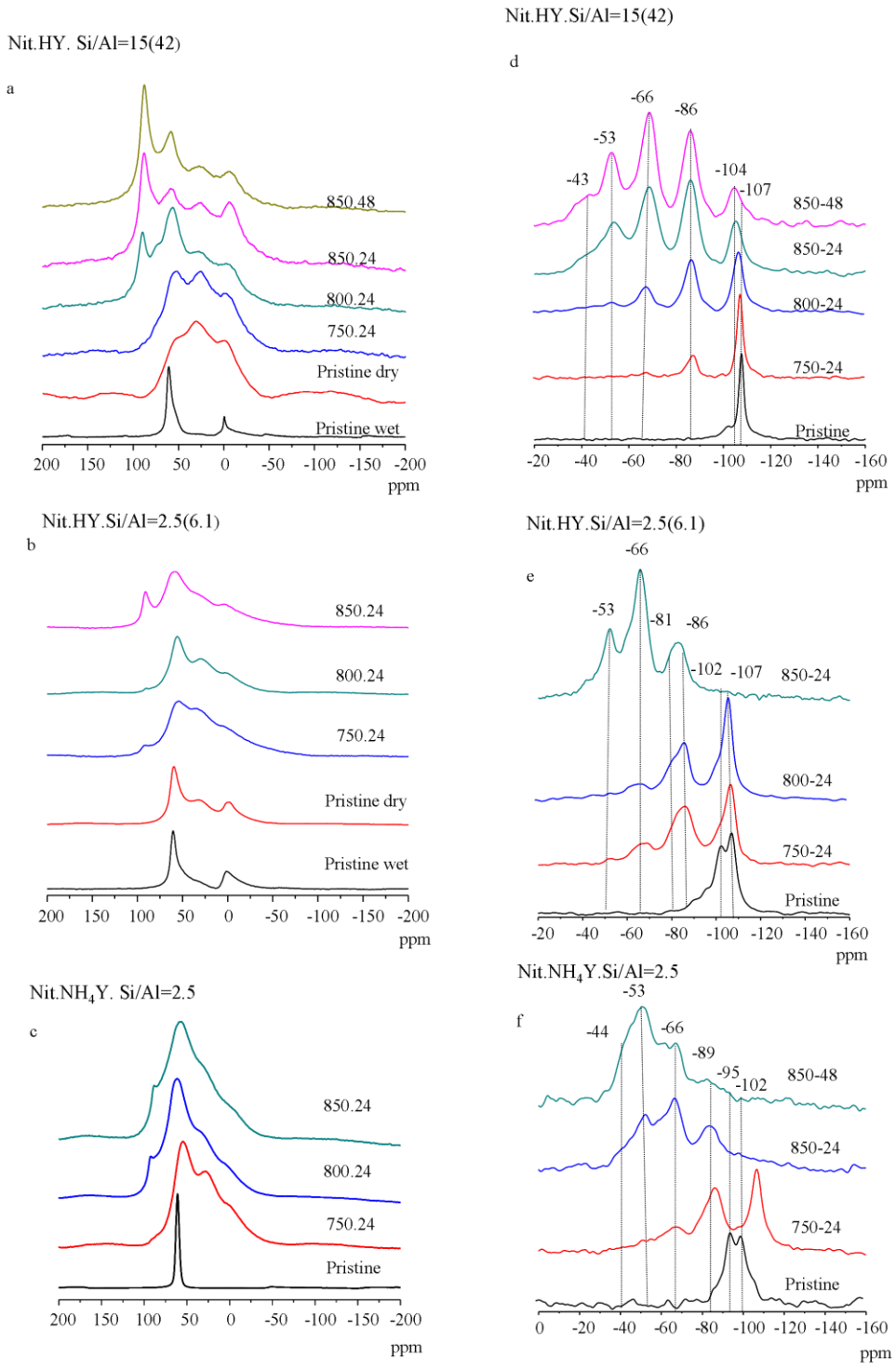

Figure 4.1. (a), (b), (c) ^{27}Al (11.7 T) and (d), (e), (f) ^{29}Si Single Pulse MAS NMR of nitrogen substituted zeolite Y. Samples are treated at different reaction times and temperatures. Numbers within parenthesis show the actual Si/Al ratio of the framework (Calculated by ^{29}Si MAS NMR).

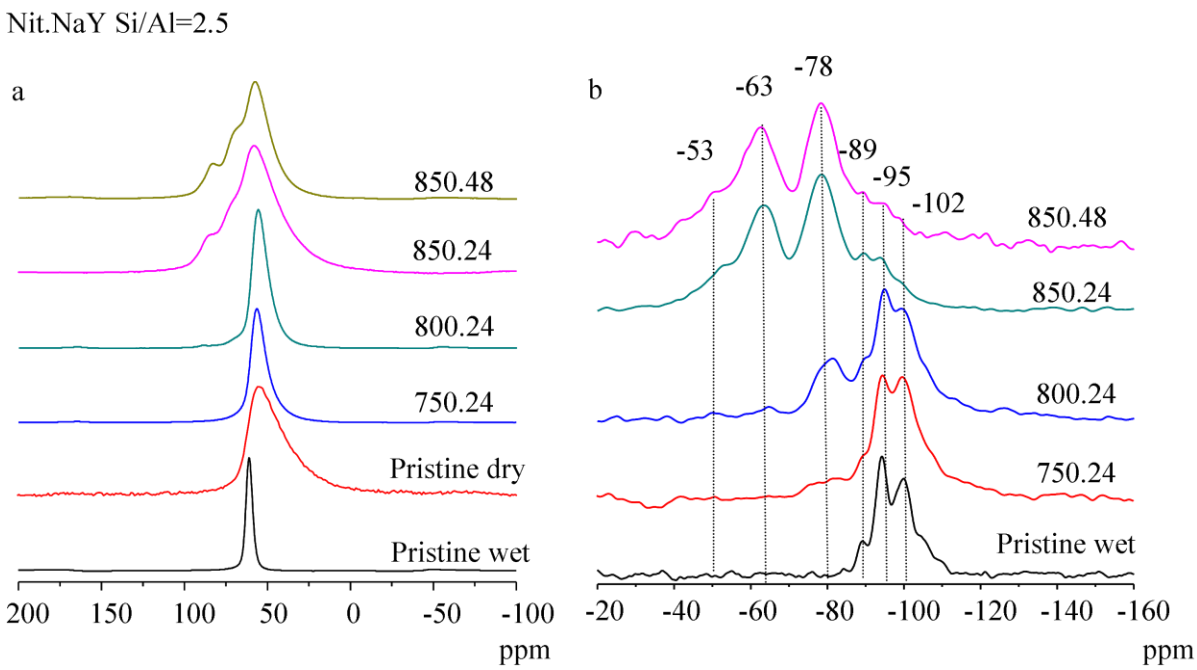

Figure 4.2. (a) ^{27}Al (11.7 T) and (b) ^{29} Si Single Pulse MAS NMR spectra of nitrogen substituted zeolite NaY treated at different reaction times and temperatures.

For HY zeolites with both high and low aluminum content (Si/Al=2.55 and Si/Al=15), comparison of the ^{27}Al MAS NMR data of the pristine dry sample with the 750^{o}C sample shows either formation of new aluminum environments or formation of quadrupolar lineshape due to the distortion of the aluminum environments due to possible dealumination of framework aluminum in the early stages of the nitrogen substitution reaction or nitrogen substitution. The resemblance of the lineshapes and peak maxima in -50−75 ppm region can be the result of extraframework aluminums present in the structure. The presence of dealumination can suggest that, the nitrogen substitution starts at the dealumination sites and continues from the same silicon tetrahedra forming a highly siliceous nitrogen substituted framework. This can also be supported by comparing the changes in the relative intensities of new sites in ^{29}Si NMR and ^{27}Al MAS NMR data for the nitrogen substituted zeolites at different reaction temperatures and reaction times. For example, for nitridated HY zeolite with Si/Al ratio of 2.55 treated at 850^{o}C for 24 hours, ^{29}Si NMR shows an increase in the intensity of SiQ^{4}(4N) sites and almost no Q^{4}(4O) site remaining in the framework, which means all silicons are nitrogen

substituted at least once and the degree of substitution increases gradually toward the late stages of nitridation. On the other hand, ^{27}Al MAS NMR of the same samples do not show the same trend and most of the aluminum sites either have no nitrogen substitution or are only a singly nitrogen substituted judging from the broad 60 ppm peak. The sharp peak with maxima of 90 ppm with an increasing intensity as the reaction temperature increases can be tentatively attributed to the nitrogen substituted extraframework aluminum sites or AlN_4 environments since it shows high symmetry. The same effect is also observed for the treated NH_4Y sample which shows a high degree of nitrogen substitution for the silicon sites, as observed by ^{29}Si MAS NMR (4.1.ii.c, sample treated at 850^{o}C for 48 hours) but not for aluminum sites as seen in ^{27}Al MAS NMR spectrum.

At this point, it is hard to define the number of aluminum sites and assign the peaks only by ^{27}Al MAS NMR due to the line broadening and line shapes which may be the result of second order quadrupolar interaction as well as the distribution of different aluminum environments. In order to observe the effects of quadrupolar interactions both ^{27}Al MAS NMR and MQMAS NMR experiments have been performed on two different magnetic fields, at 11.7 and 19.6 Tesla, and will be discussed in the following section.

4.3.1.2. Nature of Aluminum Species in Nitrogen Substituted NaY

As seen in the ^{27}Al MAS NMR spectra in Figure 4.2.a, samples treated at low temperatures (800 and 750^{o}C) show no pronounced change suggesting no nitrogen substitution of the Si-O-Al linkage. The low nitridation level of the framework of these low temperature treated samples is also supported by ^{29}Si MAS NMR where only singly substituted environments, namely SiO_3NH are observed for the 800^{o}C sample whereas, the 750^{o}C sample shows almost no substitution. Slight changes observed in the line broadening in the ^{27}Al spectra compared to the pure dry zeolite can be the result of decreased quadrupolar interaction due to healing effect[24,25] of both the water produced and ammonia present in the reaction environment, decreasing the distortion of the silicon tetrahedral neighbor to the aluminum environment possibly as a result of nitrogen substitution. For the samples treated at 800^{o}C and 750^{o}C, the low nitrogen substitution on the Al-O-Si bond is consistent with energy calculations, since the substitution between a

Si-O-Al site in NaY, costs more than 120 kJ/mol which is higher compared to 100 kJ/mol for substitution at a Si-O-Si site[1].

The ^{27}Al MAS NMR data (taken at 11.7 Tesla) for nitrogen substituted NaY zeolite treated at 850^{o}C with a reaction duration of 24 and 48 hours, shows at least two additional peaks with peak maxima at around 70 and 84 ppm and an increase in the linewidth of the AlO_4 peak with a slight shift towards higher field. The experiments were repeated at 19.6 Tesla and 2D MQMAS NMR was performed to obtain an accurate value of the isotropic chemical shift. Figure 4.3 includes the comparison of ^{27}Al MAS NMR spectra obtained at two different fields (11.7 and 19.6 Tesla) and the simulation of the high field data.

The ^{27}Al MAS NMR data at 19.6 Tesla for the nitrogen substituted NaY zeolite has better resolution than the 11.7 Tesla data and suggests that there are four possible aluminum sites. In order to get quantitative information on the distribution of different aluminum sites, simulation of the high field ^{27}Al MAS NMR data is also performed (Table 4.1). The simulation gives four aluminum environments with isotropic chemical shift values of 64, 78, 92 and 96 ppm. With a relative intensity of 62% for a distorted AlO_4 environment, it shows that most of the aluminum linkages are not nitrogen substituted; suggesting substitution favors Si-O-Si rather than Si-O-Al linkage. This is also supported by ^{29}Si MAS NMR of treated NaY zeolites (Figure 4.2.c). Even the sample with highest nitridation degree has mosty 1N and 2N nitrogen substitution to silicon tetrahedra and the unsubstituted silicon environments are mostly the Q^4(2Al) (-95 ppm) and Q^4(3Al) (-89 ppm) environments, therefore ones with more Si-O-Al linkages.

Figure 4.4 shows the 2D MQMAS spectra (taken at 500MHz) for the nitridated NaY zeolite treated at 850^{o}C for 24 hours. The slices of ^{27}Al MQMAS spectra were taken at the center of gravity of the 2D contours and the figures include the simulations of the slices. For some of the slices, the broad lineshapes observed are due to the large distributions of C_Q's for the aluminum site at higher frequency resonances giving broad components from lower frequency resonances. Therefore, the simulations were performed considering only the main resonance, representing the smallest C_Q's. The simulations were performed considering the NMR parameters obtained by the simulations of these slices and high field MAS spectra are given in Table 4.1 and Table

4.2, respectively. In the MQMAS spectrum, the projection of the 2D frequency domain along with δ_{F1} axis gives the purely isotropic spectrum free of second order quadrupolar broadening and shows two resolved contributions in 60-80 ppm region with δ^{iso}_{Al} of 67 and 79 ppm. The spread of intensity in F_1 and F_2 indicate a large distribution in isotropic chemical shift and quadrupolar interaction. Considering the nitiridation level and ^{29}Si MAS NMR data of the treated samples these two resonances can be assigned as distorted AlO_4 and AlO_3N sites, respectively which is also consistent with the assignments in literature[20] on ^{27}Al MAS NMR of dehydrated zeolites and aluminum oxynitrides. The distorted AlO_4 site is ascribed to nitrogen substituted tetrahedra through Si-O-Si linkage but not Si-O-Al, causing a shift and increase in C_Q, as a result of distortion in the symmetry of the site through changes in both bond angles and bond lengths of the aluminum environment. The spectral region of 90-100 ppm consists of two resonances with δ^{iso}_{Al} of 92 and 96 ppm with relatively small quadrupolar values. The resonances at 67, 79 and 92 ppm are separated by almost a 13 ppm shift suggesting that the shifts are additive, that and for each nitrogen substituted to an aluminum environment causes a shift of 13 ppm to lower fields. Therefore, the resonances in the 90 ppm region can be assigned as AlO_2N_2 sites. It should also be noted that as seen in ^{29}Si NMR, the chemical shift change per nitrogen addition, the number of (NH) groups in the local coordination shell increases, and a similar trend for the ^{27}Al spectra might be expected. Therefore, the 96 ppm resonance can be also assigned as $AlON_3$ or terminal AlO_3NH_2, as well as, AlN_4 sites, as the resonance shows relatively smaller quadrupolar values suggesting a symmetric aluminum environment.

As given in Table 4.1 the quadrupolar parameters and isotropic chemical shift values obtained by the simulation of the slices of F_2 dimensions of 2D ^{27}Al MQMAS data and the calculated value (by the formula 4.1) are consistent with each other. The isotropic chemical shift and C_Q values obtained are in agreement with the simulated and calculated values obtained from MQMAS data.

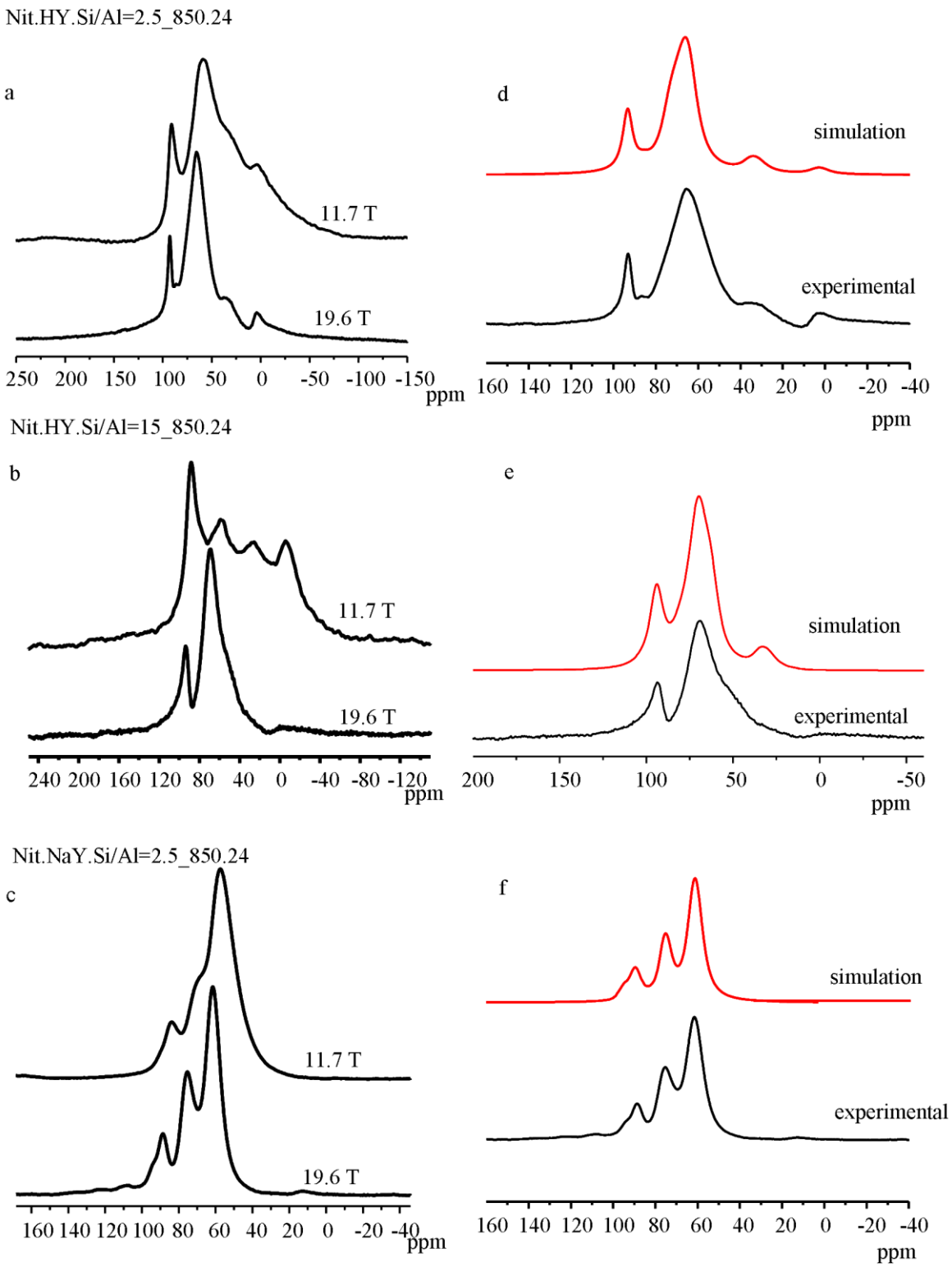

Figure 4.3. (a), (b), (c), Comparison of ^{27}Al Single Pulse MAS NMR of nitrogen substituted zeolite zeolite Y at two different field strengths and (d), (e), (f), the simulation of 19.6 Tesla data using simulation program WinSolids.

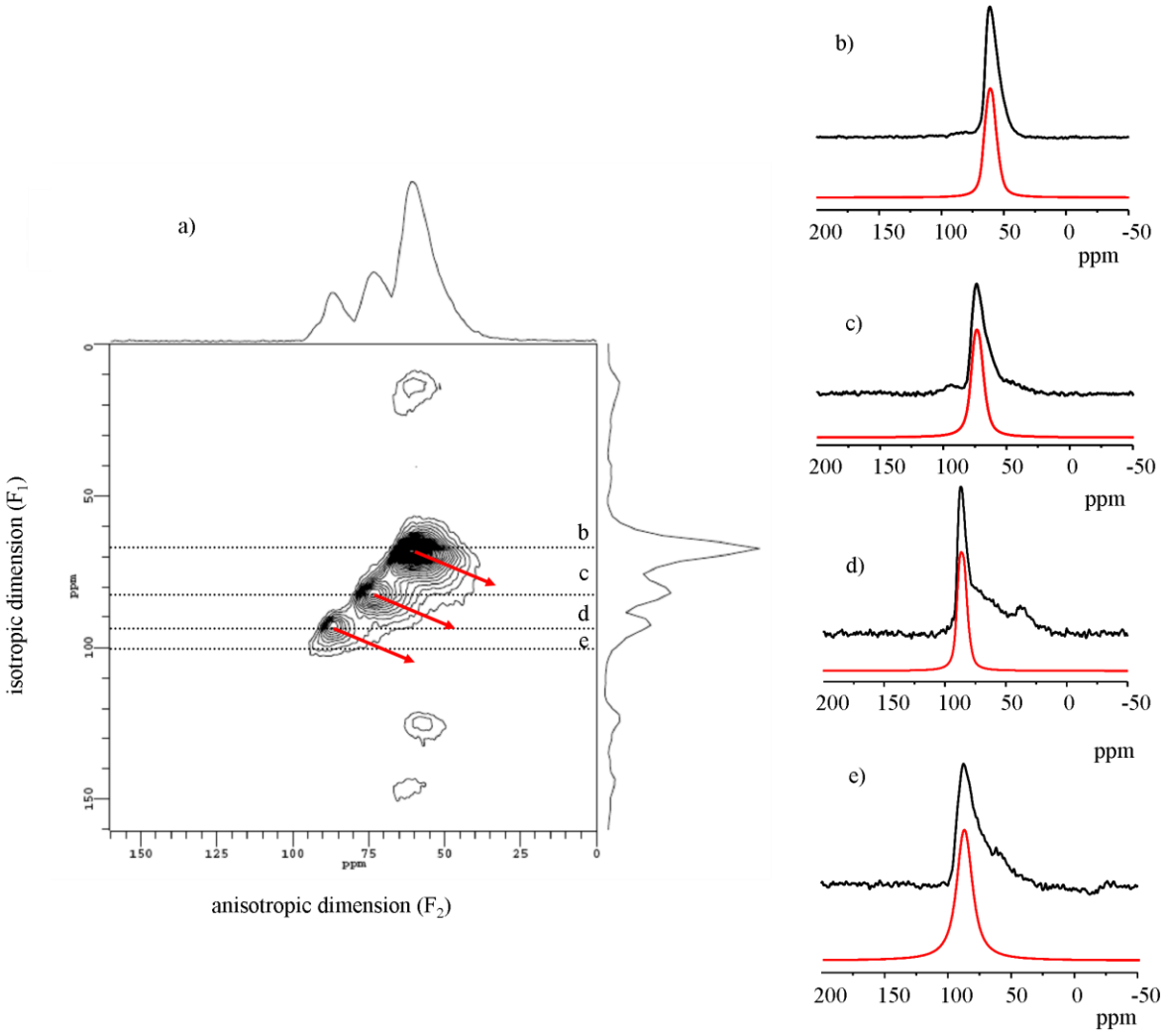

Figure 4.4. (a) ^{27}Al MQMAS spectra of Nitridated NaY zeolite treated at 850^{o}C for 24 h. Projection of F_1 and F_2 dimensions are shown on the side of the 2D spectrum. (b), (c), (d) and (e), Selected isotropic spectra taken from the slices of anisotropic dimension with the simulations are given on the left. The dotted lines in the 2-D spectrum show where the slices are taken. The arrows represent the direction of C_Q distribution.

Table 4.1. ^{27}Al NMR parameters obtained from the fitting of the slices of 2D ^{27}Al MQMAS data and calculations.

Sample/unit	δ^{iso}_{Al} (ppm)*	C_Q (MHz)*	η	δ^{iso}_{Al} (ppm)#	P_Q#	Related Slices
Nit. HY Si/Al=2.5 850.24						Figure 4.6
AlO_4	68	4.8	1.0	69	4.4	b
AlO_3N	78	4.8	0.1	77	4.8	c
AlO_2N_2	88	5.9	0.8	84	4.4	d
AlN_4	93	2.6	0.1	95	2.6	e
Nit. HY Si/Al=15 850.24						Figure 4.5
AlO_4	68	4.8	0.4	65	4.6	b
AlO_3N	71	4.4	0.8	69	4.4	c
AlO_2N_2	86	7.2	0.9	78	5.0	d
AlN_4(extraframework)	94	3.0	0.1	94	4.0	e
Nit. NaY Si/Al=2.5 850.24						Figure 4.4
AlO_4	67	4.2	0.5	67	4.2	b
AlO_3N	79	4.0	0.4	78	3.8	c
$AlO_2 N_2$	91	3.8	0.4	90	3.2	d
AlO_3NH_2/$AlON_3$/ AlN_4	94	3.6	0.4	96	4.4	e

***** Parameters obtained by the simulation of the slices of 2D ^{27}Al MQMAS data
# Parameters calculated from the observed shifts of center of gravity of the resonances ($\delta_{1(Exp.)}$ and $\delta_{2(Exp.)}$) using equation 4.1.

Table 4.2. ^{27}Al NMR parameters obtained from the simulations of high field (19.6 Tesla) MAS NMR data.

Sample/unit	δ^{iso}_{Al} (ppm)	C_Q (MHz)	% intensity
Nit. HY Si/Al=2.5 850.24			
6 coord. (extraframework)	6	5.4	2.5
5 coord. (extraframework)	38	6.2	7.0
AlO_4	68	4.8	43
AlO_3N	77	6.0	26
AlO_2N_2	88	4.4	1.5
AlN_4	94	2.8	20
Nit. NaY Si/Al=2.5 850.24			
AlO_4	64	4.4	62
AlO_3N	78	4.4	26
AlO_2N_2	92	3.8	8.4
AlN_4	96	3.0	3.6
Nit. HY Si/Al=15 850.24			
5 coord. (extraframework)	38	6.8	6.8
AlO_4	66	5.0	16.8
AlO_3N	73	4.8	28
AlO_2N_2	84	8.2	28
AlN_4	95	3.0	20.4

4.3.1.3. Nature of Aluminum Species in Nitrogen Substituted HY

^{27}Al MAS NMR spectra of nitridated HY zeolite with a Si/Al ratio of 15 show the formation of nitrogen substituted aluminum sites for the samples treated at 800^{o}C and above (Figure 4.1). ^{29}Si MAS NMR showed that these samples contain 1N, 2N and 3N substituted silicon environments. However, for the assignment of the nitrogen substitution levels around aluminum environments, the same approach can not be taken, as the ^{27}Al MAS NMR spectra of these samples obtained at 11.7 Tesla suffer from poor resolution. Comparison of the ^{27}Al NMR spectra for HY samples treated at 750 and 800^{o}C with the pristine samples indicates that, in the early stages of the reaction, a high distortion of framework aluminum and formation of extraframework aluminum environments are observed. Only a weak, sharp resonance at around 90 ppm is observed for the sample treated at 800^{o}C, the only sign of nitrogen substitution near aluminum. The MQMAS experiments (not shown here) on the low temperature treated samples (750 and 800^{o}C) also support the argument. The 2D ^{27}Al MQMAS data for the Nit.HY zeolite with Si/Al=15 treated at 750^{o}C, shows at least two aluminum sites (with poor resolution) at about 68 and 86 ppm region whereas the data on HY sample treated at 800^{o}C reveals the presence of three aluminum environments at about 65, 86 and 95 ppm region. As stated previously, ^{27}Al and ^{29}Si NMR data of HY zeolites treated at different reaction temperatures, dealumination in the framework occurs at early stages of the ammonia treatment and it is more likely that the nitrogen substitution of the zeolite framework proceeds at the dealumination sites.

The ^{27}Al NMR data of the nitrogen substituted HY zeolites with different aluminum content (HY Si/Al=15, HY Si/Al=2.55 and NH_4Y Si/Al=2.5) does not show a difference in terms of the degree of nitridation, whereas the difference is more clearly seen by ^{29}Si MAS NMR data. For example, NH_4Y zeolite treated at 850^{o}C for 24 hours shows the highest nitrogen substitution of all having mostly 3N and 4N silicon environments seen by ^{29}Si NMR, whereas HY zeolite with high aluminum content and treated under the same temperature shows a lower degree of nitrogen substitution with mostly 2N and 3N silicon environments (Figure 4.1.e). The ^{27}Al NMR spectra of the

same samples however are almost similar indicating no differences in the aluminum environments (Figure 4.1.b).

As seen in Figure 4.3, with increasing the magnetic field stregth, a noticeable change is observed in the line broadening and the discontinuities in the ^{27}Al MAS spectra of nitridated HY zeolites with both high and low aluminum content. The discontinuities are due to the 2nd order quadrupolar interaction and are mostly removed at higher field, revealing at least three possible aluminum sites for nitridated HY zeolite with low aluminum content (Si/Al=15). The 2D MQMAS data of the same sample (Figure 4.5) show two clearly resolved resonances in the 65 ppm and 95 ppm spectral regions and the simulations of the slices taken from anisotropic dimension at these regions gives isotropic chemical shifts (δ^{iso}_{Al}) of 68 and 94 ppm for these two sites. Considering the chemical shift and C_Q values of these environments, these resonances can be assigned as distorted AlO_4 and extraframework AlN_4 sites.

In nitrogen substituted HY zeolites the possible aluminum environments should be in the form of Al(NH) as proton is the charge compensation cation, whereas, for aluminum sites in the vicinity of extraframework aluminum cations, the form is AlN. The presence of extraframework aluminum species and protonated nitrogens in the framework should affect the symmetry of the aluminum site resulting in an increase in quadrupolar coupling constants for the framework aluminums. With the increase in the temperature during the ammonia flow, nitridation level of extraframework aluminum sites increases resulting in AlN_4 sites. The low C_Q value obtained for this resonance in nitrogen substituted HY zeolite can be explained by the highly symmetric aluminum environment. The 2D MQMAS data of nitridated HY zeolite with low aluminum content shows two more resonances with lower intensities with simulated shifts (δ^{iso}_{Al}) of 71 and 86 ppm with relatively higher quadrupolar coupling constants. The simulation of the anisotropic dimensions at 71 and 86 ppm gives an asymmetry parameter of 0.8 and 0.9, respectively. Considering the symmetry and chemical shift values of these sites they are assigned as AlO_3N and AlO_2N_2 environments. One major problem with the ^{27}Al NMR data of the nitridated proton type zeolite is the inconsistencies between the simulated and calculated isotropic chemical shift and quadrupolar values and the simulations between the high field ^{27}Al MAS and MQMAS NMR data of the sample. Unlike the nitridated NaY zeolite

case, when we use the parameters obtained from the MQMAS data, for the simulation of high field MAS data (Figure 4.3.c) a poor fit is obtained that does not account for two lineshapes. The program used for the simulation of the Single-Pulse ^{27}Al data can only consider one parameter at a time (either the quadrupolar interaction or chemical shift anisotropy) therefore the explanation can be either, we can not include the large CSA of the aluminum sites in the simulation, or there are multiple sites with larger quadrupolar interactions which are not determined by MQMAS as we were not able to excite the multiple quantum coherences for these sites successfully during the experiment. The latter does also explain why 5- and 6- coordinate aluminum sites are not seen in the MQMAS experiment both for nitridated HY zeolite with low and high aluminum content. Nitridated HY zeolite with higher aluminum content (Si/Al=2.55) treated at 850^{o}C for 24 hours, shows similar ^{27}Al MAS spectra with low aluminum content sample (treated at same reaction conditions) at 19.6 Tesla, suggesting similar nitrogen substitution degrees and nitrogen levels for aluminum sites. The ^{27}Al MQMAS data for the sample (Figure 4.6) shows four resolved aluminum sites with δ^{iso}_{Al} of 68, 78, 88 and 93 ppm, the first three are assigned as distorted AlO_4, AlO_3N, AlO_2N_2, respectively. The 93 ppm peak can be assigned as either framework or extraframework AlN_4 environment. The small CQ value of this resonance might suggest that it is an extraframework environment. The slight changes in the chemical shifts can be explained by the presence of residual sodium ions as extraframework cation which is supported by with EDX analysis and explained in the previous chapter.

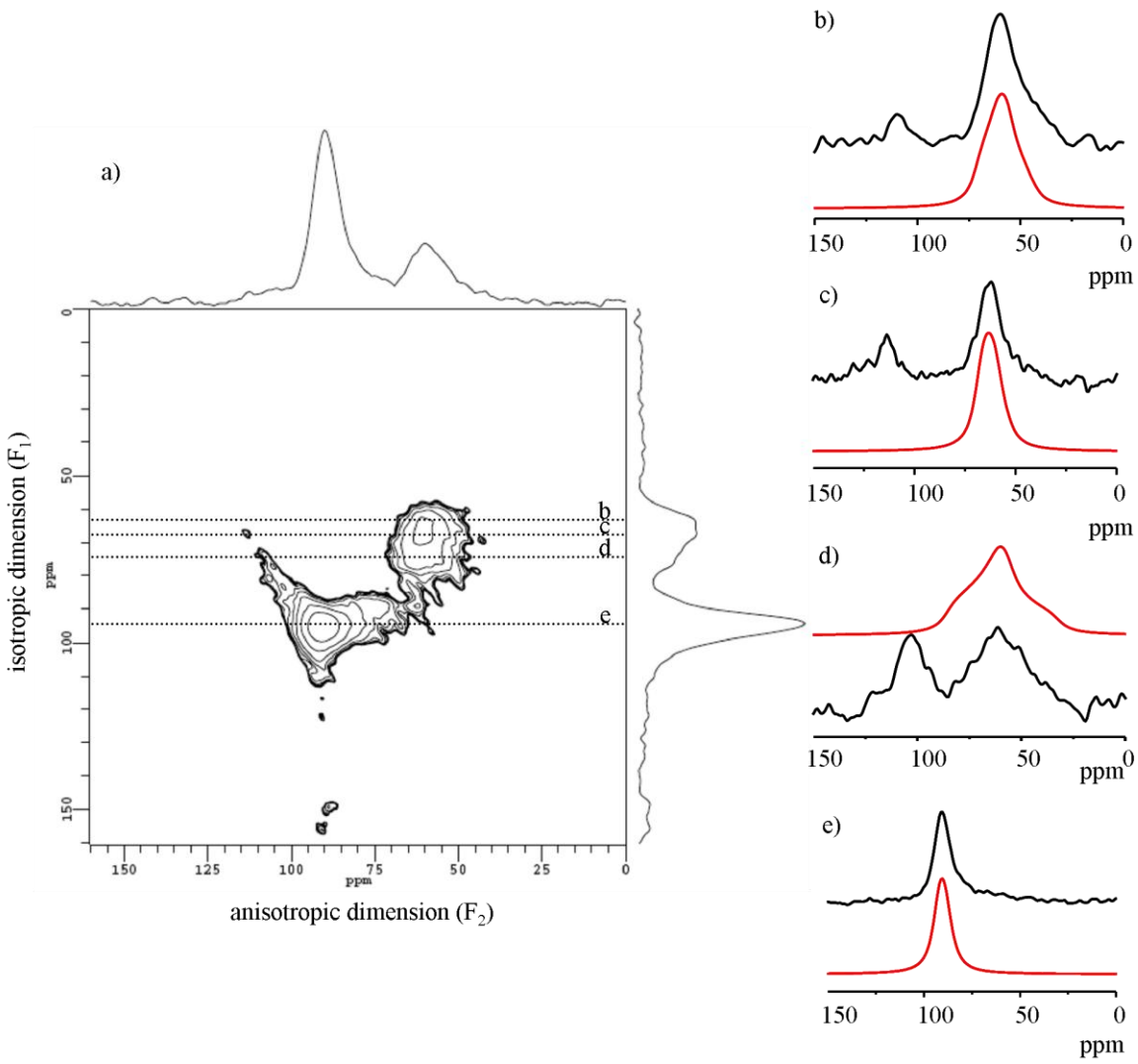

Figure 4.5 (a) ^{27}Al MQMAS spectrum of Nitridated HY zeolite with a Si/Al ratio of 15 treated at 850^{o}C for 24 h. Projection of F_1 and F_2 dimensions are shown on the side of the 2D spectrum. (b), (c), (d) and (e), Selected isotropic spectra taken from the slices of anisotropic dimension with the simulations are given on the left. The dotted lines in the 2-D spectrum show where the slices are taken.

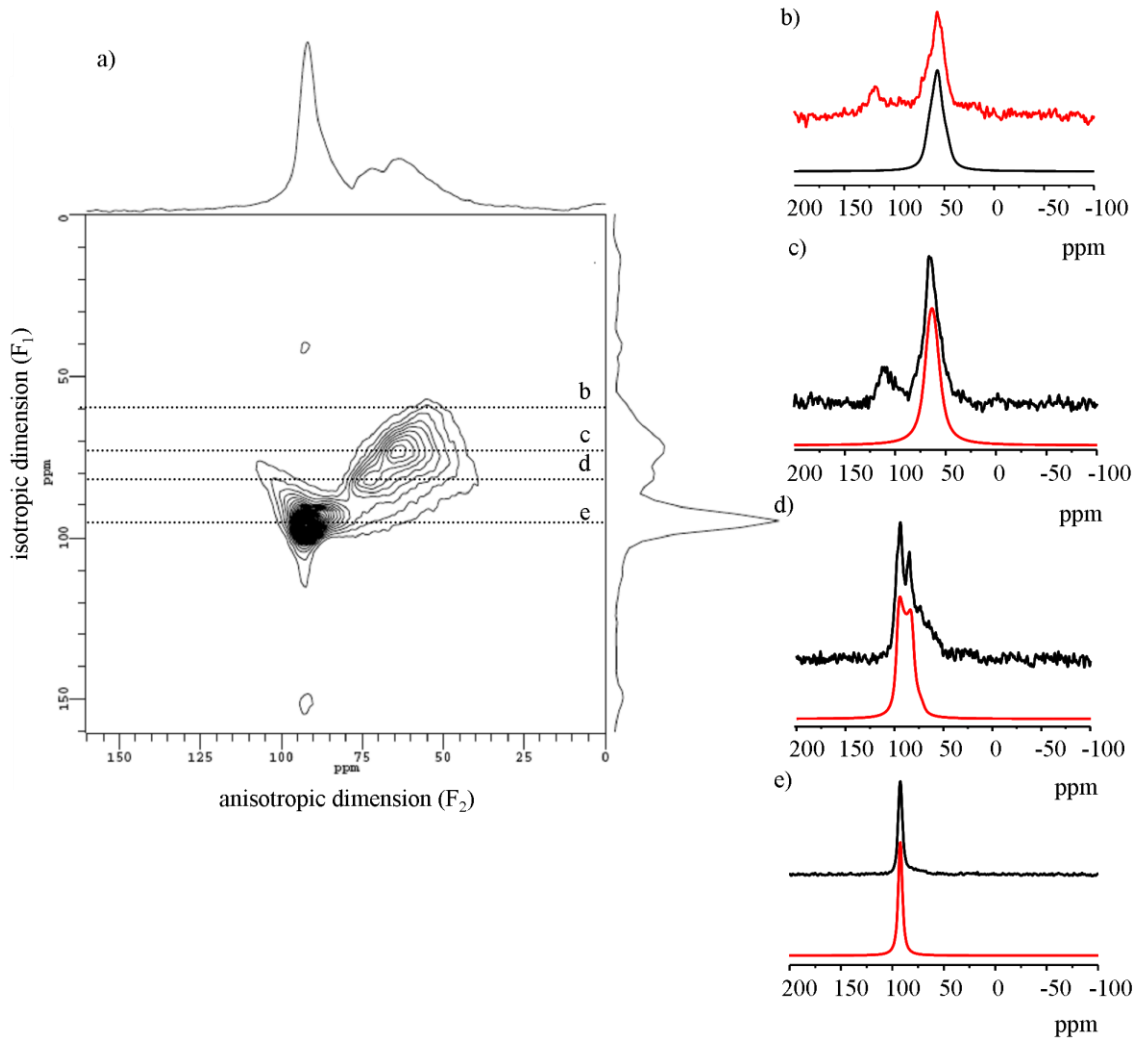

Figure 4.6 (a) ^{27}Al MQMAS spectrum of Nitridated HY zeolite with a Si/Al ratio of 2.5 treated at 850^{o}C for 24 h. Projection of F_1 and F_2 dimensions are shown on the side of the 2D spectrum. (b), (c), (d) and (e), Selected isotropic spectra taken from the slices of anisotropic dimension with the simulations are given on the left. The dotted lines in the 2-D spectrum show where the slices are taken. The arrows represent the direction of C_Q distribution.

4.3.2. ^{1}H MAS NMR

^{1}H chemical shifts for environments in pristine zeolites are in the range of approximately -0.5 to 8 ppm[12,21]. The typical chemical shifts for Bronsted acid sites in zeolites are in the range of 3.6 to 5.2 ppm and depend on the position of the site (whether in small or larger cages) and the Si/Al ratio, therefore, the mean electronegativity of the zeolitic framework. As Jiao *et al* reported, in dehydrated zeolites bridging OH groups in large cages and pores shows a ^{1}H NMR chemical shift range of 3.6-4.3 ppm, whereas the ones in small cages are in the 4.6-5.2 ppm range. Defect silanol groups show resonances between 1.2-2.4 ppm in ^{1}H MAS NMR and can be shifted downfield in the case of hydrogen bonding[24,26]. The shifts for the OH group of the extraframework aluminum are in the range of 2.4 to 3.6 ppm, and cation OH groups such as $[Zn\text{-}OH]^{+}$ in large cavities have a chemical shift range of -0.5 to 0.5 ppm[21,27]. According to very limited ^{1}H MAS NMR studies of the protonic surface groups of the ammonia chemisorbed silica and alumina, terminal $Si\text{-}NH_2$ protons give rise to a resonance at 0.8 ppm whereas terminal $Al\text{-}NH_2$ and $Al\text{-}NH_2\text{-}Al$ sites have proton resonances at -0.4 and -1.9 ppm, respectively. The bridging NH group in Al-NH-Al site is assigned to the 2.8 ppm resonances whereas, the Si-NH-Si bridging proton resonates at 0.25 ppm[19,20]. There is only one ^{1}H MAS NMR study of silicon oxynitrides where they assign the weak 7 ppm resonance to the $Si\text{-}NH_x$ groups at the surface of the pore walls. Unfortunately this study does not include any ^{1}H NMR spectra[28].

4.3.2.1. Nitrogen Substituted NaY

The possible proton sites for the pristine NaY zeolite are terminal silanol groups and protons of extraframework aluminum cations which are both expected to be minimum considering the limited dealumination of the framework and framework defects. Therefore, the possible proton sites expected for nitrogen substituted zeolite NaY, are Si-NH-Si, Si-NH-Al, terminal $SiNH_2/AlNH_2$ (if nitrogen substituted extraframework aluminum environments are not AlN_4 clusters) and non nitrogen substituted proton sites of the pristine zeolite framework.

As discussed in Chapter three, supported by the ^{29}Si NMR and EDX data, the nitrogen substitution level of Nit.NaY.750.24 is relatively low. ^{27}Al MAS NMR and ^{29}Si MAS NMR of this sample show a deformation in aluminum-containing silicon tetrahedra and a decrease in the intensity of the $Si(OAl)_2(OSi)_2$ resonance, respectively, suggesting either nitrogen substitution of the Si-O-Al linkage or possible dealumination of the framework. As discussed previously, the ^{27}Al NMR data for the dehydrated pure NaY sample shows a similar spectrum to the Nit.NaY.750.24 sample as a sign of deformation of the framework due to dehydration. Consistent with this, a similar trend is observed for ^{1}H MAS NMR of the two samples. The spectra have a sharp single peak at ~ 2.4 ppm that can be attributed to either hydrogen bonded defect silanol sites or extraframework aluminums (Figure 4.7.a) formed by the high temperature treatment or present in the pristine sample. These two resonances show no significant spinning sidebands, therefore no significant dipolar interaction. The 2.4 ppm resonance is tentatively assigned to proton sites of the extraframework aluminum, considering the proton chemical shifts reported in literature for pristine zeolites. As the nitrogen substitution increases by increasing the temperature to 800^{o}C, a new resonance is observed at ~ 0.3 ppm, while the 2.4 peak gets broader and shifts to 2.8 ppm. For the NaY zeolite nitridated at 850^{o}C for 24 and 48 hours, an additional proton resonance forms at ~ 0.8 ppm and a broad high frequency resonance forms at 3.4 ppm. Both resonances have broad spinning sideband manifolds, a sign of possible dipolar interactions (not shown). Also, the ^{1}H MAS NMR Echo experiments with different evolution/refocusing times show that the site at 3.4 ppm has a short T_2 relaxation time. Comparison of the ^{1}H MAS NMR spectra of nitrogen substituted NaY zeolite treated at different conditions, shows that the new low frequency sites are protons of newly formed amine groups. Various samples, which are not presented here, prepared under different conditions and therefore with different nitrogen content showed that the relative intensity of these sites increase gradually as the nitrogen substitution level increases. In order to confirm the proton assignments, $^{1}H/^{14}N$ and $^{1}H/^{27}Al$ TRAPDOR experiments were performed on the NaY sample with a high nitrogen content. This experiment uses the dipole interaction between ^{1}H and ^{14}N or ^{27}Al, which scales as the cube of the through-space distance between the two nuclei. Thus, the most pronounced TRAPDOR effect, which is related with the intensity of the difference

spectra (as presented in Figure 4.8), is expected for the proton groups coordinated to N or Al, respectively.

The difference spectrum of the $^{1}H/^{27}Al$ TRAPDOR experiment on Nit.NaY.850.24 shows a spectrum with a low intensity peak at ~ 0.3 and a broad peak at 2.8 ppm, whereas the difference spectrum of the $^{1}H/^{14}N$ TRAPDOR experiment on the same sample has more pronounced peaks centered at around 0.6 and 1.2 ppm. The difference ^{1}H /^{14}N TRAPDOR spectrum also shows signs of a nitrogen dipolar interaction with the environments that give rise to peaks around 0.3, 2.8 and 3.5 ppm, which are relatively low in intensity. Since these peaks are also observed with $^{1}H/^{27}Al$ TRAPDOR, these peaks can be assigned as the proton peaks of nitrogen substituted aluminum environments. On the other hand, the proton sites with the resonances of 0.6 and 1.2 ppm can be assigned as framework or terminal SiNH environments. The two points that should be considered here are the differences in relatively intensities of ^{1}H /^{14}N TRAPDOR and $^{1}H/^{27}Al$ TRAPDOR difference spectra and the presence of non nitrogen substituted protons sites. It should be noted that the expected TRAPDOR effect for ^{1}H /^{14}N correlation is higher than $^{1}H/^{27}Al$ regardless of the quantity of the sites as the N-H through-space dipolar coupling is higher than the Al-H distance. As the ^{1}H NMR chemical shifts for different protons sites are in close range and the peaks are relatively broad it is hard to resolve all the peaks and beneath the observed proton resonances it is possible that there are other sites with relatively low intensities. Therefore it is hard to make distinct assignments for all the zeolitic proton sites.

Considering formation of new proton sites observed by ^{1}H MAS NMR and the peaks observed in difference spectrum of ^{1}H TRAPDOR NMR, high field peaks (0.3 to 1.2 ppm) can be assigned to the protons of the Si-NH-Si environments. According to the relevant references, the terminal $SiNH_2$ groups are usually observed at lower ppm values whereas proton sites with hydrogen bonding are observed at higher ppm values [21,29]. With the same approach, low field peaks (2.4 to 3.5 ppm) can be assigned to protons of the nitrogen substituted aluminum environments. Figure 4.7.b shows the normalized ^{1}H MAS NMR data for the nitridated NaY zeolites. The results show that the formation of nitrogen substituted sites causes an increase in the proton content of the material, but, as the treatment temperature increases (as the substitution degree increases) the intensity of the

proton sites in the vicinity of aluminum environments decreases whereas the intensity of proton sites of SiNH environment increases. This might suggest that as the nitridation reaction proceeds, it is possible that condensed aluminum nitrides are formed.

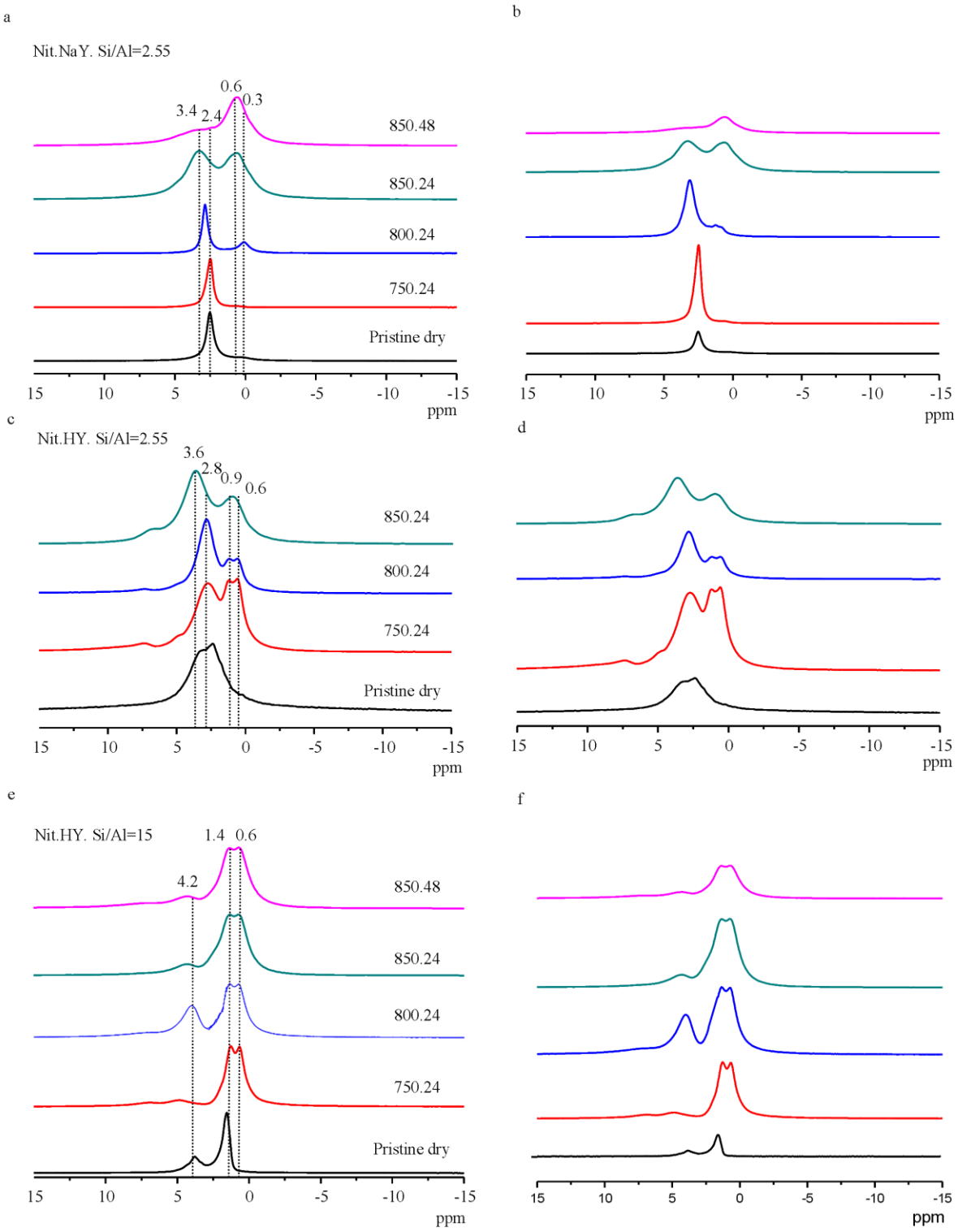

Figure 4.7. (a, c, e) ^{1}H MAS NMR spectra for the nitrogen substituted zeolite Y with different aluminum content and extraframework cations. Samples are treated at different reaction times and temperatures. (b,d,f) normalized spectra of (a, c, e), respectively.

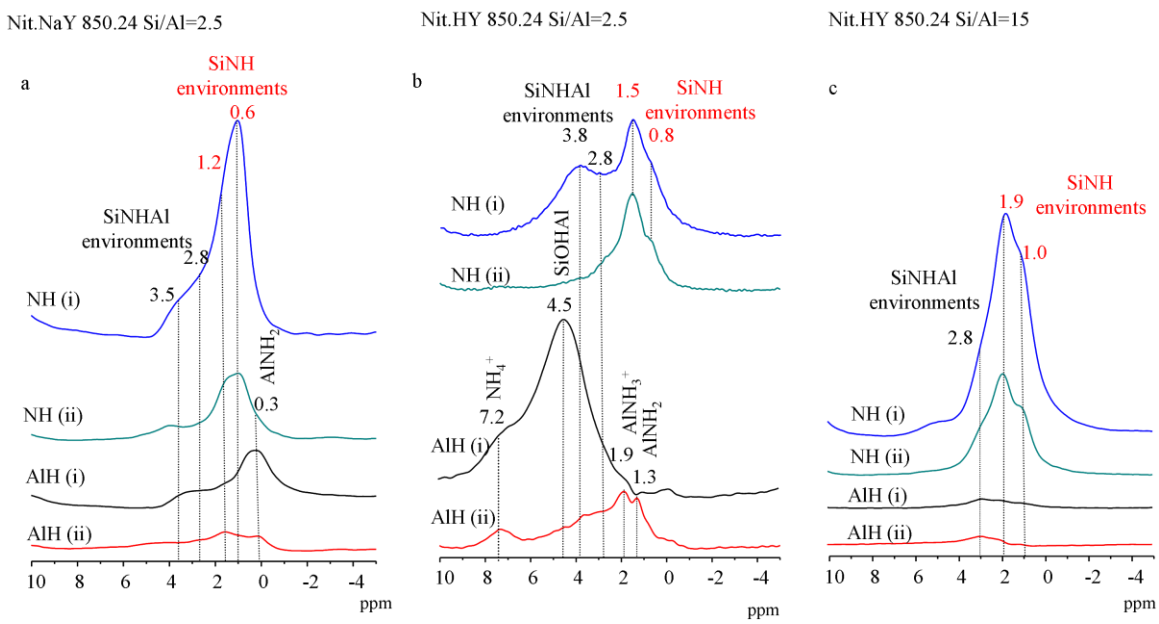

Figure 4.8. $^{1}H/^{14}N$ (NH) and $^{1}H/^{27}Al$ (AlH) TRAPDOR MAS NMR difference spectra for the nitridated zeolite (a) NaY, (b) HY high aluminum content, (c) HY low aluminum content with evolution times of (i) 200 μs and ii) 800 μs.

4.3.2.2. Nitrogen Substituted HY (Si/Al ratio=2.5)

Figure 4.7.c shows the ^{1}H MAS NMR data for nitrogen substituted zeolite HY with high aluminum content, treated at different reaction conditions. As discussed earlier, both ^{29}Si and ^{27}Al NMR showed that the pristine sample is dealuminated and therefore the major proton sites in the pristine sample are expected to be the bridging SiOHAl, terminal silanols and the protons of the extraframework aluminum (EFAL) cations. The ^{1}H NMR data of the dehydrated pure sample shows a broad proton peak with three main components with chemical shifts of 1.2, 2.3 and 3.4 ppm which are assigned as terminal SiOH, EFAL protons and bridging SiOHAl, respectively.

On treating the material under ammonia, two new resonances form at around 0.6 and 0.9 ppm that can be assigned to protons of SiNH environments; these are also observed in amine substituted NaY zeolites. The ^{29}Si MAS NMR data of the two samples treated at low temperature (750^{o}C and 800^{o}C) show relatively low levels of nitridation so

it might be expected that the nitrogen substitution starts with the terminal silanol groups (formed during the dealumination due to high temperature treatment as discussed in the ^{27}Al MAS NMR section) and proceeds with the bridging groups. Therefore the two proton sites at 0.6 and 0.9 ppm can be assigned as terminal $SiNH_2$ and bridging SiNHSi sites. With increase in the reaction temperature, and therefore higher substitution levels, a new peak is observed in the ^{1}H MAS NMR spectrum at 3.8 ppm which can be assigned as either $SiNH_2Al$ or SiNHAl bridging group protons. Comparing with the nitrogen substituted NaY zeolite the relative intensity of the 3.8 proton peak is higher for nitrogen substituted HY suggesting it is $SiNH_2Al$ environment.

The difference spectrum of ^{1}H/^{14}N TRAPDOR experiment suggests that the 3.8, 2.8, 1.5 (overlapping with 1.9 and 1.3) and 0.8 ppm peaks are proton sites nearby nitrogen. Consistent with the ^{1}H NMR assignments, the two high field peaks can be assigned as SiNHSi/ $SiNH_2$ protons. The slight shifts within the ^{1}H NMR and TRAPDOR data are due to chemical referencing errors and not the presence of different resonances. Proton sites at 2.8 and 3.8 ppm can be assigned as amines of the aluminum environments. The 3.8 ppm signal disappears with increasing the echo evolution time due to its short T_2 relaxation time. In the difference spectrum of the ^{1}H/^{27}Al TRAPDOR experiment, the dominating proton signal is at 4.5 ppm with shoulders at 2.8, 1.9 and 1.3 ppm for the first rotor period. The peak at 4.5 ppm which has a short T_2, is not seen in the ^{1}H/^{14}N TRAPDOR spectrum. Thus, this resonance is due to the protons in the vicinity of aluminums, and therefore we tentatively assign it to the bridging SiOHAl site considering its chemical shift. However, the ^{29}Si NMR spectra of this sample show that all the silicon T sites have reacted with nitrogen. Thus, it is surprising that bridging SiOHAl sites remain. This may suggest that the nitrogen substitution may not preferentially occur on the SiOHAl sites at higher temperatures. The difference spectrum of the ^{1}H/^{27}Al TRAPDOR experiment shows also two additional sites at 1.9 and 1.3 ppm that are most probably buried the main peaks in ^{1}H/^{14}N TRAPDOR spectrum; these two sites are tentatively assigned as terminal $AlNH_3$ and $AlNH_2$ groups, respectively.

4.3.2.3. Nitrogen Substituted HY (Si/Al = 15)

^{1}H MAS NMR data of dehydrated pure and nitridated HY zeolite with low aluminum content treated at varying reaction conditions are shown in Figure 4.7.e. The dehydrated pristine sample shows a main proton resonance at about 1.6 ppm which can be assigned to terminal SiOH groups created during the dealumination process. This peak shows a possible additional site with a resonance at higher frequencies as broadening due to protons of extraframework aluminum environments. There is an additional site at around 4.2 ppm which can be attributed to protons of Bronsted acid sites. For the nitrogen substituted samples, the ^{1}H MAS NMR data consist of two dominant resonances at 1.4 and 0.6 ppm with an additional peak at around 4.2 ppm. Overall, the expected proton sites are protons of Si-NH-Si, Si-NH-Al (compensated by extraframework aluminum atoms-EFAL-), Si-NH_2-Al linkages and possible terminal $SiNH_2$ goups. Since the pristine sample is highly crystalline and low in aluminum content, the new proton sites must be mostly bridging Si-NH-Si sites. The concentration of Si-NH_2-Al or Si-NH-Al sites should be low simplifying the assignments. The full spectra show that the spinning sideband manifolds mostly belong to the 1.4 and 0.6 ppm signals. Since the spinning sidebands are mainly caused by heteronuclear (H to N or Al) or homonuclear (H to H) interactions, these two signals may be due to NH groups (of the same tetrahedra) with larger dipolar interactions. As the reaction temperature and time increases the signals get broader. Since the number of nitrogen attached to a single silicon T site increases with time and temperature, this may result in line broadening because of greater dipolar interactions. The difference spectrum of ^{1}H/^{14}N and ^{1}H/^{27}Al TRAPDOR MAS NMR experiments of Nit.HY.850.24 sample is given in Figure 4.8. The difference spectra of the ^{1}H/^{14}N TRAPDOR experiment is dominated by the resonances at 1.9 and 1.0 ppm. These two sites can be assigned to Si-NH-Si sites of different T sites with various nitrogen substitution degrees, such as $Si(NHSi)_2(OSi)_2$ or $Si(NHSi)_3(OSi)$ and terminal $SiNH_2$ sites. It is more likely the low frequency site is due to terminal amines as the spinning sideband manifolds are broader for this resonance due to the H-H homonuclear dipolar coupling. The proton spectrum contains another signal as a shoulder at 2.8 ppm which is weakly observed in the ^{1}H/^{27}Al TRAPDOR spectra. This resonance

is assigned to a $SiNH_2Al$ site, the higher shift being consistent with the higher charge of these protons.

4.3.3. $^{1}H/^{29}Si$ HETCOR NMR Spectroscopy

The $^{1}H/^{29}Si$ HETCOR NMR experiments for the nitrogen substituted zeolite Y samples provide a method for identifying the presence of different nitrogen substituted silicon environments (Si-NH-Si versus Si-NH_2-Al) and their close proximities to different proton environments. A short contact time (1ms) ensures that the major peaks in the spectrum correspond to only protons in close proximity of silicon atoms.

Figure 4.9 shows the $^{1}H/^{29}Si$ HETCOR data for highly nitrogen substituted HY zeolite with high aluminum content (Si/Al= 2.5). The ^{29}Si NMR data of the sample shows nitrogen substitution at every silicon tetrahedra on both Si-O-Si and Si-OH-Al linakages. In the HETCOR spectra each of these different silicon environments are nicely resolved and give separate chemical shifts. For each nitrogen substitution degree (1N, 2N, 3N region) the center of the contours are separated from each other by about 5 ppm consistent with the ^{29}Si NMR data. Comparing the changes in the relative intensity of these different sites with different contant times on the $^{1}H/^{29}Si$ CP MAS NMR data the high frequency silicon site was tentatively assigned as Si-NH-Si site whereas the low frequency peak was assigned Si-NH_2-Al site (previous chapter). In the 2D HETCOR data, the former is correlated with the proton peak assigned to SiNH environments where as the latter is correlated with the proton site assigned as Si-NH-Al environments. Therefore the $^{1}H/^{29}Si$ HETCOR NMR data supports our assignments.

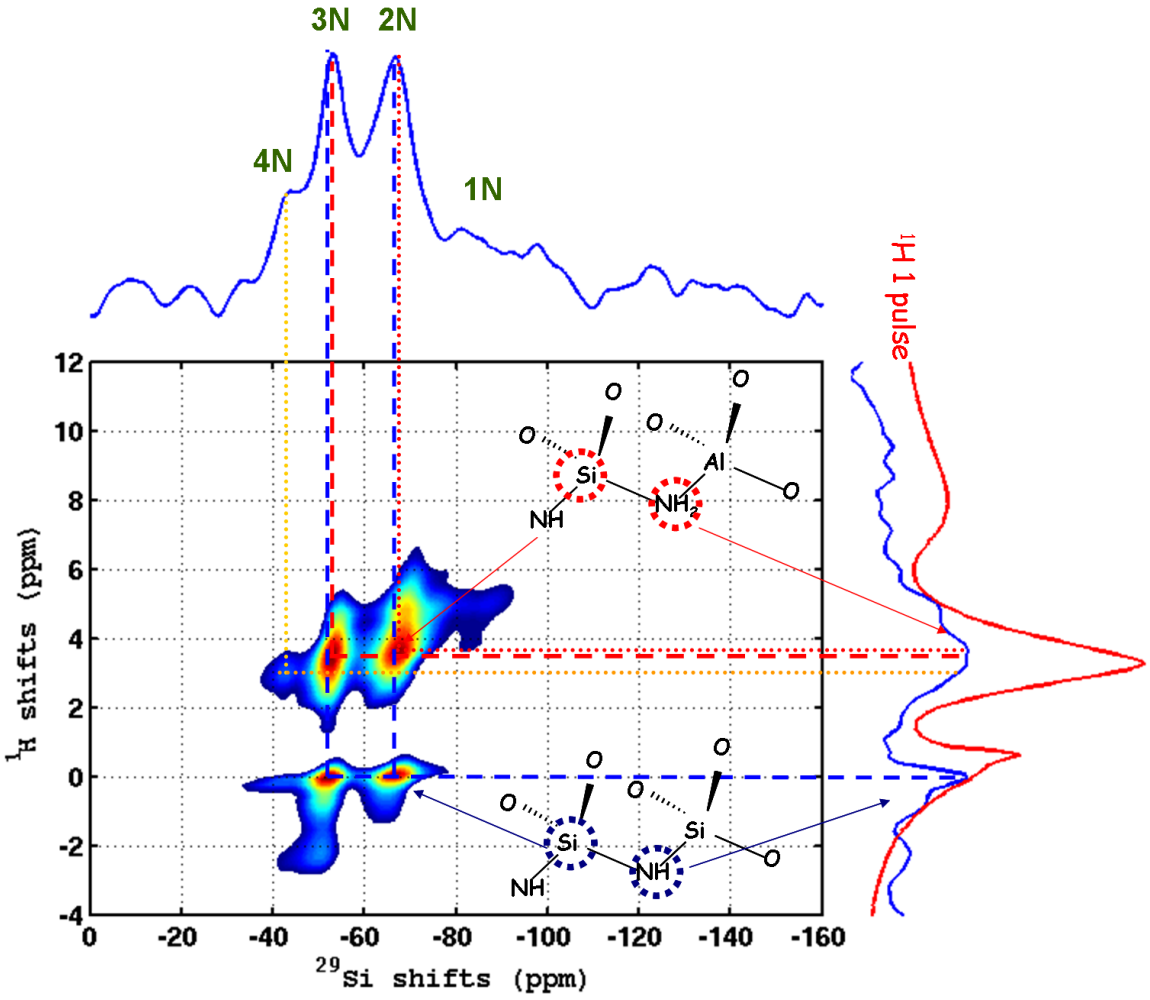

Figure 4.9. ^{1}H/^{29}Si HETCOR NMR 2D spectra for nitrogen substituted HY zeolite with Si/Al ratio of 2.5 (6.1), sample prepared at 850^{o}C for 24h, a contact time of 1 ms was used. Blue spectra are the projection of ^{29}Si and ^{1}H dimensions. Red spectrum is the 1-pulse ^{1}H NMR data.

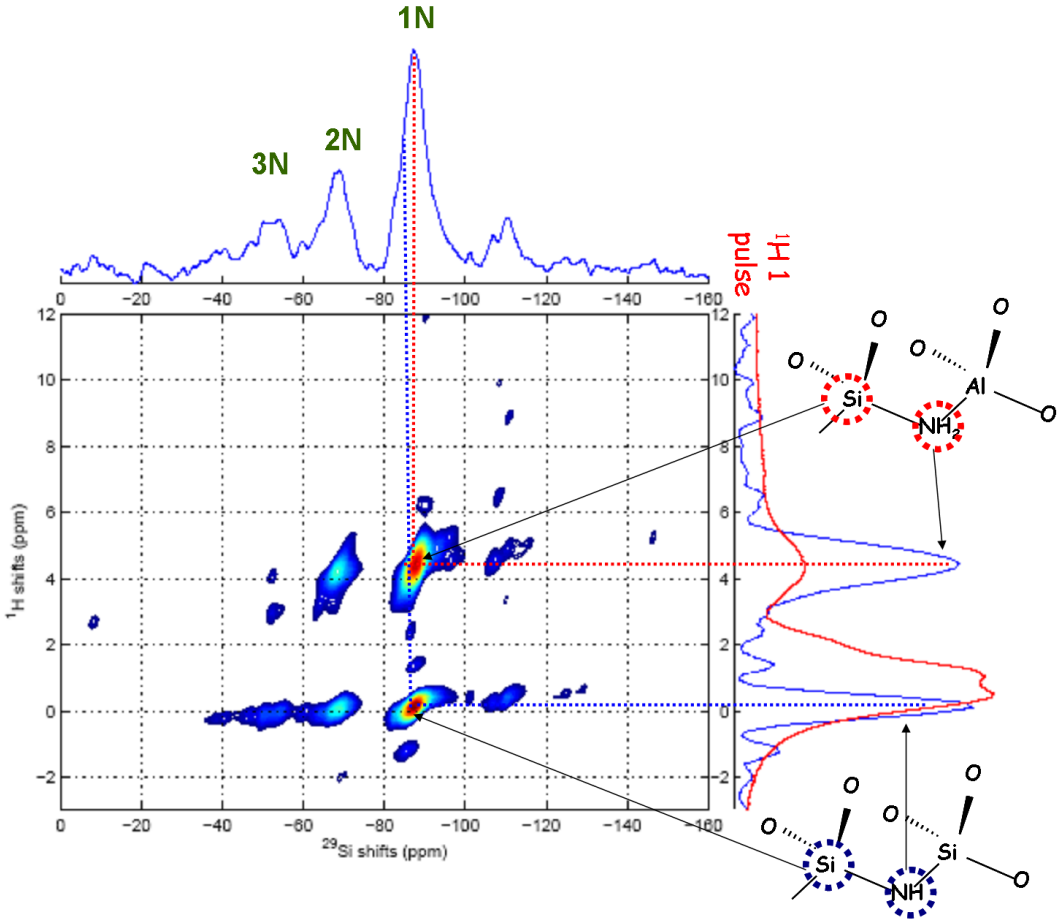

Figure 4.10. $^{1}H/^{29}Si$ HETCOR NMR 2D spectra for nitrogen substituted HY zeolite with Si/Al ratio of 15(42) sample prepared at 800°C for 24h, a contact time of 1 ms was used. Blue spectra are the projection of ^{29}Si and ^{1}H dimensions. Red spectrum is the 1-pulse ^{1}H NMR data.

Figure 4.10 shows the $^{1}H/^{29}Si$ HETCOR data for highly nitrogen substituted HY zeolite with low aluminum content (Si/Al=15). For the assignment of different silicon environments and the correlation of these with the proton environments, the same approach is used with the nitridated HY zeolite with high aluminum content. Differing from the correlations with proton environments for the HY sample with high aluminum content, the Si-NH-Si environment in the low aluminum sample is correlated with only one the proton peaks in the high field region (0.4 ppm) which was assigned as either SiNHSi or $SiNH_2$ environment. Therefore the proton peak which is not observed with the

HETCOR experiment, but present in the one pulse ^{1}H MAS NMR data, is either not in close proximity to any of the silicon environments or it is not successfully cross polarized due to high motion/ mobility of the protons of this environment.

4.3.4. Possible Nitrogen Substitution Mechanism

A detailed explanation of the nitridation mechanism can be made by careful examination of the differences in aluminum-27 data on the samples prepared at different reaction conditions and also the silicon-29 data on the same samples, as well as the nature of the aluminum environments formed. ^{27}Al MAS NMR spectra show us that all the nitridated samples (both high and low aluminum HY and NH_4Y) except NaY have similar patterns and broadening, indicating similar aluminum environments and quadrupolar interactions. The nitridation level of the NH_4Y zeolite with a Si/Al ratio of 2.55 is found to be higher than for the HY zeolite with a similar aluminum content (Si/Al ratio of 6.0 due to dealumination of the pristine material) at every nitridation temperature, which is both supported by both ^{29}Si MAS NMR and EDX analysis.

Comparing the silicon-29 NMR data of all the nitridated samples, the substitution degree follows the order NH_4Y(Si/Al=2.5), HY(Si/Al=15), HY(Si/Al=2.5) and NaY (Si/Al=2.5) from high to low substitution. The calculated values for the intensity of different aluminum environments (Table 4.2) of different zeolites are consistent with the silicon-29 data. However, a gradual increase in the relative intensity of each aluminum environment with a higher nitrogen substitution degree is not seen with time and temperature, as it was for the silicon environments. This observation suggests that once the reaction starts, further nitrogen substitution follows through the silicon tetrahedra which has already been nitrogen substituted at least once, but not through an Al-O-Si linkage. On the other hand the presence of distorted Al-O-Si linkages with a possible nitrogen substitution on the adjacent tetrahedron, even in high temperature treated, highly nitridated samples shows that, once an aluminum site is nitridated further nitrogen substitution follows through the same aluminum environment but not on a new one. This results in a non-uniform nitrogen substitution within the zeolite system.

The low nitrogen substitution on an Al-O-Si bond in NaY zeolite, especially at lower temperatures, is consistent with the reaction energy calculations, since the substitution between a Si-O-Al site in NaY, costs more than 120 kJ/mol which is higher compared to 100 kJ/mol for substitution at a Si-O-Si site. For HY zeolites, the energy calculations show that the nitrogen substitution for Si-OH-Al linkage costs about 35 kJ/mol, lower than the 100 kJ/mol for substitution at a Si-O-Si site. However, experimentally HY zeolites seem to follow a different course than NaY, showing a random nitrogen substitution especially with treatments at high reaction temperatures. The dealumination of the framework during the treatment can be reason for unbiased substitution as it leaves the nitridated framework mostly siliceous and nitridated aluminum environments as extraframework formations.

4.4. Conclusions

^{1}H and ^{27}Al MAS NMR have been used to study the proton and aluminum local environments of nitrogen substituted zeolite Y. The use of high field ^{27}Al MAS and MQMAS NMR resolves the resonances in the spectra corresponding to aluminum atoms with different nitrogen substitution degree. It is shown that in the early stages of the nitrogen substitution reaction, the Si-O-Al linkage reacts first causing dealumination of the framework in the proton type of zeolite Y, whereas, nitrogen substitution in NaY type of zeolites is preferential. For the reactions taking place at high temperatures, further nitrogen substitution takes place non uniformly for the aluminum tetrahedra resulting in a non-uniform distribution of aluminum oxides, aluminum oxy nitrides and extraframework aluminum nitrides.^{1}H MAS and $^{1}H/^{14}N$ TRAPDOR MAS NMR supports the formation of basic NH/NH_2 sites following the nitrogen substitution at high temperatures and $^{1}H/^{27}Al$ TRAPDOR NMR has defined the amine sites in the vicinity of aluminum environments. The results are in good agreement with the aluminum data suggesting preferential nitrogen substitution over Si-O-Si linkage resulting in lower amine sites with aluminum vicinity and presence of extraframework amine substituted aluminum sites. $^{1}H/^{29}Si$ HETCOR experiments have shown well resolved proton correlated silicon environment with different nitrogen substitution degree and aluminum

content. The correlations with the different proton environments allowed us to separate the Si-NH-Si environment from the Si-NH-Al environment.

4.5. References

(1) Dogan, F.; Hammond, K. D.; Tompsett, G. A.; Huo, H.; Conner, W. C.; Auerbach, S. M.; Grey, C. P. *J. Am. Chem. Soc.* **2009**, *131*, 11062.

(2) Zhang, C.; Xu, Z.; Wan, K.; Liu, Q. *Appl. Catal., A* **2004**, *258*, 55.

(3) Ernst, S.; Hartmann, M.; Sauerbeck, S.; Bongers, T. *Appl. Catal., A* **2000**, *200*, 117.

(4) Narasimharao, K.; Hartmann, M.; Thiel, H. H.; Ernst, S. *Microporous and Mesoporous Materials* **2006**, *90*, 377.

(5) Xiong, J. M.; Ding, Y. J.; Zhu, H. J.; Yan, L.; Liu, X. M.; Lin, L. W. *Journal of Physical Chemistry B* **2003**, *107*, 1366.

(6) Hammond, K. D.; Gharibeh, M.; Tompsett, G. A.; Dogan, F.; Brown, A. V.; Grey, C. P.; Auerbach, S. M.; Conner, W. C. *Chemistry of Materials* **2010**, *22*, 130.

(7) Astala, R.; Auerbach, S. M. *J. Am. Chem. Soc.* **2004**, *126*, 1843.

(8) Hammond, K. D.; Dogan, F.; Tompsett, G. A.; Agarwal, V.; Conner, W. C.; Grey, C. P.; Auerbach, S. M. *J. Am. Chem. Soc.* **2008**, *130*, 14912.

(9) G. Engelhardt, D. M. *High Resolution Solid-State NMR of Silicates and Zeolites*; John Wiley and Sons, 1987.

(10) S. M. Auerbach, K. A. C., P. K. Dutta *Handbook of Zeolite Science and Technology*; Marcel Dekker Inc., 2003.

(11) A. Auroux, A. B., E. Brunner, F. Fajula, E. Garrone, A. Jentys, J. A. Lercher, H. Pfeifer *Acidity and Basicity*; Springer: Heidelberg, 2008; Vol. 6.

(12) Mackenzie, K. J. D.; Smith, M. E. *Multinuclear Solid-State NMR of Inorganic Materials*; Pergamon Material Series, 2002; Vol. 6.

(13) Huang, J.; Jiang, Y.; Marthala, V. R. R.; Thomas, B.; Romanova, E.; Hunger, M. *J. Phys. Chem. C* **2008**, *112*, 3811.

(14) Kao, H.-M.; Grey, C. P. *J. Phys. Chem.* **1996**, *100*, 5105.

(15) Jiao, J.; Altwasser, S.; Wang, W.; Weitkamp, J.; Hunger, M. *J. Phys. Chem. B* **2004**, *108*, 14305.

(16) van Bokhoven, J. A.; Koningsberger, D. C.; Kunkeler, P.; van Bekkum, H.; Kentgens, A. P. M. *J. Am. Chem. Soc.* **2000**, *122*, 12842.

(17) Fyfe, C. A.; Bretherton, J. L.; Lam, L. Y. *Chem. Commun. (Cambridge)* **2000**, 1575.

(18) Fyfe, C. A.; Bretherton, J. L.; Lam, L. Y. *J. Am. Chem. Soc.* **2001**, *123*, 5285.

(19) Jiao, J.; Kanellopoulos, J.; Wang, W.; Ray Siddharth, S.; Foerster, H.; Freude, D.; Hunger, M. *Phys Chem Chem Phys* **2005**, *7*, 3221.

(20) Fitzgerald, J. J.; Kohl, S. D.; Piedra, G.; Dec, S. F.; Maciel, G. E. *Chemistry of Materials* **1994**, *6*, 1915.

(21) Hunger, M. *Solid State Nuclear Magnetic Resonance* **1996**, *6*, 1.

(22) Grey, C. P.; Vega, A. J. *Journal of the American Chemical Society* **1995**, *117*, 8232.

(23) Jiao, J.; Kanellopoulos, J.; Wang, W.; Ray, S. S.; Foerster, H.; Freude, D.; Hunger, M. *Physical Chemistry Chemical Physics* **2005**, *7*, 3221.

(24) Jiao, J.; Kanellopoulos, J.; Behera, B.; Jiang, Y.; Huang, J.; Marthala, V. R. R.; Ray, S. S.; Wang, W.; Hunger, M. *J. Phys. Chem. B* **2006**, *110*, 13812.

(25) Jiao, J.; Wang, W.; Sulikowski, B.; Weitkamp, J.; Hunger, M. *Microporous and Mesoporous Materials* **2006**, *90*, 246.

(26) Jiao, J.; Ray, S. S.; Wang, W.; Weitkamp, J.; Hunger, M. *Z. Anorg. Allg. Chem.* **2005**, *631*, 484.

(27) Klinowski, J. *Annual Review of Materials Science* **1988**, *18*, 189.

(28) El Haskouri, J.; Cabrera, S.; Sapina, F.; Latorre, J.; Guillem, C.; Beltran-Porter, A.; Beltran-Porter, D.; Marcos, M. D.; Amoros, P. *Advanced Materials* **2001**, *13*, 192.

(29) Puurunen, R. L.; Lindblad, M.; Root, A.; Krause, A. O. I. *Physical Chemistry Chemical Physics* **2001**, 1093.

Chapter 5

Basicity of Nitrogen Substituted Zeolites

Abstract

The basic character of the zeolite framework is increased by substitution of the framework oxygen by nitrogen through treatment of the zeolite materials under ammonia flow at high temperatures. The reaction is performed on zeolite Y, with different aluminum contents and extraframework cations. The basicity of the treated zeolites is investigated by loading an acidic probe molecule, Boric Acid Trimethyl Ester (BATE), and the interaction of the probe molecule with zeolite framework is studied by ^{11}B NMR. The results show two major ^{11}B NMR peaks, one for 3-coordinate boron and another for a 4-coordinate boron environment. As the nitrogen content of the zeolite framework increases, a distortion in the 3-coordinate site and an intensity increase in the 4-coordinate one is observed, suggesting an increased basicity of the framework. The effect of zeolite composition on the basicity of the treated zeolites is also studied by comparing the interaction of the probe molecule with the nitrogen substituted zeolite framework with different extraframework cations. The nitridated NaY zeolites shows a higher basic character than the nitridated HY zeolites prepared with identical treatment conditions.

5.1. Introduction

In the previous chapters, the synthesis of nitrogen substituted zeolites and characterization of their local structure, as well as a comparison of nitrogen substitution efficiencies of different zeolite compositions have been covered. The main driving force for the nitridation reaction is to increase the framework basicity of the zeolites, in order to form suitable solid base catalysts that can be used in various industrial applications, specifically, in the production of renewable chemicals and fuels from biomass.

Substitution of the framework oxygen by nitrogen should increase the basic strength of the zeolite framework due to the lower electronegativity of nitrogen with respect to oxygen. This was confirmed by density functional theory (DFT) calculations,[1] where the adsorption energies for various acid-base pairs in NH_3 treated and untreated zeolites were calculated to estimate the Brønsted acid and Lewis base strengths of the doped system. Zeolite Y containing Brønsted acid sites (Si-OH-Al) was found to be a stronger acid than the zeolite Y framework containing Si-NH_2-Al, whereas the Si-NH-Si linkages were found to be a much stronger Lewis bases than the Si-O-Si site.

Several methods, both theoretical and experimental, have been developed to measure the basic character of the pristine zeolites[2-5]. Experimental studies are based on the use of probe molecules (as briefly summarized in section 1.5), interacting basic oxygen sites of the zeolite framework and also testing the zeolites in appropriate catalytic reactions. However, experimentally, the basicity of the nitrogen substituted zeolites has only been studied by testing the catalyst in Knoevenagel condensation reactions (Section 1.2.2) and the nature of the basic sites has not yet been investigated with an appropriate probe molecule.

Boron-containing compounds, such as Boron Trifluoride (BF_3) and Boric Acid Trimethyl Ester (BATE), possess Lewis acidity and can be used as probe molecules to study the basic property of nitrogen substituted zeolites. Morrow *et al.* studied adsorption of BF_3 on silica in detail[6]. They found that BF_3 dissociates on the silica surface forming two species: $SiOBF_2$ and $(SiO)_2BF$ and that the dissociative adsorption depends on the degree of surface dehydroxylation. Liu *et al*. reported that BF_3 is too reactive to be used as a probe molecule for surface basicity studies and they used BATE to characterize the

basicity of metal oxides[7,8]. The group identified different basic sites of pristine zeolite Y by using BATE, detecting the binding by using IR spectroscopy.

Boric Acid Trimethyl Ester (BATE) is a Lewis acid with planar geometry, a strong interaction with surface oxygen anions converting its planar structure into a pyramidal one. This makes it possible to study the changes in the symmetry of the molecule due to the interactions with the basic sites in zeolites, by ^{11}B MAS NMR. As explained in Section 1.4.1.3, ^{11}B is a quadrupolar nuclei and it can give rise to significant broadening and distortions of the NMR resonances of compounds with asymmetrical boron environments. Boron containing oxo-compounds typically contain tetrahedral BO_4 or trigonal BO_3 configurations. The former has a relatively narrow single resonance with δ_{iso} of 2 to -4 ppm and a C_Q of 0 to 0.5 MHz whereas the latter has larger C_Q of around 2.5 MHz and δ_{iso} values ranging from 12 to 19 ppm[9]. Han and co-workers studied the basicity of pristine zeolites with BATE and ^{11}B NMR[10]. As shown in Figure 5.1. BATE has one peak at around 20 ppm for the 3-coordinate boron environment with relatively small quadrupolar coupling constant. Interaction with a strong Bronsted base, such as NaOH, results in a second ^{11}B peak at 2.3 ppm, which is assigned to a 4-coordinate site. A weaker interaction results in shifts in the peak position of the 3-coordinate site and broadens the peak due to the increase in C_Q value.

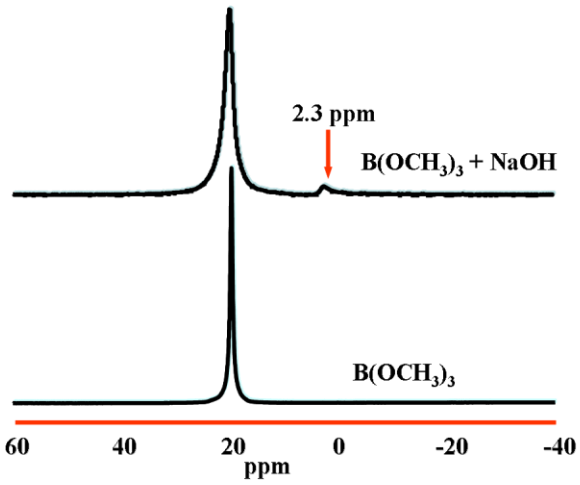

Figure 5.1. ^{11}B MAS NMR of interaction of BATE with NaOH in liquid [10]. A 4-coordinate site is seen at 2.3 ppm.

The BATE probe molecule was used by Han *et al.* to compare the basicities of alkali metal-cation exchanged Y. As already mentioned in the Section 1.3.2., the basic strength of zeolites is strongly enhanced as the electronegativity of the compensating cation decreases. The effects of the alkali ions on the basic strength of the framework are in the following order: Cs+ > Rb+ > K+ > Na+ > Li+, where the basic sites are framework oxygen ions. Figure 5.2 shows the ^{11}B MAS NMR data of the interaction of the BATE molecule with zeolite Y framework having different basicities. As the basicity of the framework increases, the formation of 4-coordinate boron site is observed and the intensity of ^{11}B NMR peak at 15 ppm region decreases a new second-order quarupolar broadened lineshape appears consistent with the distortion expected for a 3-coordinate boron environment.

The quadrupolar lineshape is close to that expected for a species with axial symmetry, such as a planar or slightly distorted BATE molecule. The lineshapes in quadrupolar nuclei can be strongly affected by motion. If the motion is slow on the time scale of the quadrupolar interaction, ω_Q^{-1}, these effects are minimal. If the molecular motion is fast on the time scale of ω_Q^{-1}, then the quadrupolar interaction averages out resulting in narrower lineshapes. If the motion is much slower, but still fast on the timescale of the second-order quadrupolar broadening, the characteristic second-order quadrupolar lineshepes will disappear, and again sharper lines will be observed. Thus, the narrow peak shapes seen for some 3-coordinate resonances most likely indicate rapid molecular motion of the BATE molecule within the zeolite pores. In general, this should indicate a weak interaction with the zeolite framework. A quadrupolar lineshape should indicate a stronger interaction, but there may be cases where lower mobility may also indicate tight packing of the molecules in the pores. Furthermore, a reduction of the rigid quadrupolar lineshape should indicate a stronger interaction with the framework, since the BATE molecule distorts to approach tetrahedral binding. In the limit, i.e., when a 4-coordinate environment is formed, the quadrupolar interaction should be very small. Thus, the lineshapes of the 3-coordiante environments will be a function of both the strength of the interactions and the generally, but not always, correlated motion.

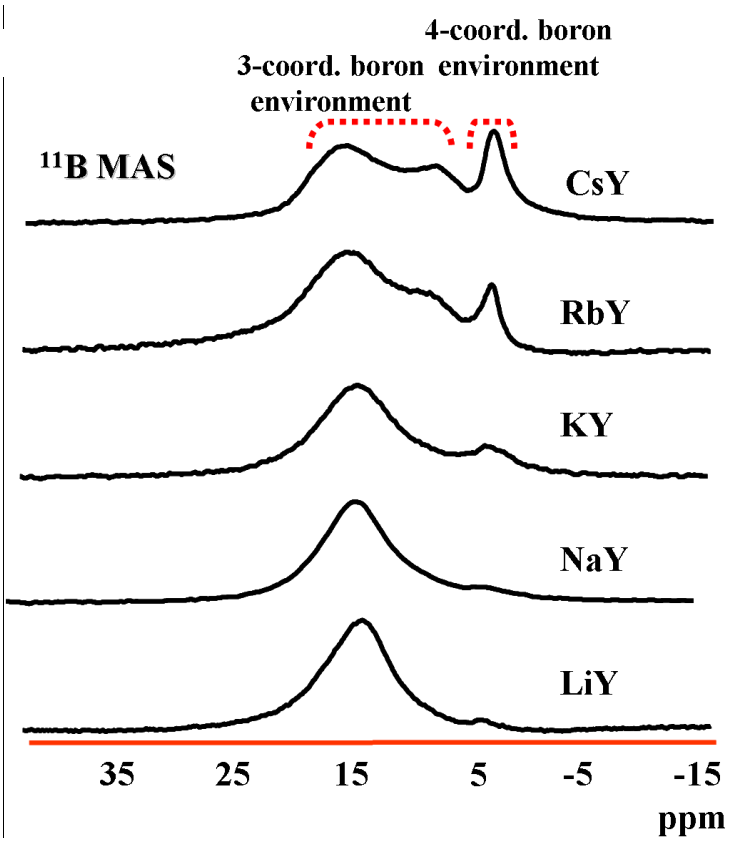

Figure 5.2. ^{11}B NMR of BATE on alkali metal-cation exchanged Y[10]. As the basicity of the framework increases, the intensity of the 4-coordinate boron resonance increase and the lineshape of 3-coordinate boron environment becomes more distorted.

Han and co workers explained the changes in the ^{11}B NMR data and the distortions in the 3-coordinate boron site by the presence of Lewis basic site with the following reaction:

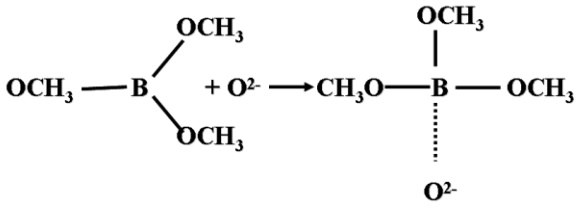

(5.1.)

With this reaction, the electron donation of the Lewis base to the BATE probe molecule results in the distortion of the molecule from planar geometry, resulting in a quadrupolar line shape of the ^{11}B NMR spectrum.

The formation of the 4-coordinate boron site was explained by the presence of the Bronsted basic sites with the reaction below,

$$B(OCH_3)_3 + OH^- \rightarrow B(OCH_3)_3OH \quad (5.2.)$$

The solid state NMR and X-ray Diffraction characterization studies of the ammonia treated zeolites have shown that nitrogen can be successfully substituted into the framework at high levels keeping the crystallinity and porosity of the material[11]. Investigation of the basicity of the treated zeolites requires either testing the material using catalytic test reactions or the use of appropriate acidic probe molecule studying their interactions with the basic sites in the nitrogen substituted zeolites. In this chapter, we study and compare the basicity of nitrogen substituted zeolites, prepared from different zeolite parent compound compositions, by using the probe molecule Boric Acid Trimethyl Ester (BATE) and ^{11}B MAS NMR as a characterization method.

5.2. Experimental

5.2.1. Materials and Method

The synthesis of nitrogen substituted zeolites used in this study is described in the previous chapter in Section 3.2.1. The NaX zeolite used was of commercial origin (faujasite NaX molecular sieve type 13-X from Aldrich Co.). The pristine dry zeolites were prepared by heating the samples first to 110^{o}C and keeping at the temperature for 3 hours under constant vacuum and then heating to 400^{o}C where they were kept still under vacuum overnight. All the samples for the characterization experiments are loaded into NMR rotors in a glovebox. The following nomenclature is used to label the samples: The first label “Nit” indicates that zeolites and nitrided. The type of the zeolite (e.g., HY, NaY) and Si/Al ratio is then given, which is then followed by the nitridation temperature in ^{o}C and the last the treatment duration in hours.

Boric Acid Trimethyl Ester (BATE) from Aldrich was used as the probe molecule to study the basicity of the nitrogen substituted zeolites. The zeolite samples were weighed before and after BATE loading and the loading was achieved using a vacuum line by the following procedure and the illustration of the experimental set-up is given in Figure 5.3.

Approximately 50 mg of sample was introduced into a glass sample holder in a nitrogen glovebox where it was tightly closed. The sample holder was then attached to the vacuum line and the zeolite sample was evacuated at room temperature for about 30 minutes. The liquid BATE in a glass holder was also attached to the set up. After the vacuum line set up was closed and leaving the inside pressure constant, the valve for liquid BATE was opened and the vacuum line filled with BATE vapor at a pressure of about 13 millitorr. The valve of the sample valve was then opened. By using the vapor pressure of the liquid, BATE adsorption was then carried out by exposing the evacuated sample to BATE vapors. The change in the pressure value of the vacuum line system was then recorded at every step. During the adsorption of the probe molecule the zeolite sample was inserted in liquid nitrogen dewar until the pressure reaches a minimum. The glass vial containing BATE loaded nitridated zeolite was then removed from the liquid nitrogen and was left at room temperature until the pressure at the vacuum line reached at a constant pressure. The amount of adsorbed molecules was calculated by using the final pressure changes in the vacuum line. In another set of experiments after the loaded samples were removed from the liquid nitrogen, they were pumped down for five minutes. The adsorbed probe molecules remaining onto the zeolite after evacuating at room temperature were assumed to correspond to chemisorbed molecules. For this set, the changes in the weight of zeolite samples were used to calculate the amount of BATE molecules loaded. All the samples were then immediately taken to a glovebox and packed into rotors for NMR experiments.

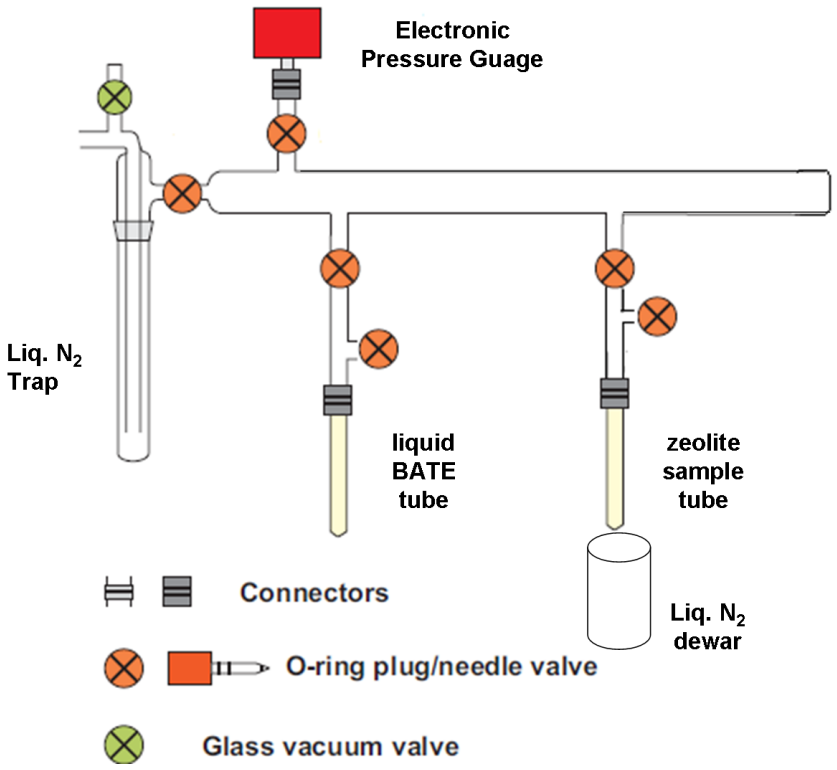

Figure 5.3. Illustration of experimental set-up for BATE loading experiments.

5.2.2. Characterization

^{11}B MAS NMR studies were carried with a double resonance 4 mm probe with a spinning rate of 10 kHz on 500 and 360 MHz spectrometers. The spectra were referenced to the secondary reference a 0.1 M solution of H_3BO_3 at 18.8 ppm[9]. Single pulse experiments were performed with a pulse width of 1.2 μs and a pulse delay of 2 s. The ^{11}B MQMAS NMR experiments were carried out by using the 'z-filter' method (Section 1.4.1.2). A standard triple quantum MAS pulse sequence with two hard pulses followed by a soft 90 degree solid pulse was applied. The experiment was performed at 10 kHz spinning rate. All the simulations were done with the WSolids NMR simulation package by K. Eichele.

5.3. Results and Discussions

5.3.1. Boric Acid Trimethyl Ester (BATE) Loading on Pristine Zeolites

Figure 5.4 shows the ^{11}B MAS NMR spectra of BATE loaded Y zeolites with different aluminum contents and extraframework cations. All the samples were dried prior to loading of the probe molecule and the zeolite samples were pumped down after loading, leaving only the BATE molecules chemisorbed to the zeolite framework. ^{11}B NMR spectra for the BATE loaded pristine zeolites consist of two peaks, 20 and 3 ppm, that can be assigned to 3- and 4-coordinate boron, respectively. A clear shift in ^{11}B NMR to lower chemical shift is observed for the 3-coordinate resonance as the expected basicity of the zeolite framework increases. Considering the cation forms and the Si/Al ratio of the three zeolites (Section 1.3.2), the basicity of the samples should be in the following order; HY Si/Al=15(41) < HY Si/Al=2.55(6.1) < NaY Si/Al=2.5.

Comparing with the data obtained by Han and co workers, the intensity of the 4-coordinate site should increase as the framework basicity increases. As stated in the introduction, the explanation for the formation and changes of these sites was due to presence of Lewis and Bronsted basic sites. However, it is also possible that, for the interaction of BATE with basic sites of the zeolite framework, there may only be a Lewis acid- base reaction and the symmetric 3-coordinate ^{11}B resonance may be due to a weakly interacting, planar BATE molecule and any distortion observed due to a weak interaction of the probe molecule with the zeolite framework. The ^{11}B peak at 0 ppm, is then assigned to the 4-coordinate boron environment formed by a strong interaction of BATE with the basic sites of the zeolites.

Differing from the BATE-loaded pristine NaY and HY sample with low aluminum content, the BATE-loaded pristine HY sample with high aluminum content (Si/Al ratio of 2.5) shows a broader peak for the 3- coordinate boron site. In order to investigate all the possible boron environments, 2D ^{11}B MQMAS NMR was performed on this sample (Figure 5.5). The slices of ^{11}B MQMAS spectra were taken at the center of gravity of the 2D contours and the figure includes simulations of the slices. The NMR parameters obtained by the simulations of these slices are also given in the figure.

As it is seen in the 2D MQMAS data, the isotropic dimension shows three resonances for 18 ppm region. The peak around 16 ppm has a small quadrupolar coupling constant therefore this site can be assigned as a weakly bound BATE molecule having higher symmetry and mobility. The other two peaks (17.8 and 16.8 ppm) have larger quadrupolar coupling constants and can be assigned as 3-coordinate boron environments weakly bonded to the zeolite framework. It should be noted that, this sample has both acidic Si-OH-Al linkages as well as a small number of Si-O-Al linkages compensated by residual Na^+ cations as the EDX analysis showed (Chapter 3). The presence of different boron environments can be explained by the presence of different basic environments in the zeolite framework.

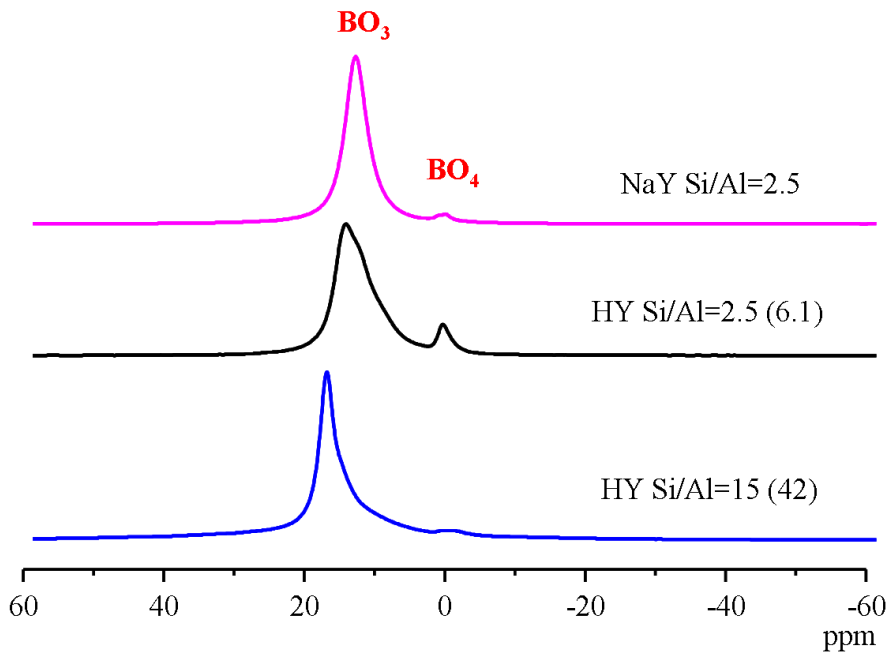

Figure 5.4. ^{11}B MAS NMR of BATE loaded zeolite Y. The effect of aluminum content and type of extraframework cation on the basicity of pristine zeolite Y. Numbers within parenthesis show the actual Si/Al ratio of the framework (Calculated by ^{29}Si MAS NMR).

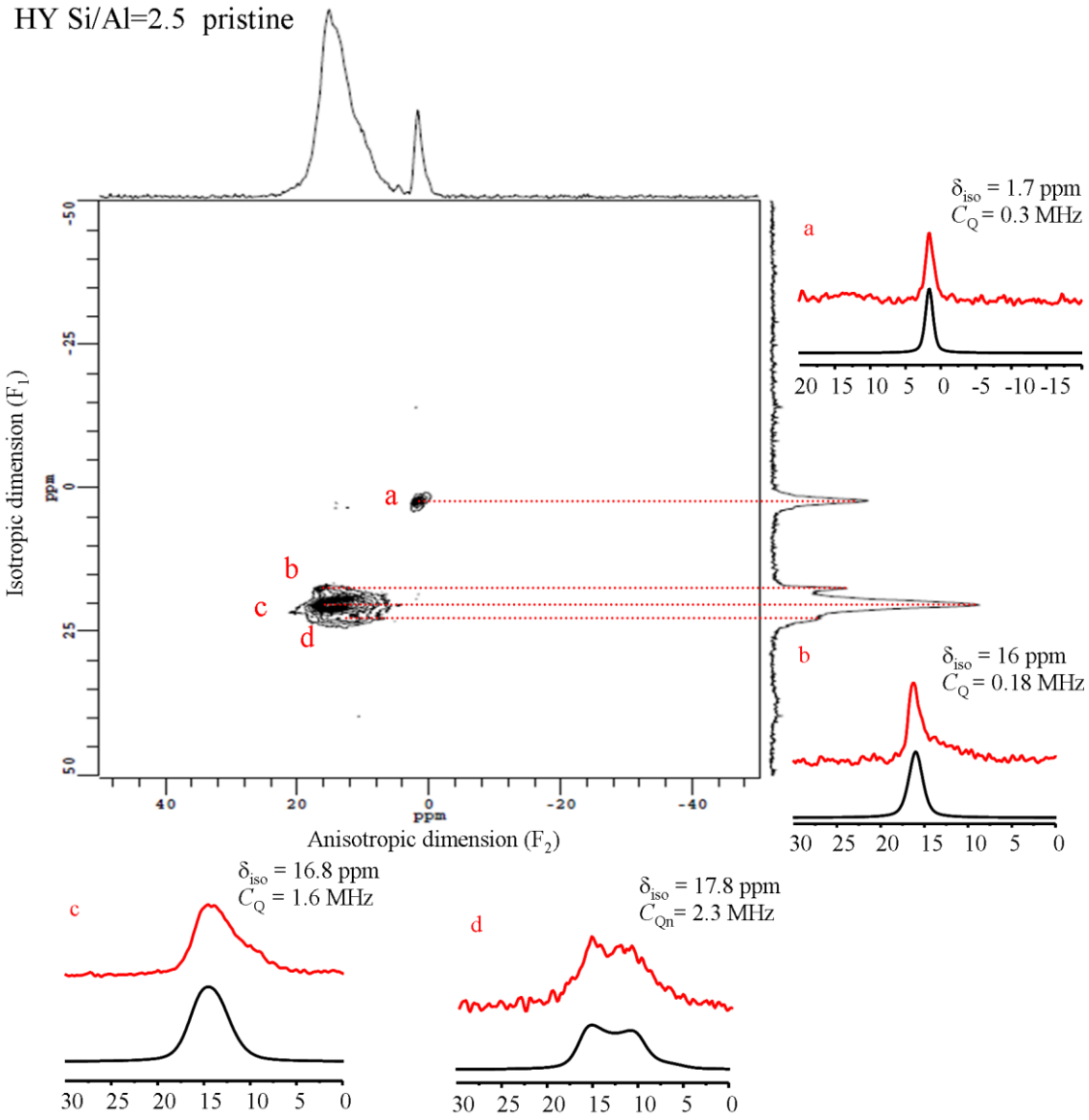

Figure 5.5. 2D ^{11}B MQMAS spectra of BATE loaded HY zeolite with a Si/Al ratio of 2.5. Projection of F_1 and F_2 dimensions are shown on the side of the 2D spectrum. (a,b,c, and d) Selected isotropic spectra taken from the slices of anisotropic dimension with the simulations and quadrupolar parameters given on the left. The dotted lines in the 2-D spectrum show where the slices are taken.

5.3.2. Boric Acid Trimethyl Ester (BATE) Loading on Nitrogen Substituted Zeolites

The basicity experiments are performed on the nitrogen substituted zeolites treated at varying reaction conditions. As discussed in Chapter 3, varying treatment conditions result in different nitrogen substitution levels in the zeolite framework. The relation between the nitrogen content of the zeolite and its basicity can be investigated by comparing the BATE loading efficiency of the zeolite samples nitridated at different conditions. The BATE loaded samples discussed in this section were not vacuumed after loading, therefore, the zeolites contain both chemisorbed and physisorbed BATE molecules.

Table 5.1. Nitrogen content, surface area analysis and amount of loaded BATE for pristine and nitrogen substituted zeolite Y.

Nitridated Zeolite	**% N substitution**	**BATE loading (# of BATE molecule/ unit cell of zeolite)**	**BET Surface Area (m^2/g)**
Nit.HY.Si/Al=15 pristine		0.240	858
Nit.HY.Si/Al=15.750.24	9.7	0.115	634
Nit.HY.Si/Al=15.800.24	25.9	0.228	597
Nit.HY.Si/Al=15.850.24	45.2	0.320	648
Nit.HY.Si/Al=15.850.48	46.6	0.235	665
Nit.NaY pristine		0.175	656
Nit.NaY.750.24	5.3	0.142	348
Nit.NaY.800.24	6.8	0.167	348
Nit.NaY.850.24	35	0.300	198
Nit.NaY.850.48	42	0.416	331
Nit.HY.Si/Al=2.5 pristine		0.220	638
Nit.HY.Si/Al=2.5.750.24	19	0.310	475
Nit.HY.Si/Al=2.5.800.24	19	0.480	
Nit.HY.Si/Al=2.5.850.24	53	0.778	427

The amount of loaded BATE molecule per unit cell of nitrogen substitued zeolites was calculated by using the pressure changes in the vacuum line during BATE loading and the weight of zeolite used. The results are given in Table 5.1 with the nitrogen content of the zeolites used and their BET surface area. A higher interaction between the adsorbent and adsorbate is expected as the basicity of the zeolite framework increases which is also correlated with nitrogen content of the samples. On the other hand, the amount of loaded BATE molecule is also related with the porosity and surface area of the nitrogen substituted zeolites. Since the high temperature treatment during nitridation reaction causes a decrease in the crystallinity and porosity of the material, this might affect the accommodation of acidic probe molecules by the zeolite framework. Therefore while the nitrogen content and basicity of the framework increase, the loading level of the BATE molecule might decrease.

As shown in Table 5.1, for the nitrogen substituted NaY zeolites, the amount of loaded BATE increases as the nitrogen content increases although the zeolite samples with high nitrogen substitution levels show a noticeable decrease in the BET surface area. Therefore, for the nitrogen substituted NaY zeolites, it can be said that BATE loading is strongly influenced by the nitrogen content (and basicity) of the framework and is not so strongly affected by porosity. On the other hand, the loading level of the parent compound (pristine material) is higher than the nitrogen substituted samples treated at low reaction temperatures (and therefore framework with lower nitrogen content). In this case, it is probable that the effect of porosity and surface area dominates and the untreated sample accommodates higher amount of probe molecule.

Figure 5.6.a shows the normalized ^{11}B NMR data of BATE loaded nitrogen substituted NaY zeolite samples nitridated at different reaction conditions. The spectra show two ^{11}B NMR peaks, around 1 and 18 ppm that can be assigned to 4 and 3-coordinate boron, respectively. As the nitrogen substitution temperature increases, the intensity of the tetrahedral boron resonance increases in response to an increase in the interaction of the basic sites in the zeolite framework and the acidic probe molecule. It should be noted since the treated zeolite framework is not completely nitrogen substituted the interactions include both basic Si-O-Al linkages and amine substituted linkages. On the other hand, the ^{29}Si NMR studies (Chapter 3) showed that increasing reaction

temperature increases nitrogen substitution degree and the ^{11}B NMR data suggest that the basicity of the framework increases as the nitrogen content increases. Therefore, ammonia treatment increases the basicity of the zeolite framework but the BATE interaction is the sum of all possible basic environments in the zeolite framework.

The 3-coordinate boron site observed by ^{11}B NMR for the pristine NaY zeolite shows a broad peak at about 18 ppm, due to the interaction of the probe molecule with basic sites of zeolite framework. As the nitrogen content of the treated NaY zeolites increases, the intensity of the peak decreases both due the decreased concentration of this species and the distortions in the lineshape of the resonance due to the increased quadrupolar interactions (compared with the pumped down sample, as seen in Figure 5.4)and presumably due to the reduced motion.

^{11}B MQMAS NMR was also performed on the BATE-loaded nitrogen substituted NaY zeolite treated at 850^{o}C for 24 hours (Figure 5.7). The 2D MQMAS data reveal that there are at least two boron coordination environments. Consistent with the single pulse data (Figure 5.6.a), the sharp peak at 1 ppm region is a single boron resonance with δ_{iso} of 1.2 ppm and C_Q of a 0.3 MHz, suggesting a symmetric 4-coordinate boron environment which can be the result of interaction of the probe molecule with the basic Si-O-Al or Si-NH-Si/Al linkages. The 2D MQMAS reveal at least two boron resonances for 3-coordination region, with δ_{iso} of 17.8 and 20 ppm and C_Q of 2.4 and 3.4 MHz. Comparing tentatively the differences in the δ_{iso} and C_Q values of the two environments, the 20 ppm peak can be assigned as a boron environment interacting with an amine site of the zeolite framework resulting in a higher C_Q due to higher asymmetry of the BO_3---N environment. The 17.8 ppm peak can be assigned as boron interacting with the basic Si-O-Al linkages of the framework which is also consistent with ^{11}B data for BATE loaded HY zeolite (Figure 5.5.) as the 3-coordinate boron site has similar quadrupolar parameters.

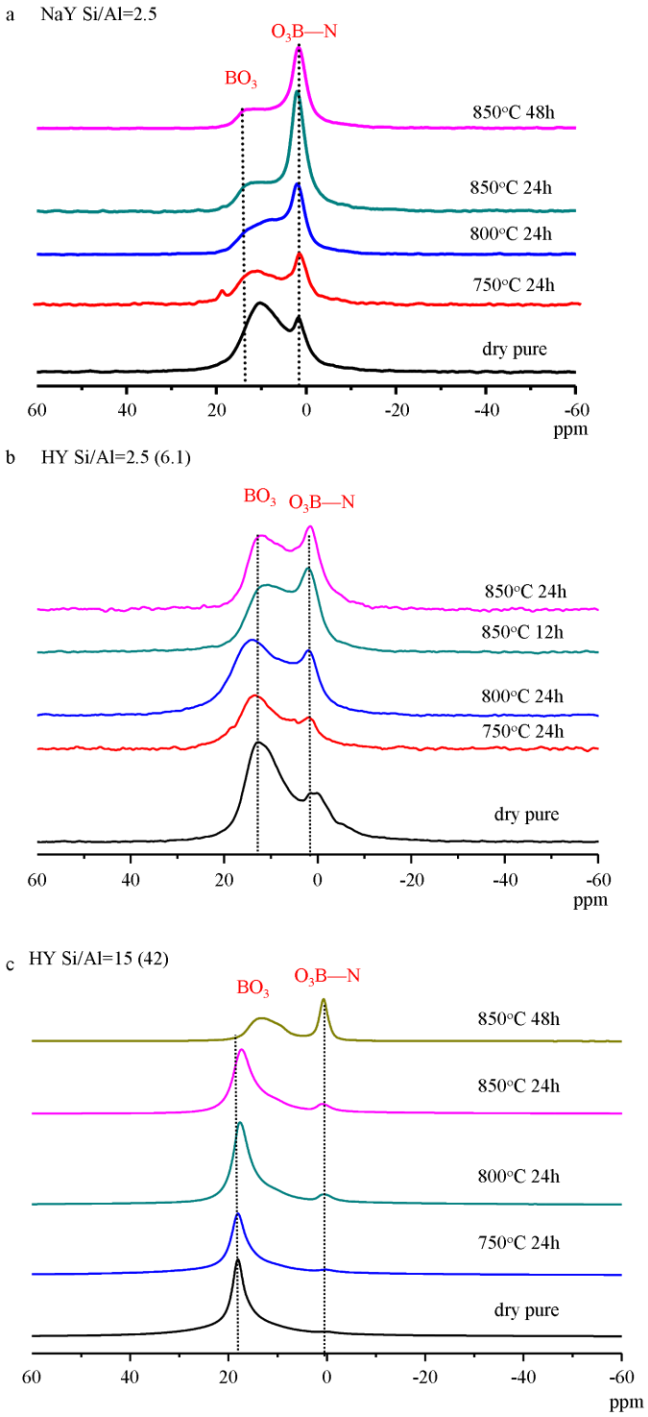

Figure 5.6. ^{11}B NMR data (11.7 T) of BATEloaded nitrogen substituted zeolite Y samples with different framework compositions and treated at different reaction conditions. Numbers within parenthesis show the actual Si/Al ratio of the framework (Calculated by ^{29}Si MAS NMR).

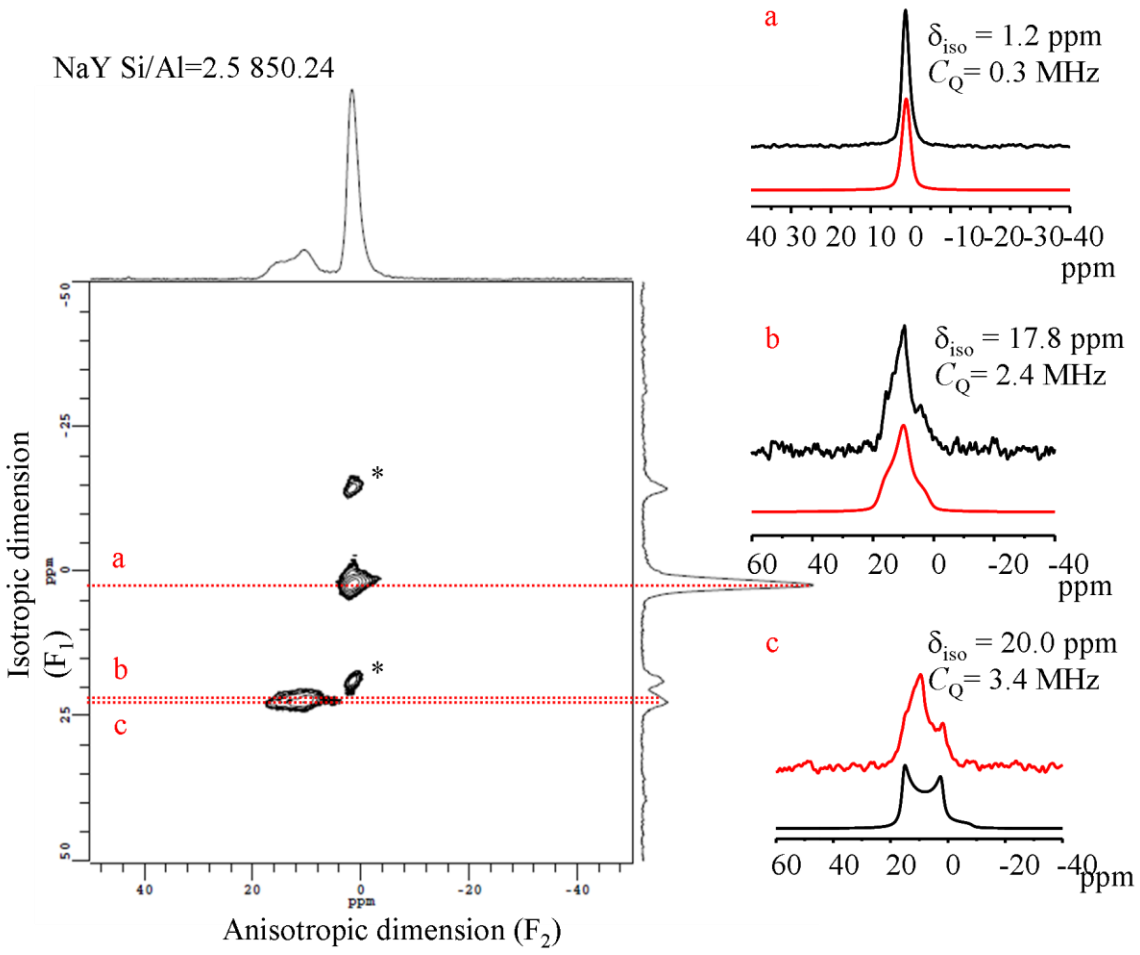

Figure 5.7. 2D ^{11}B MQMAS spectra of BATE loaded nitrogen substituted NaY zeolite with a Si/Al ratio of 2.5. The nitrogen substitution reaction was performed at 850^{o}C for 24 hours. Projection of F_1 and F_2 dimensions are shown on the side of the 2D spectrum. (a and b) Selected isotropic spectra taken from the slices of anisotropic dimension with the simulations and quadrupolar parameters given on the left. The dotted lines in the 2-D spectrum show where the slices are taken. * spinning sidebands

Figure 5.6.b shows the single pulse ^{11}B NMR data of BATE loaded nitrogen substituted HY zeolite (Si/Al ratio of 6.1) treated at different reaction conditions. Similarly with BATE loaded NaY zeolites, there are two main ^{11}B NMR peaks at about 15 and 0 ppm. With increasing nitrogen substitution degree (by increasing the nitrogen substitution reaction temperature and time) the intensity of the 0 ppm peak, which is assigned as the 4-coordinate boron environment, increases and becomes sharper. This

change shows that the amount of acidic BATE molecules strongly interacting with the basic sites of the zeolite framework increases. The intensity of the 3-coordinate boron resonance does not show a dramatic change with ammonia treatment temperature. A slight shift and a line broadening is observed as the nitrogen content increases. The 2D ^{11}B MQMAS NMR data for the BATE loaded HY zeolite (Si/Al ratio of 6.1) nitridated at 850^{o}C for 24 hours, shows two possible boron resonances from the 3-coordinate environment with δ_{iso} of 17.6 and 18.8 ppm and C_Q of 2.3 and 2.8 MHz, respectively (Figure 5.8). Compared to the ^{11}B MQMAS data of the pristine zeolite, the C_Q values gets larger and δ_{iso} values shift to higher frequencies. These changes suggest stronger interactions between the probe molecule and the basic sites of the zeolite framework and therefore an increase in the basicity of the nitrogen substituted zeolite framework. The two different ^{11}B resonances can be due the boron environment interacting with the basic oxygens of the Si-O-Si/Al linkage and basic Si-NH-Si linkage.

The simulation on the ^{11}B MQMAS data for BATE loaded nitridated HY zeolite with Si/Al ratio of 6.1 (Figure 5.8) shows that, the quadrupolar coupling constant for the 4-coordinate boron site is larger compared with the boron site in BATE loaded pristine zeolite (Figure 5.5) and the δ_{iso} value shifts to higher frequency. The resonance observed is either due to the boron environment interacting with a Bronsted base site or a strong interaction with a Lewis base site of the zeolite framework. The changes in the boron local environment (δ_{iso} and C_Q value) is due to the interaction with the amine sites of nitrogen substituted zeolite framework.

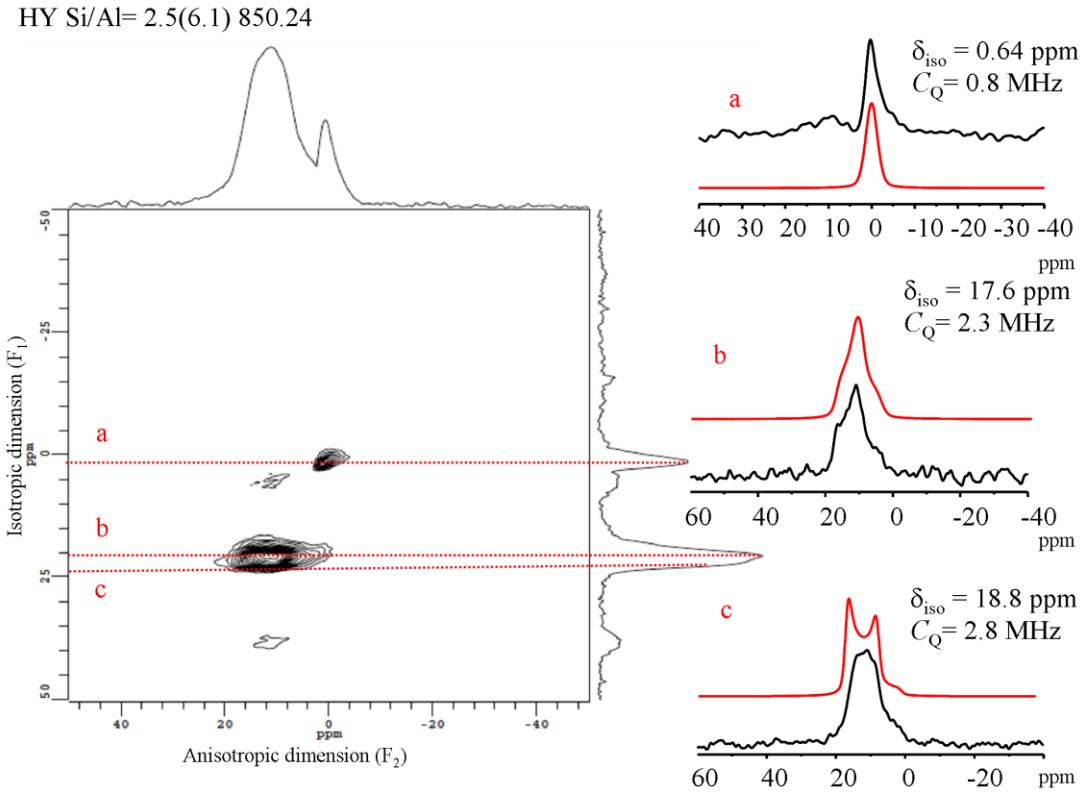

Figure 5.8. 2D ^{11}B MQMAS spectra of BATE loaded nitrogen substituted HY zeolite with a Si/Al ratio of 2.5. The nitrogen substitution reaction was performed at 850^{o}C for 24 hours. Projection of F_1 and F_2 dimensions are shown on the side of the 2D spectrum. (a and b) Selected isotropic spectra taken from the slices of anisotropic dimension with the simulations and quadrupolar parameters given on the left. The dotted lines in the 2-D spectrum show where the slices are taken.

The comparisons of single pulse ^{11}B MAS NMR data for the BATE loaded nitridated HY zeolite with low aluminum content (Si/Al ratio of 15) treated at different reaction conditions, is given in Figure 5.6.c. The low nitrogen content sample (750^{o}C 24h) shows a dominant ^{11}B peak at about 18 ppm and as the nitrogen content of the zeolite framework increases the peak gets broader, shifts to higher frequencies and its intensity decreases. This ^{11}B peak is assigned as 3-coordinate boron, either due to non-interacting BATE molecules or molecules weakly interacting with the basic sites of the zeolite. As the nitrogen content of the zeolite framework increases (zeolites treated at 800^{o}C and above), formation of the 0 ppm ^{11}B peak is observed along with a gradual intensity increase. For the BATE loaded nitrogen substituted zeolite treated at 850^{o}C for 48 hours,

a high intensity 4-coordinate ^{11}B NMR peak is observed along with a distorted 3-coordinate boron environment.

^{11}B MQMAS NMR was performed on the BATE loaded nitrogen substituted HY zeolite (Si/Al ratio of 42) treated at 850^{o}C for 24 hours (Figure 5.9). The MQMAS experiment reveals that there are at least three different boron environments due to the interaction of probe molecule with basic sites of the zeolite framework. The 2D data clearly shows that the 0 ppm resonance is a single boron environment whereas there are at three different sites in the 15-25 ppm region. The slices of the 2D MQMAS data (slices a, b, c and d in Figure 5.9) are used for simulations to get the isotropic chemical shift and quadrupolar coupling constant values. According to the obtained values, the 0 ppm ^{11}B NMR peak has a small C_Q value consistent with a more symmetric tetrahedral boron environment. The simulations show that the quadrupolar interaction for high intensity ^{11}B peak in the 15-25 ppm region (δ_{iso} of 17.6 ppm) is relatively small for a 3-coordinate ^{11}B peak and the shift is high suggesting either motion or a non-interacting boron environment of the BATE probe molecule. The discontinuity and quadrupolar line shape observed in this region is due to the presence of two ^{11}B resonances with relatively large quadrupolar interactions. The two sites with δ_{iso} of 20.8 and 24 ppm have C_Q values of 2.6 and 2.8 MHz and can be assigned to distorted 3-coordinate boron environments that are interacting with the zeolite framework. The presence of two different boron sites can be due the presence of different basic environments in the nitrogen substituted zeolite framework.

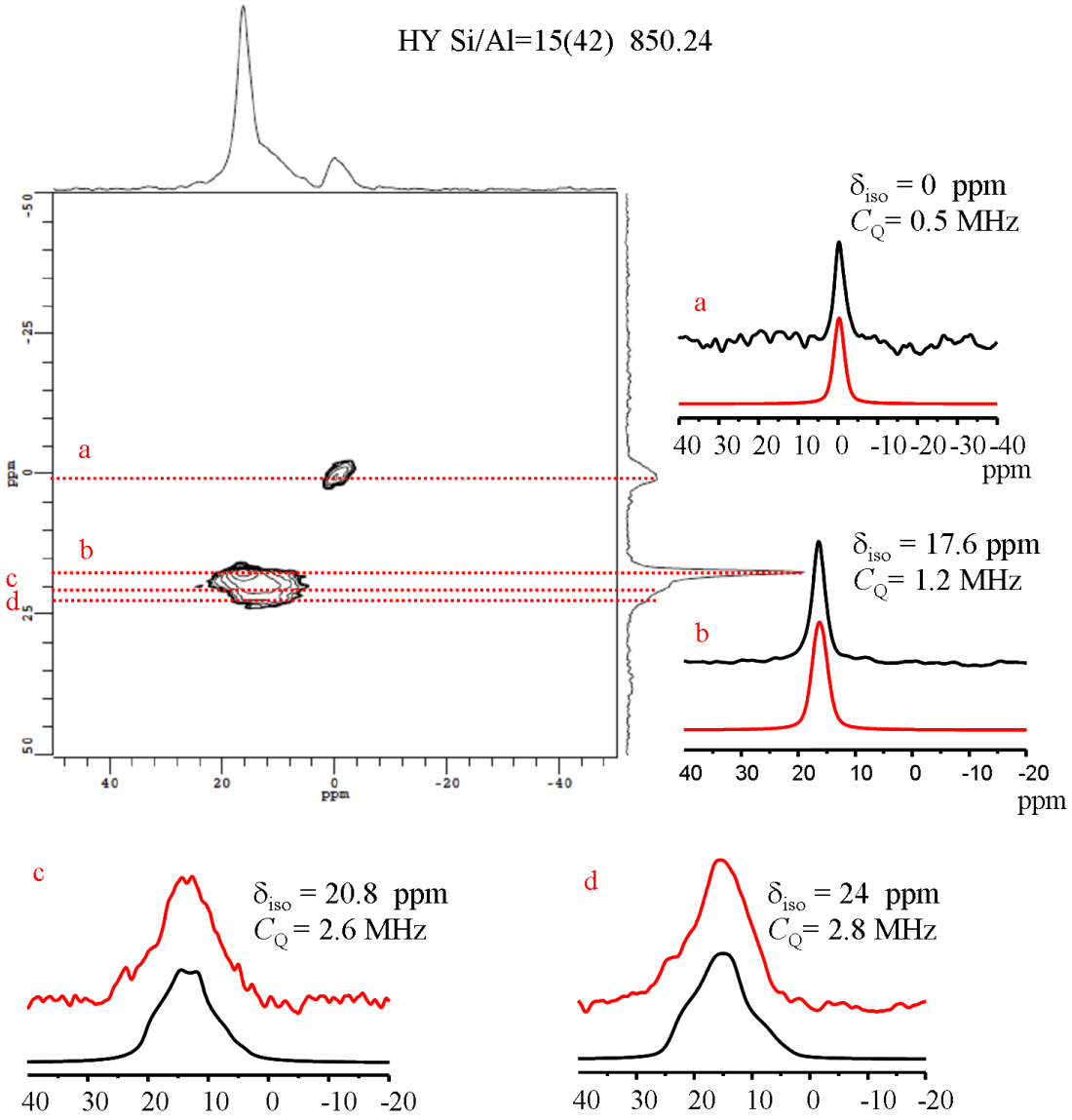

Figure 5.9. 2D ^{11}B MQMAS spectra of BATE loaded nitrogen substituted HY zeolite with a Si/Al ratio of 15. The nitrogen substitution reaction was performed at 850^{o}C for 24 hours. Projection of the F_1 and F_2 dimensions are shown on two sides of the 2D spectrum. (a, b, c and d) Selected isotropic spectra taken from the slices of anisotropic dimension with the simulations and quadrupolar parameters given on the left. The dotted lines in the 2-D spectrum show where the slices are taken.

5.3.3. The Effect of Zeolite Composition on Basicity

The studies on the loading of Boric Acid Trimethyl Ester probe molecule onto the nitrogen substituted zeolites with different nitrogen content shows that the basicity of the framework increases as the nitrogen substitution level increases. As discussed earlier, the nitrogen content is both related with the nitrogen substitution reaction conditions and the parent zeolite framework composition. On the other hand, not only the nitrogen content but also the aluminum content and nature of the extraframework cation of the zeolite framewok must have an effect on the basicity of the nitrogen substituted zeolites.

Figure 5.10 shows the ^{11}B NMR data for the zeolites with different aluminum content, nitrogen content and extraframework cations, loaded with probe molecule BATE. The data allow us to compare the basicity of the pristine zeolites with the nitrogen substituted forms and also with NaX zeolite. NaX zeolite is a faujasite type of zeolite with a high aluminum content (Si/Al ratio smaller than 2.5) and has a higher basicity than the pristine form of NaY and HY zeolites that we have been using for nitrogen substitution reactions.

For the nitrogen substituted NaY zeolite the possible basic environments are either Si-NH-Si and Si-NH-Al linkages or Si-O-Al linkages due to non nitrogen substituted sites. Due to the presence of the amine linkages, the basicity of the framework is expected to increase as compared to the pristine zeolite. In case of the nitrogen substituted HY zeolite with high aluminum content the basic environments should be same as the nitridated NaY zeolite, however, the HY form also contains Si-NH_2-Al linkages that should be acidic. Therefore, the basicity of the framework is independent from the overall nitrogen content of the treated zeolite but more dependent on the presence and amount of Si-NH-Si linkage. Having the same extraframework cation, nitrogen substituted HY zeolite with a low aluminum content also has the same basic and acidic units but, will have more Si-NH-Si linkages considering the Si/Al ratio of the framework.

Following the ^{11}B NMR data for BATE loaded zeolites given in Figure 5.2., our criteria for basicity comparison is to investigate the changes in the peak shape and distortions of the 3-coordinate boron environment (by comparing the changes in C_Q

values) as well as formation and the intensity change in the 4-coordinate boron site of the BATE probe molecule observed in ^{11}B MAS NMR. Since we are also interested in the intensities of the boron sites, another factor we should discuss is the porosity of the nitrogen substituted zeolites which might affect the loading levels of the BATE molecule and the intensity of the observed ^{11}B peaks.

As given in Table 5.1, the lowest loading levels are obtained for the nitrogen substituted HY zeolite with low aluminum content. Consistent with this, the ^{11}B NMR results have shown that the zeolite framework contains the weakest interactions with the BATE probe molecule compared to the other nitridated zeolite types treated under the same conditions, suggesting that nitridated HY zeolite with Si/Al ratio of 42 has the least basic activity. Comparing the intensity and quadrupolar coupling constants of different boron environments observed in ^{11}B NMR spectra of the BATE loaded zeolites (Figure 5.10), nitrogen substituted NaY (treated at high reaction temperature and time) has higher basicity than the other zeolites. For the nitrogen substituted HY zeolite with the high aluminum content, even the calculated loading level of BATE is the highest, the ^{11}B NMR shows boron environments with weak interaction with the zeolite framework suggesting that nitridated HY zeolites have weaker basicity than nitridated NaY zeolite.

5.3.4. The Efficiency of Nitrogen Substituted Zeolites on Furfural Conversion Reaction

Catalytic test reactions have been studied by our collaborators at University of Massachusetts, Amherst, on the nitrogen substituted zeolites. Aldol condensation of furaldehydes with acetone and propanal (Section 1.2.2) is studied on different solid base catalysts such as MgO-ZO_2, NaY, HY, nitrogen substituted HY and NaY. Nitrogen substituted NaY showed good catalytic activity comparable to MgO-ZrO_2 and much higher activity than that of untreated NaY (Figure 5.11). The nitrogen substituted NaY has shown more selectivity to monomer than MgO-ZrO_2 due to the small cage size in the faujasite structure, indicating that we have a shape selective basic catalyst.

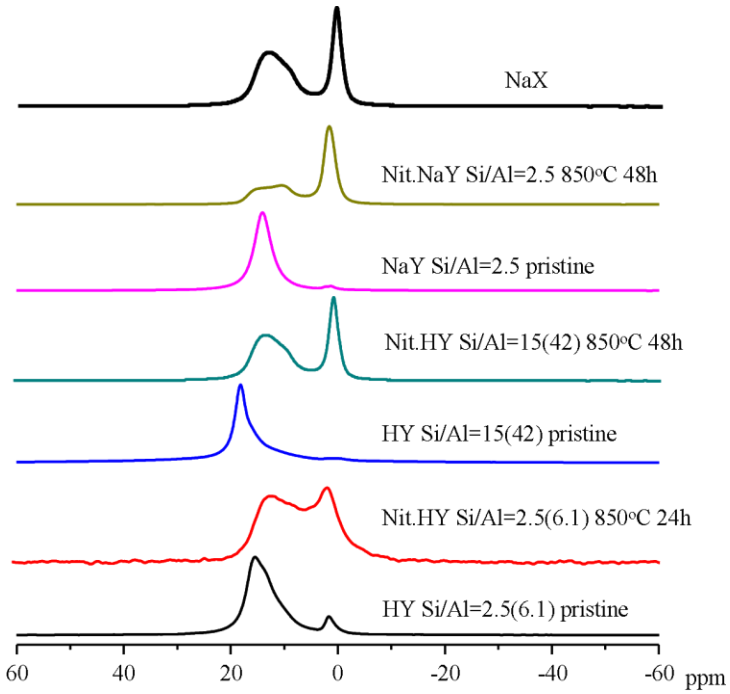

Figure 5.10. ^{11}B MAS NMR of BATE loaded faujasite zeolite allowing basicity comparisons of the nitrogen substituted zeolites with different compositions with the basicity of the pristine zeolites. Numbers within parenthesis show the actual Si/Al ratio of the framework (Calculated by ^{29}Si MAS NMR).

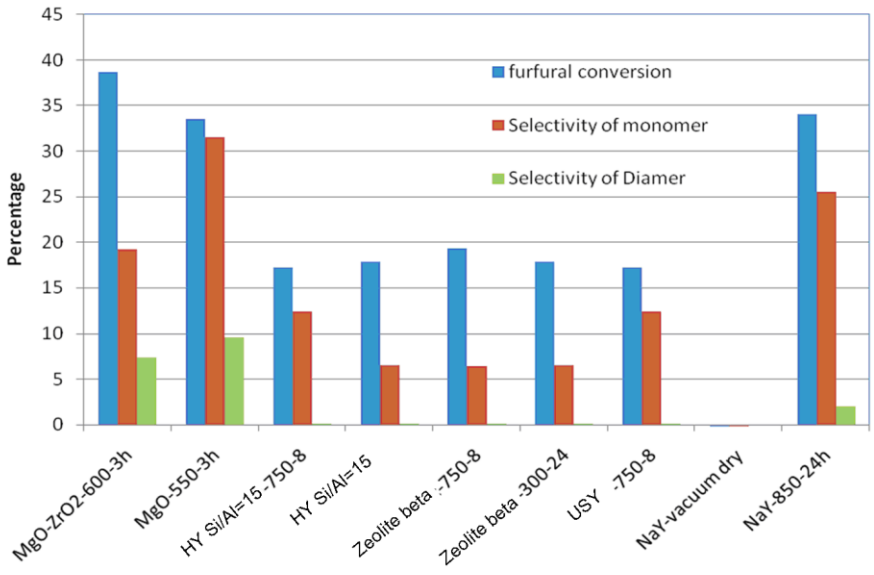

Figure 5.11. The efficiencies of the solid base catalysts for furfural conversion reaction.

5.4. Conclusions

The effect of nitrogen content and zeolite composition on the basicity of the framework has been investigated for nitrogen substituted zeolites. The basicity of the framework has been studied by using an acidic probe molecule Boric Acid Trimethyl Ester (BATE) and characterization of the boron environment interacting with the basic sites in the zeolite framework by using ^{11}B MAS NMR. The results have shown that there are two main boron environments, 3 and 4-coordinate at around 18 ppm and 0 ppm, respectively. ^{11}B MQMAS NMR has also been performed on the BATE loaded high nitrogen content zeolites to study the quarupolar interaction and distribution of different boron environments. As the interaction of the probe molecule with the zeolite framework gets stronger, the planar structure of the BATE molecule gets distorted causing an increased quadrupolar interaction for the 3-coordinate boron environment and the intensity of the 4-coordinate boron resonance increases.

The comparison of the parameters obtained from 2D ^{11}B MQMAS NMR data of BATE loaded pristine zeolite Y and nitrogen substituted zeolite with different framework compositions can allow us to compare the basicity of these materials. The results have shown that as the nitrogen content of the zeolite framework increases, the basicity increases. Compared to the nitridated HY zeolites with different aluminum content, nitridated NaY zeolite shows the highest basic character.

Aldol condensation of furaldehydes with acetone and propanal has been studied on nitrogen substituted zeolites. Nit-NaY has shown catalytic activity comparable to MgO-ZrO2 and much higher activity than that of untreated NaY. The nitrogen substituted NaY has shown more selectivity to monomer than MgO-ZrO_2 catalysts. Unfortunately, the catalyst was not stable in the water-methanol solvent with the loss in catalytic activity due to leaching of the amine sites.

Overall, the studies have shown that, nitrogen substitution, increases the basicity of the zeolite framework and nitridated zeolites are promising solid base catalysts especially for water-free catalytical reactions.

5.5. References

(1) Astala, R.; Auerbach, S. M. *J. Am. Chem. Soc.* **2004**, *126*, 1843.

(2) Sanchez-Sanchez, M.; Blasco, T. *Chemical Communications* **2000**, 491.

(3) Sanchez-Sanchez, M.; Blasco, T.; Corma, A. *J. Phys. Chem. C* **2008**, *112*, 16961.

(4) Mignon, P.; Geerlings, P.; Schoonheydt, R. *Journal of Physical Chemistry B* **2006**, *110*, 24947.

(5) Mignon, P.; Pidko, E. A.; Van Santen, R. A.; Geerlings, P.; Schoonheydt, R. A. *Chemistry-a European Journal* **2008**, *14*, 5168.

(6) Morrow, B. A.; Devi, A. *J. Chem. Soc., Faraday Trans. 1* **1972**, *68*, 403.

(7) Liu, J.; Ying, P. L.; Xin, Q.; Li, C. *Zeolites* **1997**, *19*, 197.

(8) Liu, J. K.; Ying, P. L.; Xin, Q.; Li, C. *Applied Surface Science* **1998**, *126*, 16.

(9) Mackenzie, K. J. D.; Smith, M. E. *Multinuclear Solid-State NMR of Inorganic Materials*; Pergamon Material Series, 2002; Vol. 6.

(10) Han, X.; State Key Laboratory of Catalysis Dalian Institute of Chemical Physics Chinese Academy of Sciences: Dalian, 2005.

(11) Dogan, F.; Hammond, K. D.; Tompsett, G. A.; Huo, H.; Conner, W. C.; Auerbach, S. M.; Grey, C. P. *J. Am. Chem. Soc.* **2009**, *131*, 11062.

References

Chapter 1

(1) Weitkamp, J.; Hunger, M.; Rymsa, U. *Microporous and Mesoporous Materials* **2001**, *48*, 255.

(2) Zhang, X.; Lai, E. S. M.; Martin-Aranda, R.; Yeung, K. L. *Appl. Catal., A* **2004**, *261*, 109.

(3) Han, A.-J.; He, H.-Y.; Guo, J.; Yu, H.; Huang, Y.-F.; Long, Y.-C. *Microporous Mesoporous Mater.* **2005**, *79*, 177.

(4) Xiong, J.; Ding, Y.; Zhu, H.; Yan, L.; Liu, X.; Lin, L. *J. Phys. Chem. B* **2003**, *107*, 1366.

(5) Astala, R.; Auerbach, S. M. *J. Am. Chem. Soc.* **2004**, *126*, 1843.

(6) S. M. Auerbach, K. A. C., P. K. Dutta *Handbook of Zeolite Science and Technology*; Marcel Dekker Inc., 2003.

(7) Wan, K.; Liu, Q.; Zhang, C. M.; Wang, J. C. *Bulletin of the Chemical Society of Japan* **2004**, *77*, 1409.

(8) Weitkamp, J. *Solid State Ionics* **2000**, *131*, 175.

(9) D.H., O. *Atlas of Zeolite Framework Types*; Elsevier, 2001.

(10) D.W., B. *Zeolite Molecular Sieves:Structure, Chemistry, and Use*; John Wiley&Sons,Inc., 1974.

(11) Lohse, U.; Altrichter, B.; Fricke, R.; Pilz, W.; Schreier, E.; Garkisch, C.; Jancke, K. *Journal of the Chemical Society-Faraday Transactions* **1997**, *93*, 505.

(12) Beck, J. S.; Vartuli, J. C.; Roth, W. J.; Leonowicz, M. E.; Kresge, C. T.; Schmitt, K. D.; Chu, C. T. W.; Olson, D. H.; Sheppard, E. W.; McCullen, S. B.; Higgins, J. B.; Schlenker, J. L. *Journal of the American Chemical Society* **1992**, *114*, 10834.

(13) Hu, W.; Luo, Q.; Su, Y. C.; Chen, L.; Yue, Y.; Ye, C. H.; Deng, F. *Microporous and Mesoporous Materials* **2006**, *92*, 22.

(14) Zhao, X. S.; Lu, G. Q.; Hu, X. *Microporous and Mesoporous Materials* **2000**, *41*, 37.

(15) Jentys, A.; Pham, N. H.; Vinek, H. *Journal of the Chemical Society-Faraday Transactions* **1996**, *92*, 3287.

(16) Shi, L.; Zou, Y.; He, H. Y. *Chemistry Letters* **2001**, 1164.

(17) Wouters, B. H.; Chen, T. H.; Dewilde, M.; Grobet, P. J. *Microporous and Mesoporous Materials* **2001**, *44*, 453.

(18) A. Auroux, A. B., E. Brunner, F. Fajula, E. Garrone, A. Jentys, J. A. Lercher, H. Pfeifer *Acidity and Basicity*; Springer: Heidelberg, 2008; Vol. 6.

(19) Barthomeuf, D. *Microporous Mesoporous Mater.* **2003**, *66*, 1.

(20) Ernst, S.; Hartmann, M.; Sauerbeck, S.; Bongers, T. *Appl. Catal., A* **2000**, *200*, 117.

(21) Suppes, G. J.; Dasari, M. A.; Doskocil, E. J.; Mankidy, P. J.; Goff, M. J. *Applied Catalysis a-General* **2004**, *257*, 213.

(22) Chheda, J. N.; Dumesic, J. A. *Catalysis Today* **2007**, *123*, 59.

(23) van Bokhoven, J. A.; van der Eerden, A. M. J.; Koningsberger, D. C. *Journal of the American Chemical Society* **2003**, *125*, 7435.

(24) van Bokhoven, J. A.; Koningsberger, D. C.; Kunkeler, P.; van Bekkum, H.; Kentgens, A. P. M. *J. Am. Chem. Soc.* **2000**, *122*, 12842.

(25) Jiao, J.; Ray, S. S.; Wang, W.; Weitkamp, J.; Hunger, M. *Z. Anorg. Allg. Chem.* **2005**, *631*, 484.

(26) Jiao, J.; Altwasser, S.; Wang, W.; Weitkamp, J.; Hunger, M. *J. Phys. Chem. B* **2004**, *108*, 14305.

(27) Hattori, H. *Chemical Reviews* **1995**, *95*, 537.

(28) Weitkamp, J.; Hunger, M.; Rymsa, U. *Microporous Mesoporous Mater.* **2001**, *48*, 255.

(29) Zhang, X. F.; Lai, E. S. M.; Martin-Aranda, R.; Yeung, K. L. *Applied Catalysis a-General* **2004**, *261*, 109.

(30) Climent, M. J.; Corma, A.; Fornes, V.; Frau, A.; GuilLopez, R.; Iborra, S.; Primo, J. *Journal of Catalysis* **1996**, *163*, 392.

(31) Wiame, H. M.; Cellier, C. M.; Grange, P. *Journal of Physical Chemistry B* **2000**, *104*, 591.

(32) Xia, Y.; Mokaya, R. *J. Phys. Chem. C* **2008**, *112*, 1455.

(33) El Haskouri, J.; Cabrera, S.; Sapina, F.; Latorre, J.; Guillem, C.; Beltran-Porter, A.; Beltran-Porter, D.; Marcos, M. D.; Amoros, P. *Advanced Materials* **2001**, *13*, 192.

(34) Xiong, J. M.; Ding, Y. J.; Zhu, H. J.; Yan, L.; Liu, X. M.; Lin, L. W. *Journal of Physical Chemistry B* **2003**, *107*, 1366.

(35) Zhang, C.; Liu, Q.; Xu, Z. *J. Non-Cryst. Solids* **2005**, *351*, 1377.

(36) Narasimharao, K.; Hartmann, M.; Thiel, H. H.; Ernst, S. *Microporous and Mesoporous Materials* **2006**, *90*, 377.

(37) Zhang, C.; Xu, Z.; Wan, K.; Liu, Q. *Appl. Catal., A* **2004**, *258*, 55.

(38) Chino, N.; Okubo, T. *Microporous Mesoporous Mater.* **2005**, *87*, 15.

(39) Grey, C. P.; Vega, A. J. *Journal of the American Chemical Society* **1995**, *117*, 8232.

(40) Iuga, D.; Morais, C.; Gan, Z. H.; Neuville, D. R.; Cormier, L.; Massiot, D. *Journal of the American Chemical Soceity* **2005**, *127*, 11540.

(41) Millot, Y.; Man, P. P. *Solid State Nuclear Magnetic Resonance* **2002**, *21*, 21.

(42) Klinowski, J. *Annual Review of Materials Science* **1988**, *18*, 189.

(43) Mackenzie, K. J. D.; Smith, M. E. *Multinuclear Solid-State NMR of Inorganic Materials*; Pergamon Material Series, 2002; Vol. 6.

(44) Loewenstein, W. *Am. Mineral.* **1954**, *39*, 92.

(45) Zhang, C.; Xu, Z.; Liu, Q. *J. Wuhan Univ. Technol., Mater. Sci. Ed.* **2005**, *20*, 32.

(46) Ciraolo, M. F.; Hanson, J. C.; Grey, C. P. *Microporous Mesoporous Mater.* **2001**, *49*, 111.

(47) Young, R. A. *Int. Union Crystallogr. Monogr. Crystallogr.* **1993**, *5*, 1.

(48) Abeykoon, A. M. M.; Donner, W.; Brunelli, M.; Castro-Colin, M.; Jacobson, A. J.; Moss, S. C. *J Am Chem Soc* **2009**, *131*, 13230.

(49) Narkhede, V. V.; Gies, H. *Chemistry of Materials* **2009**, *21*, 4339.

(50) Martinez-Inesta, M. M.; Peral, I.; Proffen, T.; Lobo, R. F. *Microporous and Mesoporous Materials* **2005**, *77*, 55.

(51) Martinez-Inesta, M. A. M.; Lobo, R. F. *Journal of Physical Chemistry C* **2007**, *111*, 8573.

(52) Sanchez-Sanchez, M.; Blasco, T. *Chemical Communications* **2000**, 491.

(53) Sanchez-Sanchez, M.; Blasco, T.; Corma, A. *J. Phys. Chem. C* **2008**, *112*, 16961.

(54) Mignon, P.; Geerlings, P.; Schoonheydt, R. *Journal of Physical Chemistry B* **2006**, *110*, 24947.

(55) Mignon, P.; Pidko, E. A.; Van Santen, R. A.; Geerlings, P.; Schoonheydt, R. A. *Chemistry-a European Journal* **2008**, *14*, 5168.

(56) Sanderson, R. T. *Journal of the American Chemical Society* **1983**, *105*, 2259.

(57) Varekova, R. S.; Jirouskova, Z.; Vanek, J.; Suchomel, S.; Koca, J. *International Journal of Molecular Sciences* **2007**, *8*, 572.

(58) Yang, C.; Wang, J.; Xu, Q. H. *Microporous Materials* **1997**, *11*, 261.

(59) Liu, J.; Ying, P. L.; Xin, Q.; Li, C. *Zeolites* **1997**, *19*, 197.

Chapter 2

(1) Guo, J.; Han, A.-J.; Yu, H.; Dong, J.-p.; He, H.; Long, Y.-C. *Microporous Mesoporous Mater.* **2006**, *94*, 166.

(2) Han, A.-J.; He, H.-Y.; Guo, J.; Yu, H.; Huang, Y.-F.; Long, Y.-C. *Microporous Mesoporous Mater.* **2005**, *79*, 177.

(3) Zhang, C.; Xu, Z.; Wan, K.; Liu, Q. *Appl. Catal., A* **2004**, *258*, 55.

(4) Wakihara, T.; Saito, Y.; Tatami, J.; Kometa, K.; Meguro, T.; Mackenzie, K. J. D.; Takagi, S.; Yokouchi, M. *J. Ceram. Soc. Jpn.* **2008**, *116*, 980.

(5) Ernst, S.; Hartmann, M.; Sauerbeck, S.; Bongers, T. *Appl. Catal., A* **2000**, *200*, 117.

(6) Narasimharao, K.; Hartmann, M.; Thiel, H. H.; Ernst, S. *Microporous and Mesoporous Materials* **2006**, *90*, 377.

(7) Guan, X.; Li, N.; Wu, G.; Chen, J.; Zhang, F.; Guan, N. *J. Mol. Catal. A Chem.* **2006**, *248*, 220.

(8) Mackenzie, K. J. D.; Smith, M. E. *Multinuclear Solid-State NMR of Inorganic Materials*; Pergamon Material Series, 2002; Vol. 6.

(9) Zhang, C.; Liu, Q.; Xu, Z. *J. Non-Cryst. Solids* **2005**, *351*, 1377.

(10) Chino, N.; Okubo, T. *Microporous Mesoporous Mater.* **2005**, *87*, 15.

(11) Weitkamp, J.; Hunger, M.; Rymsa, U. *Microporous Mesoporous Mater.* **2001**, *48*, 255.

(12) Zhang, C.; Xu, Z.; Liu, Q. *J. Wuhan Univ. Technol., Mater. Sci. Ed.* **2005**, *20*, 32.

Chapter 3

(1) S. M. Auerbach, K. A. C., P. K. Dutta *Handbook of Zeolite Science and Technology*; Marcel Dekker Inc., 2003.

(2) Weitkamp, J. *Solid State Ionics* **2000**, *131*, 175.

(3) Haw, J. F. *Phys. Chem. Chem. Phys.* **2002**, *4*, 5431.

(4) Wan, K.; Liu, Q.; Zhang, C.; Wang, J. *Bull. Chem. Soc. Jpn.* **2004**, *77*, 1409.

(5) Weitkamp, J.; Hunger, M.; Rymsa, U. *Microporous and Mesoporous Materials* **2001**, *48*, 255.

(6) Barthomeuf, D. *Microporous Mesoporous Mater.* **2003**, *66*, 1.

(7) Narasimharao, K.; Hartmann, M.; Thiel, H. H.; Ernst, S. *Microporous and Mesoporous Materials* **2006**, *90*, 377.

(8) Zhang, X.; Lai, E. S. M.; Martin-Aranda, R.; Yeung, K. L. *Appl. Catal., A* **2004**, *261*, 109.

(9) Ernst, S.; Hartmann, M.; Sauerbeck, S.; Bongers, T. *Appl. Catal., A* **2000**, *200*, 117.

(10) Zhang, X. F.; Lai, E. S. M.; Martin-Aranda, R.; Yeung, K. L. *Applied Catalysis a-General* **2004**, *261*, 109.

(11) Suppes, G. J.; Dasari, M. A.; Doskocil, E. J.; Mankidy, P. J.; Goff, M. J. *Applied Catalysis a-General* **2004**, *257*, 213.

(12) Yamamoto, K.; Sakata, Y.; Nohara, Y.; Takahashi, Y.; Tatsumi, T. *Science (Washington, DC, U. S.)* **2003**, *300*, 470.

(13) Kerr, G. T.; Shipman, G. F. *J. Phys. Chem.* **1968**, *72*, 3071.

(14) Chino, N.; Okubo, T. *Microporous Mesoporous Mater.* **2005**, *87*, 15.

(15) Xiong, J. M.; Ding, Y. J.; Zhu, H. J.; Yan, L.; Liu, X. M.; Lin, L. W. *Journal of Physical Chemistry B* **2003**, *107*, 1366.

(16) Han, A.-J.; He, H.-Y.; Guo, J.; Yu, H.; Huang, Y.-F.; Long, Y.-C. *Microporous Mesoporous Mater.* **2005**, *79*, 177.

(17) Zhang, C.; Xu, Z.; Liu, Q. *J. Wuhan Univ. Technol., Mater. Sci. Ed.* **2005**, *20*, 32.

(18) Zhang, C.; Liu, Q.; Xu, Z. *J. Non-Cryst. Solids* **2005**, *351*, 1377.

(19) El Haskouri, J.; Cabrera, S.; Sapina, F.; Latorre, J.; Guillem, C.; Beltran-Porter, A.; Beltran-Porter, D.; Marcos, M. D.; Amoros, P. *Advanced Materials* **2001**, *13*, 192.

(20) Hammond, K. D.; Dogan, F.; Tompsett, G. A.; Agarwal, V.; Conner, W. C.; Grey, C. P.; Auerbach, S. M. *J. Am. Chem. Soc.* **2008**, *130*, 14912.

(21) Astala, R.; Auerbach, S. M. *J. Am. Chem. Soc.* **2004**, *126*, 1843.

(22) Lesthaeghe, D.; Van Speybroeck, V.; Marin, G. B.; Waroquier, M. *J. Phys. Chem. B* **2005**, *109*, 7952.

(23) Martinez-Inesta, M. M.; Peral, I.; Proffen, T.; Lobo, R. F. *Microporous and Mesoporous Materials* **2005**, *77*, 55.

(24) Proffen, T.; Billinge, S. J. L.; Egami, T.; Louca, D. *Zeitschrift Fur Kristallographie* **2003**, *218*, 132.

(25) Loewenstein, W. *Am. Mineral.* **1954**, *39*, 92.

(26) Kao, H.-M.; Grey, C. P. *J. Phys. Chem.* **1996**, *100*, 5105.

(27) Luz, Z.; Vega, A. J. *J. Phys. Chem.* **1987**, *91*, 374.

(28) Wouters, B. H.; Chen, T.; Grobet, P. J. *J. Phys. Chem. B* **2001**, *105*, 1135.

(29) Ciraolo, M. F.; Hanson, J. C.; Norby, P.; Grey, C. P. *J. Phys. Chem. B* **2001**, *105*, 2604.

Chapter 4

(1) Dogan, F.; Hammond, K. D.; Tompsett, G. A.; Huo, H.; Conner, W. C.; Auerbach, S. M.; Grey, C. P. *J. Am. Chem. Soc.* **2009**, *131*, 11062.

(2) Zhang, C.; Xu, Z.; Wan, K.; Liu, Q. *Appl. Catal., A* **2004**, *258*, 55.

(3) Ernst, S.; Hartmann, M.; Sauerbeck, S.; Bongers, T. *Appl. Catal., A* **2000**, *200*, 117.

(4) Narasimharao, K.; Hartmann, M.; Thiel, H. H.; Ernst, S. *Microporous and Mesoporous Materials* **2006**, *90*, 377.

(5) Xiong, J. M.; Ding, Y. J.; Zhu, H. J.; Yan, L.; Liu, X. M.; Lin, L. W. *Journal of Physical Chemistry B* **2003**, *107*, 1366.

(6) Hammond, K. D.; Gharibeh, M.; Tompsett, G. A.; Dogan, F.; Brown, A. V.; Grey, C. P.; Auerbach, S. M.; Conner, W. C. *Chemistry of Materials* **2010**, *22*, 130.

(7) Astala, R.; Auerbach, S. M. *J. Am. Chem. Soc.* **2004**, *126*, 1843.

(8) Hammond, K. D.; Dogan, F.; Tompsett, G. A.; Agarwal, V.; Conner, W. C.; Grey, C. P.; Auerbach, S. M. *J. Am. Chem. Soc.* **2008**, *130*, 14912.

(9) G. Engelhardt, D. M. *High Resolution Solid-State NMR of Silicates and Zeolites*; John Wiley and Sons, 1987.

(10) S. M. Auerbach, K. A. C., P. K. Dutta *Handbook of Zeolite Science and Technology*; Marcel Dekker Inc., 2003.

(11) A. Auroux, A. B., E. Brunner, F. Fajula, E. Garrone, A. Jentys, J. A. Lercher, H. Pfeifer *Acidity and Basicity*; Springer: Heidelberg, 2008; Vol. 6.

(12) Mackenzie, K. J. D.; Smith, M. E. *Multinuclear Solid-State NMR of Inorganic Materials*; Pergamon Material Series, 2002; Vol. 6.

(13) Huang, J.; Jiang, Y.; Marthala, V. R. R.; Thomas, B.; Romanova, E.; Hunger, M. *J. Phys. Chem. C* **2008**, *112*, 3811.

(14) Kao, H.-M.; Grey, C. P. *J. Phys. Chem.* **1996**, *100*, 5105.

(15) Jiao, J.; Altwasser, S.; Wang, W.; Weitkamp, J.; Hunger, M. *J. Phys. Chem. B* **2004**, *108*, 14305.

(16) van Bokhoven, J. A.; Koningsberger, D. C.; Kunkeler, P.; van Bekkum, H.; Kentgens, A. P. M. *J. Am. Chem. Soc.* **2000**, *122*, 12842.

(17) Fyfe, C. A.; Bretherton, J. L.; Lam, L. Y. *Chem. Commun. (Cambridge)* **2000**, 1575.

(18) Fyfe, C. A.; Bretherton, J. L.; Lam, L. Y. *J. Am. Chem. Soc.* **2001**, *123*, 5285.

(19) Jiao, J.; Kanellopoulos, J.; Wang, W.; Ray Siddharth, S.; Foerster, H.; Freude, D.; Hunger, M. *Phys Chem Chem Phys* **2005**, *7*, 3221.

(20) Fitzgerald, J. J.; Kohl, S. D.; Piedra, G.; Dec, S. F.; Maciel, G. E. *Chemistry of Materials* **1994**, *6*, 1915.

(21) Hunger, M. *Solid State Nuclear Magnetic Resonance* **1996**, *6*, 1.

(22) Grey, C. P.; Vega, A. J. *Journal of the American Chemical Society* **1995**, *117*, 8232.

(23) Jiao, J.; Kanellopoulos, J.; Wang, W.; Ray, S. S.; Foerster, H.; Freude, D.; Hunger, M. *Physical Chemistry Chemical Physics* **2005**, *7*, 3221.

(24) Jiao, J.; Kanellopoulos, J.; Behera, B.; Jiang, Y.; Huang, J.; Marthala, V. R. R.; Ray, S. S.; Wang, W.; Hunger, M. *J. Phys. Chem. B* **2006**, *110*, 13812.

(25) Jiao, J.; Wang, W.; Sulikowski, B.; Weitkamp, J.; Hunger, M. *Microporous and Mesoporous Materials* **2006**, *90*, 246.

(26) Jiao, J.; Ray, S. S.; Wang, W.; Weitkamp, J.; Hunger, M. *Z. Anorg. Allg. Chem.* **2005**, *631*, 484.

(27) Klinowski, J. *Annual Review of Materials Science* **1988**, *18*, 189.

(28) El Haskouri, J.; Cabrera, S.; Sapina, F.; Latorre, J.; Guillem, C.; Beltran-Porter, A.; Beltran-Porter, D.; Marcos, M. D.; Amoros, P. *Advanced Materials* **2001**, *13*, 192.

(29) Puurunen, R. L.; Lindblad, M.; Root, A.; Krause, A. O. I. *Physical Chemistry Chemical Physics* **2001**, 1093.

Chapter 5

(1) Astala, R.; Auerbach, S. M. *J. Am. Chem. Soc.* **2004**, *126*, 1843.

(2) Sanchez-Sanchez, M.; Blasco, T. *Chemical Communications* **2000**, 491.

(3) Sanchez-Sanchez, M.; Blasco, T.; Corma, A. *J. Phys. Chem. C* **2008**, *112*, 16961.

(4) Mignon, P.; Geerlings, P.; Schoonheydt, R. *Journal of Physical Chemistry B* **2006**, *110*, 24947.

(5) Mignon, P.; Pidko, E. A.; Van Santen, R. A.; Geerlings, P.; Schoonheydt, R. A. *Chemistry-a European Journal* **2008**, *14*, 5168.

(6) Morrow, B. A.; Devi, A. *J. Chem. Soc., Faraday Trans. 1* **1972**, *68*, 403.

(7) Liu, J.; Ying, P. L.; Xin, Q.; Li, C. *Zeolites* **1997**, *19*, 197.

(8) Liu, J. K.; Ying, P. L.; Xin, Q.; Li, C. *Applied Surface Science* **1998**, *126*, 16.

(9) Mackenzie, K. J. D.; Smith, M. E. *Multinuclear Solid-State NMR of Inorganic Materials*; Pergamon Material Series, 2002; Vol. 6.

(10) Han, X.; State Key Laboratory of Catalysis Dalian Institute of Chemical Physics Chinese Academy of Sciences: Dalian, 2005.

(11) Dogan, F.; Hammond, K. D.; Tompsett, G. A.; Huo, H.; Conner, W. C.; Auerbach, S. M.; Grey, C. P. *J. Am. Chem. Soc.* **2009**, *131*, 11062.